JOURNAL OF PETROLOGY | VOLUME 48 | NUMBER 9 | PAGES 1681–1724 | 2007 | doi:10.1093/petrology/egm035

Garnet-bearing Xenoliths from Salt Lake Crater, Oahu, Hawaii: High-Pressure Fractional Crystallization in the Oceanic Mantle

SHANTANU KESHAV[1,2]*, GAUTAM SEN[1] AND DEAN C. PRESNALL[2,3]

[1]DEPARTMENT OF EARTH SCIENCES, FLORIDA INTERNATIONAL UNIVERSITY, MIAMI, FL 33199, USA

[2]GEOPHYSICAL LABORATORY, CARNEGIE INSTITUTION OF WASHINGTON, WASHINGTON, DC 20015, USA

[3]DEPARTMENT OF GEOSCIENCES, UNIVERSITY OF TEXAS AT DALLAS, BOX 830688, RICHARDSON, TX 75083, USA

RECEIVED NOVEMBER 1, 2004; ACCEPTED JUNE 14, 2007
ADVANCE ACCESS PUBLICATION AUGUST 18, 2007

The focus of this study is a suite of garnet-bearing mantle xenoliths from Oahu, Hawaii. Clinopyroxene, olivine, and garnet constitute the bulk of the xenoliths, and orthopyroxene is present in small amounts. Clinopyroxene has exsolved orthopyroxene, spinel, and garnet. Many xenoliths also contain spinel-cored garnets. Olivine, clinopyroxene, and garnet are in major element chemical equilibrium with each other; large, discrete orthopyroxene does not appear to be in major-element chemical equilibrium with the other minerals. Multiple compositions of orthopyroxene occur in individual xenoliths. The new data do not support the existing hypothesis that all the xenoliths formed at 1·6–2·2 GPa, and that the spinel-cored garnets formed as a consequence of almost isobaric subsolidus cooling of a spinel-bearing assemblage. The lack of olivine or pyroxenes in the spinel–garnet reaction zones and the embayed outline of spinel grains inside garnet suggest that the spinel-cored garnets grew in the presence of a melt. The origin of these xenoliths is interpreted on the basis of liquidus phase relations in the tholeiitic and slightly silica-poor portion of the $CaO–MgO–Al_2O_3–SiO_2$ *(CMAS) system at pressures from 3·0 to 5·0 GPa. The phase relations suggest crystallization from slightly silica-poor melts (or transitional basaltic melts) in the depth range ~110–150 km beneath Oahu. This depth estimate puts the formation of these xenoliths in the asthenosphere. On the basis of this study it is proposed that the pyroxenite xenoliths are high-pressure cumulates related to polybaric magma fractionation in the asthenosphere, thus making Oahu the only locality among the oceanic regions where such deep magmatic fractional crystallization processes have been recognized.*

KEY WORDS: *xenolith; asthenosphere; basalt; CMAS; cumulate; oceanic lithosphere; experimental petrology; mantle; geothermobarometry; magma chamber*

INTRODUCTION

The Hawaiian–Emperor chain provides a good example of the evolution of a mid-plate volcanic chain and continues to play an important role in our understanding of mantle melting processes on a global scale. It is perhaps the location of the Hawaiian Islands, which is far from trenches, ridges, and regions of active plate motions, that has attracted geologists and geophysicists alike. Volcanic activity along this chain has now lasted for almost 80 Myr and has been thought to be the surface expression of a mantle plume rooted deep in the Earth's interior (Wilson, 1963; Morgan, 1971). Hawaii presents an opportunity to study and better understand melting processes in mid-plate oceanic regions. However, there are very weak or no physical constraints on the dimension (either in the past or at present) of the presumed plume, its depth extent, and its precise thermal and compositional nature. Additionally, in recent times, keen interest has developed in constraining the seismically defined lithospheric thickness beneath Hawaii, inasmuch as this thickness constrains the locus of lithosphere–asthenosphere interaction and depth of primary magma formation and magma ponding. Strong shear-wave velocity reductions seen at depths of ~80–85 km have been interpreted as marking the lithosphere–asthenosphere transition beneath the island of Oahu (Bock, 1991; Woods & Okal, 1996). Similar velocity reductions, interpreted to be indicative of melting at depths of ~130–140 km, beneath the island of Hawaii have also been reported (Li *et al.*, 2000).

*Corresponding author. Present address: Bayerisches Geoinstitut, Universität Bayreuth, 95440 Bayreuth, Germany. Telephone: +49-921-55-3719. Fax: +49-921- 55-3769.
E-mail: keshav@uni-bayreuth.de

Studies of Hawaiian volcanism have revealed a great variety of crustal and mantle xenoliths, mostly recovered from the island of Oahu. These xenoliths have been brought to the surface by the Honolulu Volcanics (HV), a stage in Hawaiian volcanism marking the rejuvenation of eruptive activity on Oahu. Here we focus on a large suite of garnet-bearing xenoliths from Salt Lake Crater (SLC) on the island of Oahu. Garnet-bearing xenoliths were chosen for the following reasons: (1) they provide evidence for deep melting and crystallization processes in the mantle; (2) Hawaii is the only oceanic island setting where such unusual xenoliths occur; (3) these xenoliths might tell us something more about how magmatic processes work in mid-plate locations, and thus if Hawaii is unique; (4) these xenoliths can provide invaluable constraints on mantle dynamics beneath Hawaii.

In this study, we address the following issues: (1) petrographic and mineral chemical variability shown by the xenolith suite; (2) petrogenesis of the xenoliths (residues of melt extraction, frozen melts, or magmatic cumulates); (3) the depths at which the xenoliths formed; (4) the relationship between the xenoliths and the parental magmas of the Hawaiian lavas.

We first present the petrography and major element mineral chemistry of 28 garnet-bearing xenoliths. We utilize mineral chemical information to assess the state of major-element equilibrium between the major silicate minerals in individual xenoliths. Exchange mineral thermometers are then used to place constraints on the thermal equilibration state of these xenoliths. This state perhaps reflects the last thermal equilibration stage experienced by the xenoliths. With some caveats, information on 'pre-exsolution' temperatures in these xenoliths, by 'dissolving' the exsolved phase back into the host phase, is also provided. Also, high-pressure liquidus phase relations in the $CaO–MgO–Al_2O_3–SiO_2$ (CMAS) system are used to evaluate the initial depth(s) of origin of the xenoliths. A unified petrogenetic model on the basis of combined petrography, mineral assemblage, mineral chemistry, and high-pressure liquidus phase relations is presented, and constraints are placed on the minimum depth of magma formation and subsequent ponding beneath the Oahu lithosphere.

SAMPLE DESCRIPTION AND PREVIOUS WORK

Several mafic and ultramafic xenolith localities are known from the Hawaiian Islands, and many of them are on the island of Oahu (White, 1966; Jackson & Wright, 1970; Sen, 1987; Appendix A). Almost all the Oahu xenoliths occur in the post-erosional Honolulu Volcanics (HV), which erupted <1 Myr ago (Lanphere & Dalrymple, 1980). A number of researchers have documented specific geographic distribution patterns of the various xenolith suites on the Koolau shield (Jackson, 1968; Sen & Presnall, 1986): dunites are abundant in vents that are proximal to the Koolau caldera, whereas spinel lherzolites are dominant elsewhere. Jackson & Wright (1970) reported finding dunites at Salt Lake Crater, but later studies concluded that these 'dunites' are actually spinel lherzolites (Sen & Presnall, 1986; Sen, 1988). In contrast to dunites and spinel lherzolites, garnet-bearing xenoliths occur exclusively on the 'flanks' of the exposed part of the tholeiitic shield (Jackson & Wright, 1970; Sen & Presnall, 1986; Sen, 1988). Much work has been done on the dunite and spinel lherzolite xenoliths (Jackson & Wright, 1970; Sen, 1983, 1987, 1988; Sen & Presnall, 1986; Vance *et al.*, 1989; Sen & Leeman, 1991; Sen *et al.*, 1993), with the conclusion that the dunites represent cumulates from magmas that underwent fractional crystallization at crustal levels (Sen & Presnall, 1986), whereas the spinel lherzolites are lithospheric fragments (restites) that have undergone variable degrees of metasomatism subsequent to a mid-ocean ridge basalt (MORB) extraction event (Sen, 1988; Sen *et al.*, 1993; Yang *et al.*, 1998; Ducea *et al.*, 2002; Bizimis *et al.*, 2003*a*). However, new trace-element and isotopic data have shown that this relatively simple scenario for the origin of spinel lherzolites as MORB-related residues may be more complicated, as some of the spinel lherzolites from Salt Lake Crater could represent fragments of ancient (>500 Ma) oceanic lithosphere (Bizimis *et al.*, 2005*a*, 2005*b*).

Salt Lake Crater is best known for its unusual suite of garnet-bearing xenoliths. Although garnet-bearing xenoliths have been described from Salt Lake Crater and from the island of Kauai (Garcia & Presti, 1987), it is only those from Salt Lake Crater that have been extensively studied (Green, 1966; Beeson & Jackson, 1970; Wilkinson, 1976; Herzberg, 1978; Frey, 1980; Sen, 1983, 1987, 1988; Sen & Leeman, 1991; Sen *et al.*, 1993, 2002, 2005; Lassiter *et al.*, 2000; Keshav & Sen, 2001, 2002, 2003, 2004; Keshav *et al.*, 2001; Bizimis *et al.*, 2005*c*).

In the past, xenoliths of the pyroxenite suite at Salt Lake Crater have also been called eclogites (Yoder & Tilley, 1962; Green, 1966; Kuno, 1969). Their true eclogitic nature and the genetic significance of this suite have been debated for the last four decades (Green, 1966; Beeson & Jackson, 1970; Frey, 1980; Sen, 1988; Sen & Leeman, 1991; Sen *et al.*, 1993, 2005; Keshav & Sen, 2001, 2003, 2004). Prior to the era of isotope and geochemical analysis of these xenoliths, the debate was focused on whether these xenoliths are the source/residue of Hawaiian magmas or are fractionation products (crystal accumulates) from Hawaiian- or MORB-type magmas (Jackson & Wright, 1970; Frey, 1980; Sen, 1988). Some researchers grouped all the garnet-bearing xenoliths into one type (the pyroxenite group), with a common mode of origin as high-pressure

(1·6–2·2 GPa; 50–70 km) crystal accumulates from Honolulu Volcanics-related magmas (Green, 1966; Frey, 1980; Sen, 1988). This conclusion was reached on the basis of petrography, mineral chemistry (major and trace element composition), and limited radiogenic isotope data. Some very rare composite xenoliths, in which a garnet-clinopyroxenite vein was seen to intrude spinel lherzolite, were also found (Sen, 1988), suggesting an igneous origin for the garnet pyroxenites. Rare olivine-rich xenolith types, such as 66SAL-1 (modally a garnet websterite) were thought to represent fertile upper mantle fragments (Jackson & Wright, 1970; Mysen & Kushiro, 1977), although Sen (1988) and Sen & Leeman (1991) suggested that such xenoliths represent physical mixtures of spinel lherzolite and garnet clinopyroxenite.

A rare garnet–spinel dunite xenolith from Salt Lake Crater with distinct cumulate texture was suggested to have originated at pressures of ~3·0 GPa (Sen & Jones, 1990). In two recent studies, rare majoritic garnets and xenoliths with ilmenite exsolution in the host garnet were described, implying their deep upper mantle origin (~180–240 km; Keshav & Sen, 2001; Keshav *et al.*, 2001). In another study, an olivine-bearing garnet-clinopyroxenite xenolith intruded by a composite vein containing cumulus Mg–Al-titanomagnetite + pleonaste + garnet was found. This unusual mineral association indicates the likely presence of very CO_2-rich kimberlite-like melts in the uppermost part of the asthenosphere beneath Oahu (Keshav & Sen, 2003). A recent report on the presence of nano-diamonds in a rare garnet-bearing xenolith from Salt Lake Crater (Wirth & Rocholl, 2003) provides further constraints on the depths of formation of these xenoliths and the host melts that brought the xenoliths to the surface. Complex assemblages of C–O–H–S fluid/melt inclusions and microdiamonds in these fluid/melt inclusions in Salt Lake Crater garnet pyroxenites suggest that some of these xenoliths may have formed at pressures significantly greater than 5–6 GPa (Frezzotti and Peccerillo, 2005), than those inferred by Sen (1988), Bizimis *et al.* (2005*c*), and Sen *et al.* (2005). These studies have opened up a new range of possibilities for the processes that have shaped the Hawaiian mantle.

The xenoliths described here come from the Jackson Collection (Smithsonian Institution) and the Presnall Collection [samples with 77-prefix; Florida International University (FIU)]. Only garnet-bearing xenoliths are described. Composite xenoliths, such as those described by Sen (1988), were not examined.

TEXTURES AND PETROGRAPHY

The garnet-bearing xenoliths are black to dark gray in hand specimen and are very easily distinguished from the light green spinel lherzolite xenoliths. Most of the studied xenoliths are pale to dark green in thin section, reflecting the color of the modally abundant clinopyroxene. They consist of variable modal proportions of clinopyroxene (usually the major phase), olivine, orthopyroxene, spinel, and garnet. Phlogopite and ilmenite, although present in some xenoliths, are not modally abundant. Modal abundances of the phases are shown in Fig. 1. The small size of many xenoliths (<5 cm) relative to the coarse size of the individual minerals produces some uncertainty in the estimation of the modal abundances. Sample numbers and brief petrographic descriptions are provided in Appendices B and C.

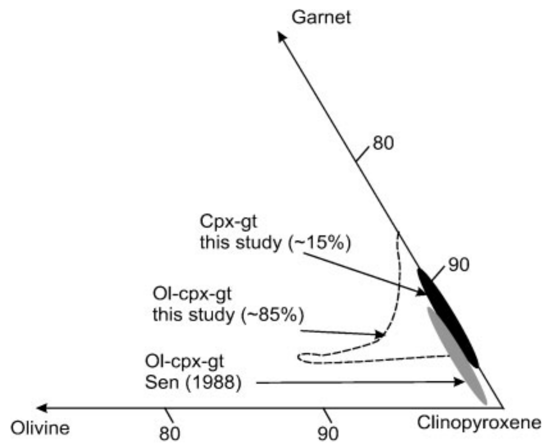

Fig. 1. A corner of the olivine–garnet–clinopyroxene ternary (vol.%) showing the modal distribution of garnet-bearing xenoliths from Salt Lake Crater. Also shown are the modes determined by Sen (1988).

Clinopyroxene

Large clinopyroxene (~0·5–1·5 mm) crystals are generally the dominant phase, forming >65% by mode of the xenoliths. They are present in all but one of the 28 xenoliths reported here. The one exception is sample 69SAL-204, which is essentially a garnetite (Fig. 2a) with <10% cpx. Clinopyroxene crystals are generally subhedral (Fig. 2b) and the larger crystals contain variable amounts of exsolved opx, spinel, and garnet. Sometimes a large cpx crystal can contain as much as ~35–40% exsolved phases. However, not all of these exsolved phases occur in the same cpx crystal; adjacent grains may contain distinct exsolution assemblages; for example, one cpx crystal may contain only exsolved garnet whereas the adjacent cpx crystal may contain exsolved spinel + opx (see also Sen & Jones, 1988), perhaps indicating different *P*–*T* paths along which the exsolution occurred. Exsolved garnets occur as round to elliptical blebs (Fig. 2c) and their size (~50–200 μm) and distribution vary greatly. The smaller garnet blebs are generally uniformly distributed in the cores of cpx crystals, whereas the larger, more elliptical to irregularly shaped blebs are somewhat randomly distributed. Large cpx crystals rarely show deformation textures. Exsolved opx can vary from perfect lamellae to highly irregular blebs

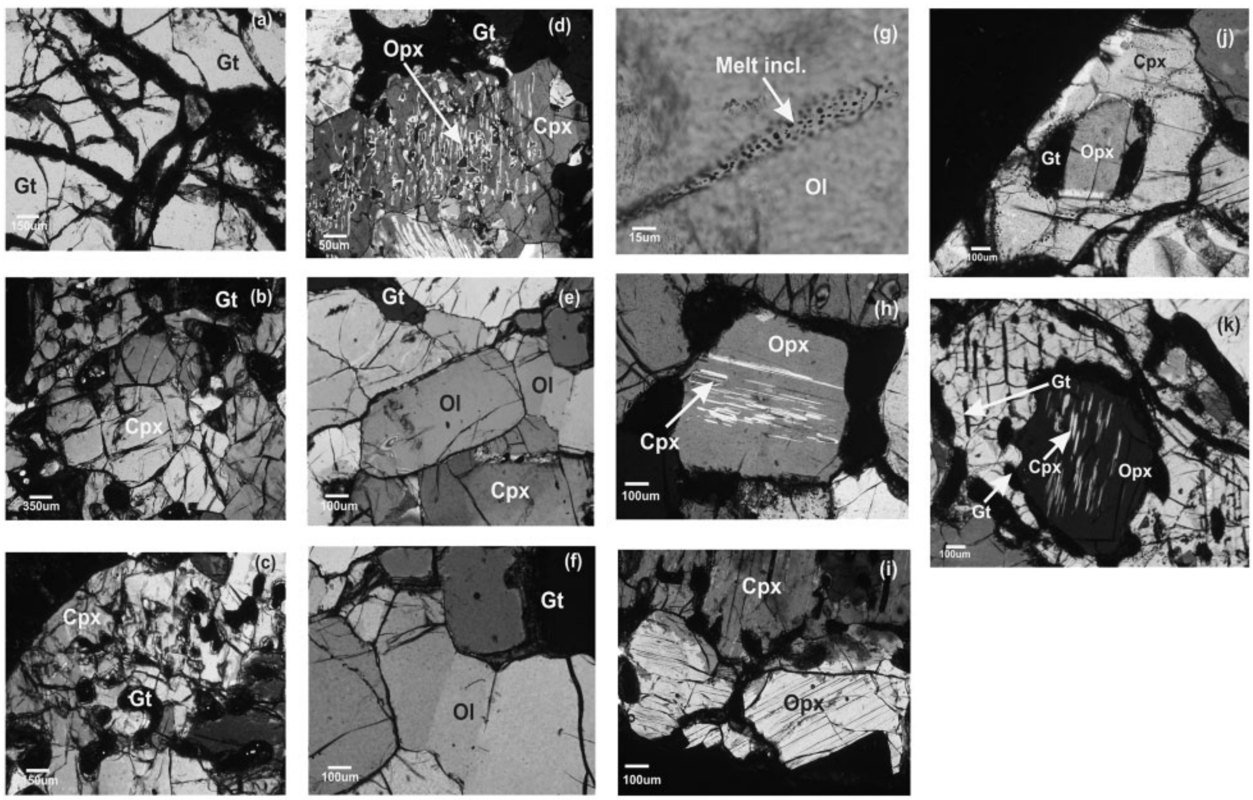

Fig. 2. Petrography of Salt Lake Crater xenoliths (a) almost a pure garnetite (69SAL-204); (b) subhedral cpx (77SL-54); (c) thick exsolved blebs of garnet in host cpx (77SL-48); (d) blebs and lamellae of exsolved opx in cpx (77SL-48); (e) euhedral olivine (77SL-10); (f) deformation bands in olivine (77SL-7); (g) melt/fluid inclusion trail in olivine (114923-55); (h) large opx with cpx exsolution (only in the center; 77SL-35); (i) large opx without exsolution near the edge of a xenolith (114923-167); (j) an inclusion of opx, surrounded by blebby garnet in primary cpx (69SAL-214); (k) an inclusion of opx in a crystal of primary cpx. The inclusion is surrounded by garnet and has also exsolved cpx. The primary crystal of cpx has exsolved garnet (69SAL-214). Abbreviations are identical to those used in the text. All photographs are taken with crossed polars.

(Fig. 2d). Annealed fractures with trapped fluid inclusions and deformation are rare in large cpx crystals. Smaller neoblasts of cpx are generally free of exsolution and deformation features. Additionally, large cpx crystals have inclusions of opx, although, depending on the orientation of the thin section, it is not always possible to determine if the opx is the product of exsolution. Sometimes olivine is also present as an inclusion. However, garnet has not been observed as an inclusion in large cpx. In view of its abundance, subhedral nature, and physical contact with large olivine and garnet, the large cpx in this suite of xenoliths is treated as a primary phase.

Clinopyroxene also occurs as an exsolved phase in large opx crystals, is generally lamellar, and ranges in size from 20 to 200 μm across. In many cases, exsolved cpx is present only in the core of the host opx.

Olivine

Olivine occurs as large (~0·2–1·0 mm; Fig. 2e), euhedral to subhedral, discrete crystals, as well as inclusions in large cpx. Rarely, it is anhedral in outline. There is some transition between euhedral and subhedral habits of olivine. Large olivine crystals occur in 22 out of 28 xenoliths described here and their modal abundance ranges from ~5 to 12%. The absence of olivine in some cases and the range in its modal abundance has been confirmed for a different batch of garnet-pyroxenite xenoliths from Salt Lake Crater (Bizimis *et al.*, 2005*c*). Previous studies have reported a much greater abundance of olivine in garnet-bearing wehrlites, websterites, and lherzolites (Kuno, 1969; Jackson & Wright, 1970; Sen, 1988; Sen & Leeman, 1991). There is no significant textural difference between the large olivine crystals found in the present suite of xenoliths and those examined by previous researchers. Euhedral olivine has also been reported in the past (Sen & Jones, 1990; Keshav & Sen, 2003). Deformation bands and subgrain boundaries are common in large crystals (Fig. 2f). Triple junctions between adjacent olivine grains are sometimes present. The grain margins of large olivines do not show evidence of alteration, in contrast to the large garnets. Large olivine is in physical contact with large cpx and/or garnet crystals with or without a spinel core. Large olivines in these xenoliths are locally fractured and melt/fluid inclusions have annealed such fractures (Fig. 2g).

Olivine in the suite of xenoliths described here is treated as a primary phase (petrographically). This conclusion is reached on the basis of the following observations: (1) large olivine crystals are euhedral to subhedral (Kuno, 1969; Sen & Leeman, 1991; Keshav & Sen, 2003); (2) primary, magmatic olivine (euhedral) in similar garnet-bearing xenoliths has been described previously (Sen & Jones, 1990; Keshav & Sen, 2003); (3) large olivine crystals (sometimes deformed) are in physical contact with large crystals of garnet (with or without a spinel core) and subhedral cpx.

Orthopyroxene

Large (~0·5–1·5 mm) prismatic to sub-prismatic crystals of orthopyroxene (opx; Fig. 2h), often containing exsolution lamellae of cpx (± spinel), occurs in 12 out of the 28 xenoliths described here. Orthopyroxene is a minor phase in these xenoliths, forming up to 2–3% of the mode. Garnet does not occur as an exsolved phase in the large opx. In this sense, the SLC xenoliths are distinct from the garnet-pyroxenite bodies in the orogenic peridotites of the French Pyrenees in which the garnet pyroxenites contain opx crystals with exsolved garnet (Sautter & Fabriès, 1990). Smaller neoblasts of opx are generally free of exsolution (Fig. 2i), and appear to be more common than those that contain exsolved cpx. Large opx, with or without exsolution, tends to occur in clusters, and is sometimes in physical contact with large garnet (with or without a spinel core). In some xenoliths, opx occurs as inclusions in cpx, and can be of two kinds: one with no exsolution (Fig. 2j) and one with exsolved cpx (Fig. 2k). Both the inclusion types are surrounded by garnet which also occurs as an exsolved phase in the host cpx. In these cases, opx is interpreted to be an inclusion and not an exsolved phase, mantled by garnet that had been subsequently exsolved from the host cpx.

Orthopyroxene is also found within a vein in one xenolith (Fig. 3a; sample 114923-158), interpreted to be of intrusive origin. In this particular xenolith, two intrusive episodes appear to be recorded: an earlier one, composed of opx (the spots are ink stains), and a later event that resulted in the formation of garnet (garnet cumulate?) and resorption of pre-existing opx (Fig. 3a). Orthopyroxene occurring as an exsolved phase in large cpx displays complex textures. It occurs as oriented lamellae and blebs with a size range of 25–100 μm and 40–200 μm, respectively. Orthopyroxene occurring at the grain boundaries of large garnets is, in rare circumstances, also associated with spinel. Out of 22 xenoliths with opx, seven have only the opx that occurs at grain boundaries of large garnets. This opx is suggested to be of secondary origin.

Garnet

Garnet is found in all the xenoliths and occurs in many forms. Where large and discrete, it is generally subhedral but in places appears to be euhedral; however, the euhedral habit is somewhat obscured by grain boundary kelyphitization. In general, large garnet grains are ~0·2–2 mm across and are in physical contact with large olivine and/or cpx crystals. Sometimes such garnet grains are also in physical contact with large opx crystals (with or without exsolution). Garnet also commonly forms rims on spinel, giving rise to the classic spinel-cored garnets (Fig. 3b). Significantly, spinel crystals present as cores in garnets show embayed and amoeboidal grain boundaries. Garnets with and without a spinel core are present in some individual xenoliths (Fig. 3c).

Garnet also occurs as an exsolved phase in host cpx (Fig. 3d), and is present both as thin, oriented rods (40–70 μm) and blebs (50–100 μm) and as relatively larger blobs (100–250 μm). Some of the exsolved garnet appears to have migrated out of the host cpx, forming rims around it that give rise to the so-called 'garland' texture (Fig. 3e). Such rim-forming garnet is generally amoeboid and irregular in outline, and in many cases can be traced back into its 'parent' exsolved garnet bleb within the host cpx. In some xenoliths, exsolved garnet constitutes as much as 35–40% of the host cpx (Fig. 3f). Garnet as an exsolved phase in host opx has not been found in the studied suite of xenoliths.

Large garnets with or without a spinel core are considered primary for the following reasons. (1) Some xenoliths in the studied suite have been extensively veined by garnet, garnet–spinel, and garnet–opx, pointing to an igneous origin of these veins as well as the host rock. Sen (1988) and Keshav & Sen (2003) also described such textures. (2) Interstitial, primary magmatic garnet has been reported in a garnet–spinel dunite from Salt Lake Crater (Sen & Jones, 1990). (3) Garnet rims around a spinel core are reminiscent of reaction rims around phenocrysts in erupted lavas. (4) Large garnet crystals (with or without a spinel core) in physical contact with large, euhedral or subhedral grains of olivine and cpx also support a magmatic origin, although now the xenoliths are 'metamorphic rocks'.

Spinel

Spinel exhibits varied textures. It commonly forms the cores of large garnet grains and also occurs as an exsolved phase in large cpx and opx crystals. Spinel occurring as a core in large garnet crystals is generally round and amoeboid. Interstitial spinel is rare. Zoned spinel occurring in proximity with opx is found at grain boundaries of large garnet.

When exsolved in cpx, spinel has blade-like forms (20–150 μm), and also occurs as rhomboids (30–150 μm), lamellae (20–100 μm), and rods varying in size from

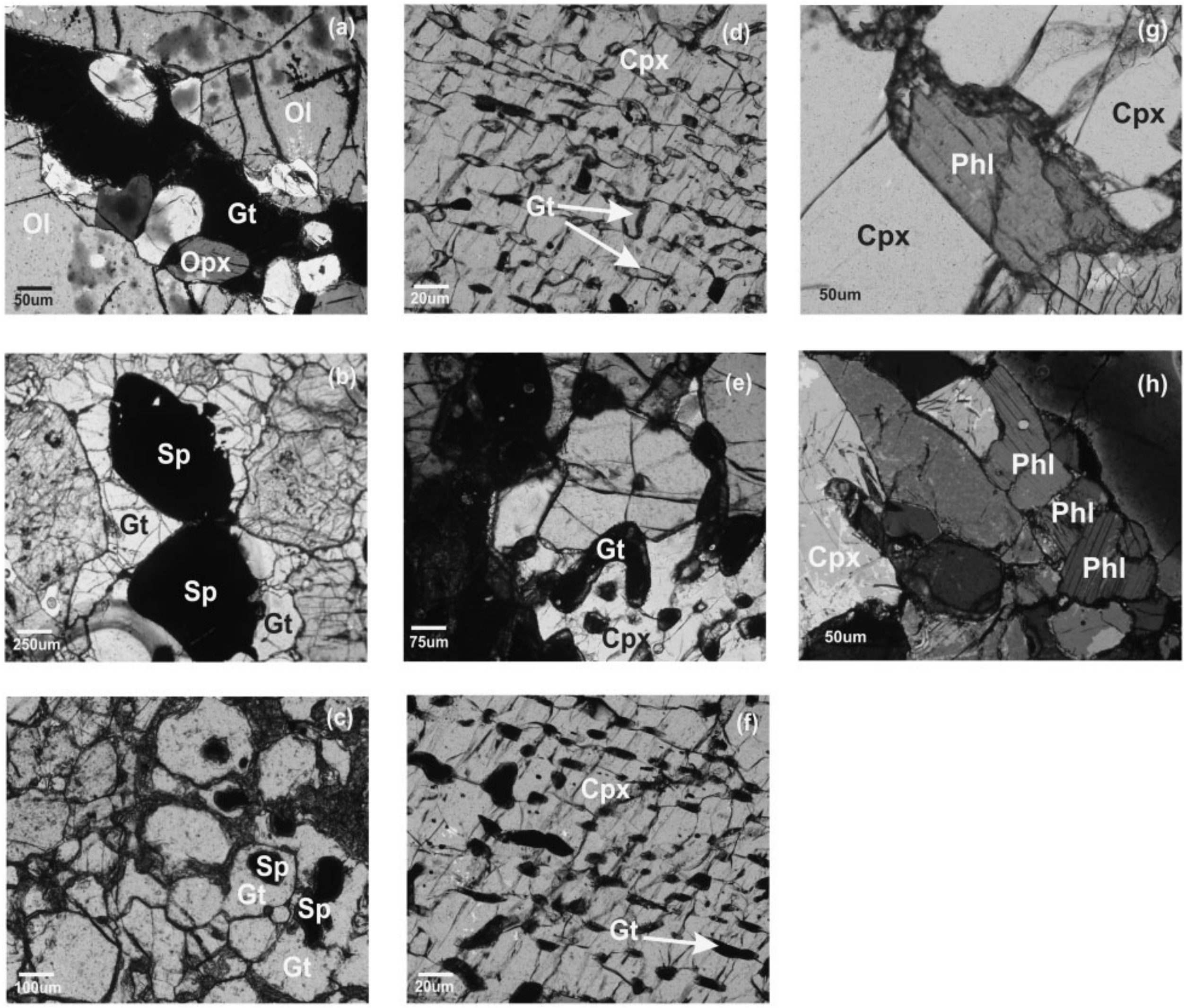

Fig. 3. Texture variations in Salt Lake Crater garnet-pyroxenite xenoliths (a) garnet (black) and opx (grey) veins in a porphyroclastic olivine (greenish blue). The rounded margins of opx in garnet (114923-158) should be noted. (b) spinel-cored garnet (114954-20A). The absence of other phase(s) between spinel and garnet should be noted; also the smooth outlines of spinel in the core. (c) Two types of garnet in the same xenolith: one with a spinel core and the other without (115954-20C). (d) Exsolved garnet in cpx (69SAL-214). (e) Grain boundary garnet in cpx. It should be noted how the grain boundary garnet can be traced back into its 'parent' (77SL-48). (f) Densely exsolved garnet in cpx (69SAL-214). (g) Phlogopite in physical contact with large cpx. Both the sharp and the irregular grain boundary of phlogopite should be noted (77SL-62). (h) Vein of phlogopite that is in continuation with garnet and opx in the same vein as described in (a) (114923-158). Photographs (b–d) and (f) were taken in plane-polarized light, whereas the rest were taken with crossed polars.

~30 to 120 μm. Spinel exsolution, varying between 25 and 100 μm, in opx is rare. Some xenoliths also have well-developed large and discrete spinels occurring with garnets. A cumulus origin for such xenoliths is indicated (Keshav & Sen, 2003).

Phlogopite

Phlogopite is an accessory mineral in the garnet-bearing xenoliths. Four xenoliths containing phlogopite are described here. Primarily, phlogopite occurs as large, euhedral grains (77SL-62), ranging in size between ~0·2 and 0·6 mm across (Fig. 3g). In some cases, phlogopite has a sharp contact with the neighboring cpx. Phlogopite veins (~200–600 μm) also occur in one xenolith (114923-158; Fig. 3h). We suggest that the vein-forming phlogopite intruded the host garnet clinopyroxenite and therefore is 'secondary', although it is still of magmatic origin. Discrete phlogopite crystals with sharp contacts with other silicate minerals may have formed more or less simultaneously with the other silicates, and could be primary. Sen (1988) used compositional arguments to suggest a primary origin for discrete phlogopites in the Hawaiian garnet clinopyroxenites. However, as mentioned below, the earlier view on the primary nature of phlogopite by Sen (1988) does not seem to be correct.

Ilmenite

Ilmenite occurs as an exsolved phase in cpx and also as a large discrete phase. Exsolved ilmenite in cpx ranges from being irregular (~40 μm) to very fine-grained lamellae (<25 μm). In some xenoliths (114954-20A), it is difficult to determine if ilmenite is an inclusion or an exsolved phase in cpx. Large (150–500 μm) ilmenite is commonly subhedral, and is in physical contact either with large cpx or garnet.

One xenolith (77SL-10) has lamellae of ilmenite in the host cpx, a texture that has been widely reported from megacrysts in kimberlites (Boyd & Nixon, 1973; Gurney *et al.*, 1973). This type of texture has been variously interpreted as the result of exsolution (Dawson & Reid, 1970), decomposition of a high-pressure titanium garnet (Ringwood & Lovering, 1970), eutectic crystallization (Boyd, 1971; Gurney *et al.*, 1973; Wyatt, 1977), or metasomatic replacement (Haggerty, 1991). The origin(s) of the coherent ilmenite lamellae in the host cpx at Salt Lake Crater remains inconclusive (S. E. Haggerty, personal communication, 2003).

ANALYTICAL TECHNIQUES

Analyses of individual minerals were performed with an automated electron microprobe (JEOL SuperProbe, JSM 8900R) equipped with five wavelength-dispersive spectrometers at the Florida Center for Analytical Electron Microscopy (FCAEM), FIU. An energy-dispersive spectrometer (EDS) was used for reconnaissance work, prior to quantitative analyses; all analyses reported here were made using the wavelength-dispersive spectrometers, which are equipped with crystals of LDE2, TAP, LIF, PETJ, LEDH2, TAPH, LIFH, and PETH. The accelerating voltage was 15 kV, and the beam current was 20 nA at the Faraday cup. The beam diameter was 1–2 μm and all analyses were performed in a fixed spot mode. The on-peak time was 10–20 s for major elements (Mg, Al, Ca, Fe, and Si) and 30–60 s for minor elements (Ti, K, Cr, and Mn), except for Na (10 s), for both standards and unknowns, and half the on-peak time for the high and low side background for the elements mentioned. A combination of natural and synthetic oxides and silicates were used as standards. Mg, Al, Si, Fe, and Ca were measured using pyrope garnet, enstatite, olivine, and diopside. Mn, K, Ti, Cr, and Na were measured using rhodonite, sanidine, rutile, chromium oxide, and albite standards supplied by Structured Probe Inc (SPI). Raw data were reduced using CITZAF. Uncertainties for major (≥5%) and minor (≤5%) oxides analyzed by microprobe are better than 2% and 5% of the quoted values, respectively.

MINERAL CHEMISTRY

Major element composition data for the minerals in the SLC xenoliths are presented in Tables 1–7. Rare chemical zoning is limited to spinel and opx that occur as breakdown products around large garnet grains. Compositional heterogeneity is more pronounced in large opx crystals. In individual thin sections, garnet, cpx, and olivine grains are homogeneous; however, cpx and garnet of different composition are present in some rare xenoliths. We briefly describe the major element chemistry of individual minerals in the following sub-sections.

Olivine

Olivine in the xenoliths is unzoned. Also, there is no compositional difference between the large (deformed or undeformed) discrete grains and small neoblasts in the same xenolith, or the olivine forming inclusions in cpx in the same xenolith (Table 1). Olivine compositions in garnet-bearing xenoliths range from ~Fo_{71} to ~Fo_{85} (Fo, forsterite content, or molar Mg-number; Fig. 4; Table 1) and include significantly more Fe-rich compositions than those in the spinel lherzolites (Fo_{88-92}) from Salt Lake Crater (Sen, 1988). Previous studies on a smaller suite of garnet-bearing xenoliths at Salt Lake Crater found a small range in the Fo contents (81–84; Fig. 4; Sen, 1987, 1988; Sen & Jones, 1990; Sen & Leeman, 1991). The CaO content of olivines varies from a low of 0·00 to a high of 0·21 wt % (average ~0·08 wt %), and does not correlate with Fo content. The concentrations of Cr_2O_3 and TiO_2 vary from 0·00–0·05 wt % and 0·00–0·04-wt %, respectively.

Some xenoliths require special mention. Sample 77SL-62 contains two distinct olivine compositions, Fo_{82} and Fo_{85} (Table 1). On the basis of K_d $(Mg/Fe)^{cpx/gt}$ (Walter, 1998), olivine of composition Fo_{82} appears to be in Mg-number equilibrium with the large cpx and garnet in the same xenolith. The olivine with the higher Fo content appears to be a xenocryst. Samples 114954-20A and 115954-20B have olivine occurring as an inclusion in a large cpx and also as a large, discrete phase. The Fo content of olivines in both xenoliths is almost identical (Table 1).

The relatively high Fe/Mg (low Mg-number) of olivine in these xenoliths precludes them from being products of melt extraction (restites). Their similarity to olivine phenocrysts in Hawaiian basalts [Fodor *et al.*, 1977; Basaltic Volcanism Study Project (BSVP), 1981; Baker *et al.*, 1996; Garcia, 1996; Frey *et al.*, 2000] suggests that the olivines in SLC xenoliths are of 'cumulus' (*sensu lato*) origin.

Clinopyroxene

Individual cpx grains are unzoned. In some rare xenoliths, compositionally distinct kinds of cpx also occur (Table 2). Post-exsolution cpx is a low-Cr_2O_3 (0·01–0·93 wt %), high-Na_2O (1·18–3·20 wt%),

Table 1: Major element composition of olivines

Sample no.:	1	1	2	3	4	4	5	5	6	7	8	9	10	11	12	13
Type:	Inc	P	P	P	P	Inc	Inc	P	P	P	P	P	P	P	P	P
SiO_2	39·80	39·69	39·94	39·42	38·84	38·40	39·26	38·56	38·70	39·13	39·83	38·43	39·88	39·50	39·88	39·69
TiO_2	0·00	0·00	0·01	0·04	0·04	0·00	0·02	0·03	0·00	0·02	0·00	0·00	0·00	0·00	0·00	0·00
Al_2O_3	0·05	0·01	0·02	0·01	0·04	0·01	0·01	0·01	0·01	0·02	0·00	0·00	0·01	0·00	0·01	0·01
Cr_2O_3	0·05	0·00	0·00	0·00	0·00	0·00	0·00	0·00	0·05	0·01	0·00	0·01	0·01	0·01	0·00	0·00
FeO*	14·75	15·05	16·22	23·30	23·23	22·45	23·00	23·09	23·00	21·12	17·61	23·20	15·97	15·91	16·69	15·78
MnO	0·17	0·15	0·16	0·10	0·17	0·17	0·00	0·00	0·15	0·15	0·00	0·18	0·07	0·13	0·09	0·07
MgO	43·9	44·44	43·67	37·48	39·05	37·27	39·70	39·39	38·20	39·99	42·54	37·40	43·45	43·50	43·11	43·39
CaO	0·08	0·06	0·03	0·21	0·04	0·05	0·05	0·15	0·07	0·06	0·04	0·04	0·06	0·06	0·07	0·04
Na_2O	0·02	0·03	0·00	0·04	0·01	0·01	0·00	0·00	0·00	0·03	0·00	0·00	0·01	0·01	0·01	0·01
K_2O	0·00	0·00	0·00	0·00	0·00	0·00	0·00	0·00	0·00	0·00	0·00	0·00	0·00	0·00	0·00	0·00
Sum	98·83	99·43	100·08	99·24	101·1	99·05	101·03	100·20	100·14	100·53	99·46	99·28	99·49	98·68	99·49	99·02
Si	1·009	1·002	1·006	1·006	0·998	1·008	1·009	1·006	1·006	1·005	1·006	1·009	1·009	1·006	1·007	1·008
Ti	0·000	0·000	0·000	0·000	0·000	0·000	0·000	0·000	0·000	0·000	0·000	0·000	0·000	0·000	0·000	0·000
Al(IV)	0·000	0·000	0·000	0·000	0·000	0·000	0·000	0·000	0·000	0·000	0·000	0·000	0·000	0·000	0·000	0·000
Al(VI)	0·000	0·000	0·000	0·000	0·000	0·000	0·000	0·000	0·000	0·000	0·000	0·000	0·000	0·000	0·000	0·000
Cr	0·001	0·000	0·000	0·001	0·000	0·000	0·000	0·000	0·000	0·001	0·000	0·000	0·000	0·000	0·000	0·000
Fe	0·313	0·317	0·341	0·354	0·499	0·492	0·494	0·521	0·500	0·453	0·427	0·509	0·338	0·329	0·391	0·335
Mn	0·003	0·003	0·003	0·002	0·003	0·003	—	—	0·003	0·003	—	0·004	0·001	0·002	0·001	0·001
Mg	1·660	1·672	1·640	1·630	1·497	1·496	1·483	1·460	1·480	1·530	1·558	1·464	1·639	1·652	1·588	1·643
Ca	0·002	0·001	—	0·005	0·001	0·001	0·001	0·004	0·001	0·001	0·001	0·001	0·001	0·001	0·002	0·001
Na	0·000	0·000	0·000	0·000	0·000	0·000	0·000	0·000	0·000	0·000	0·000	0·000	0·000	0·000	0·000	0·000
K	0·000	0·000	0·000	0·000	0·000	0·000	0·000	0·000	0·000	0·000	0·000	0·000	0·000	0·000	0·000	0·000
O	4	4	4	4	4	4	4	4	4	4	4	4	4	4	4	4
Sum	2·990	2·997	2·993	2·993	3·001	2·992	2·989	2·993	2·993	2·996	2·994	2·990	2·990	2·993	2·992	2·991
Fo	84·13	84·02	82·75	73·68	74·97	75·08	75·98	75·71	74·74	77·13	81·28	74·17	82·90	82·52	82·19	83·04

Sample no.:	14	15	16	17	18	19	19	19	20	21	22	22
Type:	P	P	P	P	P	P	V	Inc	P	P	P1	P2
SiO_2	38·60	39·31	38·61	39·52	38·35	39·89	40·12	39·90	39·56	39·84	39·80	39·40
TiO_2	0·00	0·00	0·01	0·00	0·01	0·00	0·00	0·00	0·01	0·00	0·00	0·00
Al_2O_3	0·00	0·02	0·01	0·01	0·02	0·01	0·01	0·00	0·03	0·00	0·01	0·01
Cr_2O_3	0·02	0·00	0·00	0·00	0·00	0·00	0·04	0·00	0·02	0·01	0·05	0·01
FeO*	23·12	17·36	25·06	15·93	23·70	15·92	16·36	16·72	15·67	17·50	16·78	14·91
MnO	0·08	0·12	0·14	0·00	0·15	0·00	0·00	0·00	0·15	0·17	0·15	0·11
MgO	39·37	42·81	36·94	43·34	37·52	43·47	43·63	43·50	43·45	42·45	43·05	44·92
CaO	0·11	0·06	0·15	0·05	0·06	0·08	0·00	0·06	0·08	0·07	0·06	0·06
Na_2O	0·00	0·00	0·04	0·00	0·03	0·00	0·00	0·01	0·04	0·01	0·00	0·03
K_2O	0·00	0·00	0·00	0·00	0·00	0·00	0·00	0·00	0·00	0·00	0·00	0·00
Sum	100·01	99·73	100·98	98·87	99·81	99·81	100·24	100·23	99·01	100·09	99·88	99·46
Si	1·010	1·000	1·004	1·006	1·004	1·005	1·009	1·002	1·006	1·009	1·007	0·994
Ti	0·000	0·000	0·000	0·000	0·000	0·000	0·000	0·000	0·000	0·000	0·000	0·000
Al(IV)	0·000	0·000	0·000	0·000	0·000	0·000	0·000	0·000	0·000	0·000	0·000	0·000
Al(VI)	0·000	0·000	0·000	0·000	0·000	0·000	0·000	0·000	0·000	0·000	0·000	0·000
Cr	0·001	0·000	0·000	0·000	0·000	0·000	0·000	0·000	0·000	0·000	0·000	0·000
Fe	0·357	0·369	0·545	0·339	0·519	0·348	0·344	0·352	0·333	0·370	0·355	0·314
Mn	0·001	0·002	0·003	—	0·003	—	—	—	0·003	0·003	0·003	0·002
Mg	1·615	1·624	1·432	1·645	1·465	1·638	1·635	1·634	1·647	1·603	1·625	1·690
Ca	0·002	0·001	0·004	—	0·001	—	0·001	0·001	0·002	0·002	0·001	0·001
Na	0·000	0·000	0·000	0·000	0·000	0·000	0·000	0·000	0·000	0·000	0·000	0·000
K	0·000	0·000	0·000	0·000	0·000	0·000	0·000	0·000	0·000	0·000	0·000	0·000
O	4	4	4	4	4	4	4	4	4	4	4	4
Sum	2·990	2·999	2·999	2·993	2·995	2·994	2·991	2·994	2·994	2·991	2·992	3·005
Fo	75·97	81·46	72·42	82·90	73·82	82·96	82·61	82·24	83·16	81·21	82·04	85·51

Inc, inclusion; V, vein; P, primary.
*Total Fe given as FeO.

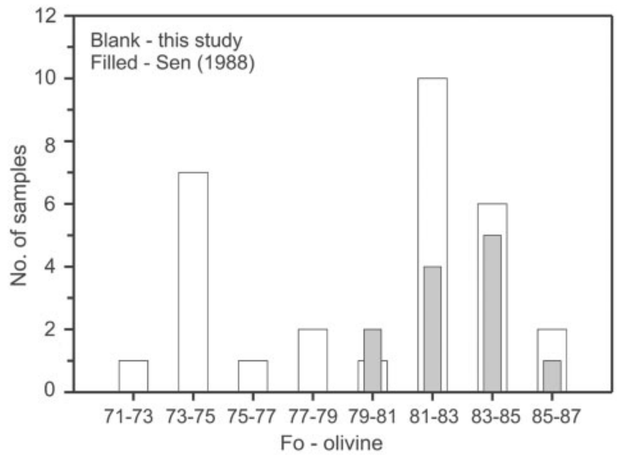

Fig. 4. Range of forsterite content of olivines [Fo or molar Mg-number = Mg/(Mg + Fe)] in Salt Lake Crater garnet pyroxenites. (See text for further details.)

high-Al_2O_3 (5·73–8·29 wt %), and high-TiO_2 (0·69–1·26 wt %) type. The Mg-number of this cpx varies between 71 and 86, a range that is virtually identical to that of the large olivines. Bizimis *et al.* (2005*c*) reported Mg-number of cpx as low as 68 in some garnet-pyroxenite xenoliths from Salt Lake Crater. The range of chemistry of large cpx grains is shown in Fig. 5a–c; this is much wider than that reported by Sen (1988).

The projected compositions of these clinopyroxenes range from $Wo_{41}En_{43}Fs_{16}$ to $Wo_{46}En_{45}Fs_{9}$ and $Jd_{13}Di_{38}Hy_{49}$ to $Jd_{21}Di_{36}Hy_{43}$ (Table 2), and partially overlap the composition of cpx phenocrysts in Hawaiian tholeiites and alkalic lavas (Fig. 6; Fodor *et al.*, 1975; BVSP, 1981; Frey *et al.*, 2000). In terms of Al_2O_3 (Fig. 7), this overlap is virtually absent; however, in TiO_2–Mg-number space (Fig. 8), cpx in the xenoliths are compositionally similar to the cpx phenocrysts in Hawaiian tholeiites and

Table 2: Major element composition of clinopyroxenes

Sample no.:	1	1	1	1	2	2	2	3	3	4
Type:	P	H	R	E	P	H	R	H	R	H
SiO_2	51·49	51·58	51·66	51·38	51·76	50·87	46·89	51·21	50·44	50·91
TiO_2	0·77	0·76	0·73	0·80	0·71	0·95	0·82	1·14	1·09	1·08
Al_2O_3	7·40	8·12	8·01	7·66	6·52	7·44	12·66	7·23	8·46	6·85
Cr_2O_3	0·42	0·21	0·20	0·43	0·15	0·15	0·22	0·03	0·03	0·05
FeO*	4·63	4·71	4·89	4·81	5·38	5·42	7·26	8·24	8·83	7·40
MnO	0·11	0·11	0·11	0·10	0·08	0·13	0·13	0·08	0·10	0·08
MgO	13·64	13·51	14·01	13·39	14·13	14·09	15·63	12·66	12·89	12·13
CaO	18·62	18·38	17·67	18·34	19·43	19·35	15·56	16·76	15·80	17·71
Na_2O	2·03	1·98	1·90	1·95	1·66	1·73	1·53	2·29	2·11	2·39
K_2O	0·00	0·00	0·00	0·01	0·01	0·00	0·00	0·00	0·00	0·00
Sum	98·97	99·24	99·22	98·92	99·85	99·84	100·04	99·67	99·79	99·29
Si	1·885	1·881	1·881	1·883	1·889	1·860	1·687	1·884	1·854	1·884
Ti	0·021	0·020	0·020	0·022	0·019	0·026	0·022	0·031	0·030	0·030
Al(IV)	0·114	0·118	0·118	0·116	0·110	0·139	0·312	0·115	0·145	0·115
Al(VI)	0·205	0·230	0·226	0·214	0·169	0·181	0·234	0·198	0·221	0·184
Cr	0·012	0·006	0·005	0·012	0·004	0·004	0·009	—	—	0·001
Fe	0·137	0·143	0·149	0·147	0·164	0·141	0·168	0·253	0·271	0·202
Mn	0·007	0·003	0·003	0·003	0·002	0·004	0·004	0·002	0·003	0·002
Mg	0·744	0·727	0·760	0·731	0·768	0·743	0·853	0·694	0·706	0·680
Ca	0·730	0·718	0·689	0·720	0·760	0·758	0·610	0·661	0·622	0·720
Na	0·144	0·140	0·134	0139	0·117	0·134	0·108	0·163	0·150	0·171
K	0·000	0·000	0·000	0·000	0·000	0·000	0·000	0·000	0·000	0·000
O	6	6	6	6	6	6	6	6	6	6
Sum	3·999	3·990	3·990	3·992	4·007	4·000	4·018	4·007	4·007	3·994
Wo	45·30	45·18	43·12	45·03	44·89	46·15	37·40	41·07	38·88	44·95
En	46·17	45·78	47·55	45·74	45·40	45·24	52·28	43·16	44·14	42·42
Fs	8·51	9·03	9·31	9·22	9·69	8·59	10·30	15·76	16·97	12·61
Jd	18·28	19·11	18·62	18·60	14·69	16·31	17·73	18·40	18·27	18·19
Di	36·94	36·46	35·02	36·58	38·24	38·53	30·69	33·46	31·48	36·71
Hy	44·76	44·41	46·35	44·41	47·06	45·15	51·56	48·13	49·64	45·09
Mg-no.	83·42	83·51	83·61	83·22	82·39	82·41	83·52	73·24	72·62	74·49
Cr-no.	5·58	2·56	2·55	5·57	2·54	2·37	3·89	0·47	0·42	0·79

(continued)

Table 2: Continued

Sample. no.:	4	5	5	6	6	7	7	8	8	9
Type:	R	H	R	H	R	H	R	H	R	H
SiO_2	50·54	51·09	48·46	50·87	48·77	50·89	49·39	51·44	50·92	50·67
TiO_2	1·09	0·13	0·96	0·81	1·20	0·78	0·70	1·26	1·21	0·85
Al_2O_3	7·49	6·52	10·60	7·55	8·34	7·07	9·44	6·96	7·77	7·20
Cr_2O_3	0·05	0·04	0·04	0·07	0·07	0·01	0·01	0·12	0·12	0·01
FeO*	7·74	7·06	8·91	7·45	9·50	6·57	7·70	5·60	6·00	7·68
MnO	0·10	0·00	0·09	0·10	0·09	0·07	0·11	0·08	0·10	0·08
MgO	12·42	12·49	13·28	12·11	13·08	12·81	13·35	13·39	13·52	11·44
CaO	17·65	17·69	14·54	17·66	15·58	17·94	15·97	19·10	18·39	17·53
Na_2O	2·29	2·20	1·66	1·98	2·25	2·14	1·82	1·71	1·63	2·66
K_2O	0·00	0·00	0·00	0·00	0·00	0·00	0·00	0·00	0·00	0·00
Sum	99·35	98·22	98·57	98·61	98·92	98·31	98·53	99·70	99·71	98·12
Si	1·869	1·903	1·798	1·888	1·821	1·891	1·830	1·880	1·861	1·896
Ti	0·029	0·031	0·026	0·022	0·033	0·022	0·019	0·034	0·033	0·023
Al(IV)	0·130	0·096	0·201	0·111	0·178	0·108	0·169	0·119	0·138	0·103
Al(VI)	0·196	0·189	0·262	0·219	0·189	0·201	0·243	0·180	0·196	0·214
Cr	0·001	0·001	0·001	0·001	0·002	—	—	0·003	0·003	—
Fe	0·211	0·219	0·276	0·231	0·237	0·204	0·238	0·171	0·183	0·223
Mn	0·003	—	0·003	0·003	0·003	0·002	0·003	0·002	0·003	0·002
Mg	0·685	0·693	0·734	0·670	0·728	0·709	0·737	0·729	0·736	0·638
Ca	0·699	0·706	0·578	0·702	0·623	0·714	0·634	0·748	0·720	0·703
Na	0·164	0·158	0·119	0·142	0·163	0·154	0·130	0·121	0·115	0·193
K	0·000	0·000	0·000	0·000	0·000	0·000	0·000	0·000	0·000	0·000
O	6	6	6	6	6	6	6	6	6	6
Sum	3·993	4·000	4·002	3·993	4·000	4·008	4·006	3·993	3·994	3·992
Wo	43·83	43·60	36·37	43·79	39·23	43·86	39·36	45·37	43·90	44·492
En	42·01	42·81	46·21	41·78	45·81	43·59	45·80	44·24	44·90	40·78
Fs	13·25	13·58	17·41	14·42	14·94	12·54	14·83	10·38	11·18	14·29
Jd	18·47	17·75	19·38	18·44	18·23	17·90	18·83	15·63	16·12	20·65
Di	35·66	35·85	29·26	35·64	32·02	35·95	31·87	38·21	36·75	35·58
Hy	45·86	46·38	51·35	45·90	49·74	46·13	49·28	46·15	47·11	43·75
Mg-no.	73·89	75·91	74·63	74·33	75·29	77·65	76·81	80·99	80·05	74·04
Cr-no.	0·75	0·61	0·52	0·52	0·64	0·22	0·21	2·01	1·86	0·13

(continued)

alkalic lavas (Fodor *et al.*, 1975; BVSP, 1981; Frey *et al.*, 2000). Compared with the compositions of cpx phenocrysts in Hawaiian lavas (Fodor *et al.*, 1975; BVSP, 1981; Frey *et al.*, 2000), the cpx in the xenoliths is much more sodic (Fig. 9). The cpx compositions in the SLC xenoliths are very different from those in abyssal peridotites (Johnson & Dick, 1992; Johnson *et al.*, 1990).

With a few exceptions, the neoblast cpx is compositionally indistinguishable from the large cpx in the same xenolith (Table 2). Neoblast cpx does not show much compositional variation, with compositions averaging at $\sim Wo_{44}En_{46}Fs_{10}$ and $Jd_{17}Di_{37}Hy_{46}$ and Mg-number of 83 (Table 2). Where the exsolved phase(s) were thick enough to permit compositional analysis, 'original' (host + exsolution) cpx was reconstructed from the composition of exsolved and host phases. This 'original' cpx is broadly aluminous sub-augitic in composition (Table 2).

Salt Lake Crater clinopyroxenes, when compared with clinopyroxenes in eclogite or garnet-bearing pyroxenites from kimberlites (Snyder *et al.*, 1997, and references therein; S. E. Haggerty, personal communication, 2003), form a relatively tight cluster in the hypersthene–diopside–jadeite (Hy–Di–Jd) ternary (Fig. 10). In this respect, these Salt Lake Crater clinopyroxenes are similar to those in garnet

Table 2: Continued

Sample no.:	10	10	10	11	11	12	13	13	14	14
Type:	H	R	E	P	E	P	H	R	P1	P2
SiO_2	51·80	52·06	51·66	52·20	51·55	51·45	52·55	51·26	52·41	51·99
TiO_2	0·77	0·71	0·85	0·63	0·75	0·72	0·69	0·64	0·90	0·68
Al_2O_3	7·58	7·58	7·25	6·47	7·45	6·39	6·22	6·65	7·86	6·20
Cr_2O_3	0·37	0·35	0·16	0·26	0·30	0·22	0·26	0·28	0·06	0·12
FeO*	4·96	5·48	5·43	5·24	5·18	6·10	4·98	5·57	7·00	5·80
MnO	0·09	0·09	0·11	0·07	0·09	0·06	0·07	0·08	0·09	0·12
MgO	13·87	15·56	13·92	13·97	13·80	14·26	14·24	15·75	12·14	14·21
CaO	17·83	15·96	17·66	18·33	18·21	17·46	19·45	17·39	14·43	18·36
Na_2O	1·97	1·77	1·90	1·88	1·95	2·19	1·54	1·38	3·20	1·75
K_2O	0·00	0·00	0·00	0·00	0·00	0·00	0·00	0·00	0·00	0·00
Sum	99·29	99·36	98·97	99·10	99·32	98·89	99·04	99·05	98·11	99·23
Si	1·888	1·889	1·892	1·911	1·883	1·896	1·894	1·877	1·932	1·906
Ti	0·021	0·019	0·023	0·017	0·020	0·020	0·019	0·017	0·024	0·018
Al(IV)	0·111	0·110	0·107	0·088	0·116	0·103	0·105	0·122	0·067	0·093
Al(VI)	0·214	0·204	0·206	0·190	0·204	0·173	0·164	0·165	0·273	0·174
Cr	0·010	0·010	0·004	0·007	0·008	0·006	0·007	0·008	0·002	0·007
Fe	0·151	0·166	0·166	0·160	0·158	0·167	0·153	0·170	0·215	0·177
Mn	0·002	0·003	0·003	0·002	0·003	0·002	0·002	0·002	0·003	0·003
Mg	0·754	0·842	0·759	0·762	0·752	0·783	0·780	0·860	0·667	0·776
Ca	0·696	0·620	0·693	0·719	0·713	0·689	0·765	0·682	0·570	0·721
Na	0·139	0·124	0·135	0·133	0·138	0·156	0·110	0·098	0·228	0·124
K	0·000	0·000	0·000	0·000	0·000	0·000	0·000	0·000	0·000	0·000
O	6	6	6	6	6	6	6	6	6	6
Sum	3·991	3·991	3·992	3·994	3·999	3·994	4·002	4·006	3·982	4·001
Wo	43·48	38·09	46·90	43·79	43·92	42·04	45·07	39·84	39·22	43·04
En	47·06	51·68	47·92	46·41	46·32	47·76	45·90	50·18	45·92	46·33
Fs	9·45	10·21	10·27	9·78	9·75	10·19	9·02	9·96	14·85	10·61
Jd	18·53	17·20	17·58	16·79	17·79	17·01	14·20	13·68	25·72	15·26
Di	35·35	31·48	35·19	36·38	36·03	34·84	38·61	34·34	29·07	36·39
Hy	46·10	51·31	42·21	46·81	46·16	48·14	47·17	51·97	45·20	48·34
Mg-no.	83·27	83·50	82·03	82·58	82·60	83·40	83·57	83·43	75·56	81·36
Cr-no.	4·82	4·76	2·24	3·80	4·12	3·63	4·40	4·78	0·72	1·95

Sample no.:	15	15	16	16	17	17	17	18	18	19
Type:	H	R	H	R	H	R	E	H	R	E
SiO_2	51·20	48·32	51·39	46·71	50·10	50·28	50·22	50·13	49·11	50·20
TiO_2	1·04	0·90	1·15	1·68	0·76	0·67	0·63	0·44	0·40	0·95
Al_2O_3	7·64	9·92	7·51	8·42	7·82	7·86	8·20	7·79	9·23	8·04
Cr_2O_3	0·03	0·02	0·08	0·01	0·28	0·26	0·25	0·01	0·01	0·29
FeO*	5·77	6·43	7·88	10·23	5·63	5·96	5·59	7·47	7·98	5·32
MnO	0·09	0·05	0·09	0·06	0·00	0·00	0·00	0·06	0·09	0·00
MgO	13·29	13·56	12·10	11·43	13·31	15·76	13·26	12·21	12·01	13·73
CaO	18·45	17·66	16·59	17·14	18·33	15·78	18·38	19·40	18·02	18·10
Na_2O	2·01	1·97	2·46	2·39	2·00	1·71	1·98	2·01	1·81	1·98
K_2O	0·00	0·00	0·00	0·00	0·00	0·00	0·00	0·00	0·00	0·00
Sum	98·55	98·87	99·30	98·12	98·11	98·31	98·52	98·66	98·68	98·63
Si	1·859	1·788	1·894	1·782	1·858	1·852	1·857	1·868	1·831	1·852
Ti	0·028	0·025	0·032	0·082	0·021	0·018	0·017	0·012	0·011	0·026
Al(IV)	0·140	0·211	0·105	0·217	0·141	0·147	0·142	0·131	0·168	0·147
Al(VI)	0·193	0·222	0·220	0·161	0·200	0·194	0·214	0·211	0·237	0·201
Cr	—	—	0·002	0·001	0·008	0·007	0·007	—	—	0·008
Fe	0·162	0·161	0·243	0·244	0·139	0·170	0·155	0·191	0·222	0·146
Mn	0·002	0·001	0·002	0·002	—	—	—	—	—	—
Mg	0·734	0·748	0·664	0·650	0·753	0·865	0·731	0·655	0·667	0·754
Ca	0·732	0·700	0·655	0·701	0·728	0·622	0·728	0·774	0·720	0·715
Na	0·144	0·141	0·176	0·177	0·143	0·122	0·141	0·145	0·131	0·141
K	0·000	0·000	0·000	0·000	0·000	0·000	0·000	0·000	0·000	0·000
O	6	6	6	6	6	6	6	6	6	6
Sum	3·996	3·995	3·997	3·992	3·996	3·997	3·995	3·993	3·992	3·995
Wo	44·96	43·49	41·91	43·91	44·94	37·56	45·11	47·76	44·74	44·27
En	45·05	46·45	42·52	40·74	46·45	52·18	45·20	40·40	41·45	46·69
Fs	9·97	10·04	15·55	15·33	8·59	10·25	9·60	11·83	13·80	9·03
Jd	17·19	18·44	20·31	17·51	17·87	16·37	18·39	18·00	18·62	17·89
Di	37·16	35·43	33·34	36·17	36·91	31·41	36·81	39·11	36·34	36·35
Hy	45·63	46·12	46·34	46·13	45·20	52·20	44·78	42·87	45·03	45·75
Mg-no.	81·86	82·21	73·21	72·64	82·47	83·57	82·50	74·21	75·28	83·79
Cr-no.	0·45	0·35	0·91	0·10	3·92	3·80	3·35	0·13	0·13	4·02

(continued)

Table 2: Continued

Sample no.:	19	19	20	20	20	21	22	22	22	23
Type:	H	R	H	R	E	P	P	H	R	P
SiO_2	50·73	51·03	51·61	51·84	52·03	51·42	50·49	51·68	49·45	51·13
TiO_2	0·83	0·75	0·68	0·63	0·65	0·59	0·69	0·75	0·65	1·13
Al_2O_3	7·46	7·23	7·09	6·93	6·24	7·73	9·00	7·26	9·29	7·24
Cr_2O_3	0·33	0·31	0·51	0·48	0·49	0·25	0·26	0·41	0·71	0·31
FeO^*	5·47	6·01	4·88	5·28	5·37	5·34	5·40	5·38	6·87	7·56
MnO	0·00	0·00	0·12	0·12	0·09	0·10	0·12	0·09	0·09	0·09
MgO	13·93	15·72	13·88	15·27	14·11	13·01	13·96	13·71	16·19	12·19
CaO	17·96	15·92	18·77	17·14	18·72	18·04	19·69	19·74	14·48	15·58
Na_2O	1·97	1·76	1·92	1·76	1·89	2·13	1·97	2·23	1·81	2·96
K_2O	0·00	0·00	0·00	0·00	0·00	0·00	0·00	0·00	0·00	0·00
Sum	98·70	98·76	99·48	99·50	99·59	98·74	99·01	99·49	99·59	98·44
Si	1·869	1·871	1·885	1·887	1·901	1·888	1·852	1·887	1·804	1·905
Ti	0·023	0·021	0·018	0·017	0·017	0·016	0·019	0·020	0·018	0·031
Al(IV)	0·130	0·128	0·114	0·112	0·098	0·111	0·147	0·112	0·195	0·094
Al(VI)	0·193	0·184	0·190	0·184	0·170	0·223	0·242	0·200	0·204	0·222
Cr	0·009	0·009	0·014	0·014	0·014	0·007	0·007	0·012	0·020	0·009
Fe	0·153	0·184	0·149	0·160	0·164	0·160	0·165	0·164	0·183	0·234
Mn	—	—	0·003	0·003	0·002	0·003	0·003	0·002	0·003	0·002
Mg	0·765	0·859	0·755	0·828	0·768	0·734	0·709	0·746	0·880	0·673
Ca	0·709	0·625	0·734	0·668	0·733	0·701	0·712	0·702	0·566	0·619
Na	0·141	0·125	0·136	0·124	0·133	0·152	0·140	0·158	0·128	0·212
K	0·000	0·000	0·000	0·000	0·000	0·000	0·000	0·000	0·000	0·000
O	6	6	6	6	6	6	6	6	6	6
Sum	3·996	4·009	4·004	4·002	4·005	4·000	3·999	4·008	3·996	4·006
Wo	43·58	37·49	44·81	40·33	44·00	43·93	44·86	43·53	34·73	42·78
En	47·00	51·46	46·08	49·95	46·13	45·99	44·67	46·27	54·01	46·56
Fs	9·41	11·04	9·10	9·70	9·85	10·06	10·45	10·18	11·25	10·65
Jd	17·47	16·03	17·22	16·27	16·04	19·33	19·68	18·65	17·77	23·45
Di	35·96	31·47	37·00	33·69	36·88	35·37	35·95	35·34	28·50	32·68
Hy	46·55	52·48	45·76	41·92	47·06	45·29	44·36	45·99	53·71	43·85
Mg-no.	83·31	82·33	83·50	83·73	82·50	81·18	81·99	81·96	82·74	74·18
Cr-no.	4·77	4·73	7·16	7·06	7·65	3·23	3·02	5·66	9·16	3·93

(continued)

pyroxenites (not shown in Fig. 10) from the Lherz Massif (Bodinier *et al.*, 1987) and a few xenoliths and megacrysts from the kimberlites in Canada (Kopylova *et al.*, 1999; Schmidberger & Francis, 1999). However, compared with the cpx in the SLC xenoliths, the cpx in the Canadian xenoliths and megacrysts is more Mg-rich, and is less aluminous, ferrous, and titaniferous. Also, the Salt Lake data seem to radiate from the Hy corner toward more diopsidic (Di) compositions (Fig. 10). This observation is in accord with high-pressure liquidus phase equilibrium experiments showing that with progressive crystallization at constant pressure, a melt precipitates more diopsidic cpx (Milholland & Presnall, 1998). Also shown in Fig. 10 are the compositions of cpx in eclogitic xenoliths (in kimberlites) from Yakutia (Russia) and South Africa. Besides being orthogonal to the cpx in the SLC xenoliths, cpx compositions in the eclogitic xenoliths show a marked enrichment in the jadeite component. On this basis, either different sources or P–T conditions (coupled with possibly different melts) appear to be involved in the genesis of these xenoliths. Additionally, there does not seem to be an obvious relation between the wollastonite component of the host cpx and its Mg-number in the SLC xenoliths (Fig. 11).

Table 2: Continued

Sample no.:	24	24	24	25	26	27	27	28	28
Type:	H	E1	E2	P	P	H	R	H	R
SiO_2	50·88	52·29	51·18	50·90	50·82	49·16	45·24	51·53	50·71
TiO_2	0·75	0·72	0·81	0·87	1·29	1·26	1·93	0·82	0·73
Al_2O_3	7·29	6·41	8·29	7·32	7·80	8·29	8·50	5·73	7·35
Cr_2O_3	0·44	0·49	0·54	0·12	0·07	0·01	0·02	0·15	0·14
FeO*	5·28	5·15	5·08	8·14	7·41	6·92	12·21	5·31	6·21
MnO	0·03	0·10	0·09	0·08	0·05	0·06	0·07	0·08	0·11
MgO	14·21	14·11	13·63	12·28	12·21	11·77	11·23	14·29	15·35
CaO	18·41	18·44	18·15	16·03	17·48	18·05	16·60	19·10	16·77
Na_2O	2·05	1·88	1·98	2·37	2·36	2·52	2·30	1·49	1·27
K_2O	0·01	0·00	0·00	0·00	0·00	0·00	0·00	0·01	0·00
Sum	98·66	99·33	99·78	98·06	99·53	98·08	98·16	98·55	98·71
Si	1·876	1·909	1·861	1·899	1·871	1·842	1·742	1·904	1·865
Ti	0·020	0·019	0·022	0·024	0·035	0·035	0·056	0·022	0·020
Al(IV)	0·123	0·090	0·138	0·100	0·128	0·157	0·254	0·095	0·134
Al(VI)	0·194	0·185	0·217	0·218	0·209	0·209	0·132	0·154	0·184
Cr	0·013	0·014	0·015	0·003	0·002	—	—	0·004	0·004
Fe	0·148	0·157	0·154	0·254	0·228	0·194	0·306	0·164	0·191
Mn	0·001	0·003	0·002	0·002	0·001	0·002	0·002	0·002	0·003
Mg	0·746	0·768	0·739	0·683	0·669	0·657	0·646	0·787	0·841
Ca	0·727	0·710	0·707	0·641	0·689	0·724	0·686	0·756	0·661
Na	0·147	0·133	0·139	0·172	0·169	0·182	0·173	0·107	0·091
K	0·000	0·000	0·000	0·000	0·000	0·000	0·000	0·000	0·000
O	6	6	6	6	6	6	6	6	6
Sum	3·999	3·992	3·998	4·001	4·007	4·001	3·999	3·998	3·998
Wo	44·93	43·41	44·18	40·61	43·43	46·09	42·16	44·38	39·02
En	46·12	46·96	46·15	43·28	42·18	41·80	39·68	46·10	49·69
Fs	8·94	9·62	9·65	16·10	14·37	12·10	18·15	9·61	11·27
Jd	17·94	16·90	18·85	19·95	19·34	19·96	15·82	13·44	14·15
Di	36·84	35·99	35·79	32·45	34·99	36·84	35·44	38·26	33·42
Hy	45·20	47·09	45·35	34·72	45·66	43·19	48·73	48·28	52·41
Mg-no.	82·29	82·99	82·70	72·88	74·57	77·55	68·60	82·73	81·98
Cr-no.	6·33	7·19	6·72	1·69	1·04	0·15	0·15	2·82	2·30

P, no exsolution; E, exsolved in opx; H, host; R, reconstructed; Ps, compositionally distinct cpx in the same xenolith.
*Total Fe given as FeO.

Orthopyroxene

In contrast to olivine and cpx, compositional heterogeneity is more pronounced in opx crystals in individual xenoliths. The chemical compositions of the various petrographic types are reported in Table 3, and the range of chemical compositions is shown in Fig. 12a and b. The Mg-number of the large opx ranges between ~83 and 86. Bizimis *et al.* (2005*c*) reported a similar Mg-number range for opx, and also opx with the lowest Mg-number (~76) reported so far in the Salt Lake Crater garnet-pyroxenite literature. Neoblast opx also shows a similar range of Mg-number (~83–87), and has one of the lowest Al_2O_3 contents among all the opx types in the suite of xenoliths described here (Table 3).

Chemical differences between the neoblast and large opx are large and vary in individual xenoliths (Table 3), suggesting disequilibrium. This disequilibrium is most pronounced in terms of Mg-number and alumina content (Table 3). Sen (1988) and Sen & Jones (1990) also noted disequilibrium crystals of opx in some similar xenoliths and a rare garnet-dunite xenolith from Salt Lake Crater.

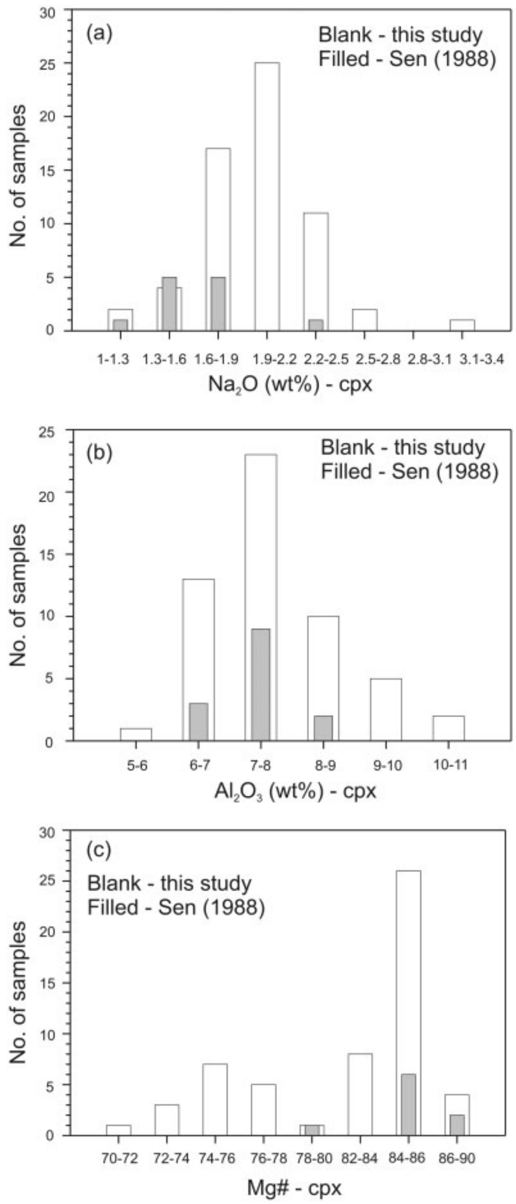

Fig. 5. Mineral chemistry of clinopyroxene in Salt Lake Crater garnet-pyroxenite xenoliths: (a) Na_2O (wt %); (b) Al_2O_3 (wt %); (c) molar Mg-number [Mg/(Mg + Fe)]. Host and other (reconstructed/without exsolution) cpx in the Al_2O_3 histogram are in the ~5–8 and >9 wt % Al_2O_3, respectively. Also, host cpx lies in the Mg-number range ~72–83. (See text for further explanation.)

The Mg-number and Al_2O_3 (wt %) of opx exsolved from cpx vary in the range of 81–85 and 3·7–5·7, respectively (Table 3). Exsolved opx appears to be in Mg-number equilibrium with its host cpx. The composition of orthopyroxene prior to exsolution of cpx ('original' opx) was reconstructed using the modal abundance and composition of host and lamellae, and its Mg-number ranges between ~86 and 88 (Table 3).

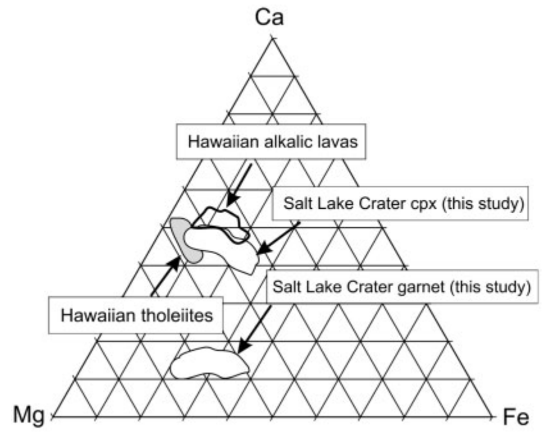

Fig. 6. Compositional projection of the Salt Lake Crater cpx and garnets in Ca–Mg–Fe ternary. Also shown for comparison are the compositions of the cpx phenocrysts in Hawaiian tholeiites and alkalic lavas (Fodor *et al.*, 1975; Clague *et al.*, 1980; Frey *et al.*, 2000).

Many xenoliths contain a highly aluminous and highly calcic type of opx. This occurs at the grain boundaries of large garnets and/or pleonaste spinels. Two or more kinds of highly aluminous opx are present in many xenoliths; however, some xenoliths (e.g. sample 114923-95) have only the highly aluminous variety. The Al_2O_3 content of this opx varies widely in a single xenolith and ranges between 9 and 15 wt % (Table 3). Similar opx has also been observed to occur in garnet-pyroxenite xenoliths from Kaula island in Hawaii (M. Bizimis, personal communication, 2006), and appears to be a metastable, melt-related product.

Garnet

Garnets in these xenoliths are homogeneous. All the petrographically distinct types are unzoned, and the compositions of these various types are given in Table 4.

Large garnets without a spinel core are dominantly pyropic and their molar pyrope and Mg-number vary in the range of 53–65 and 61–75 (Table 4), respectively. The Mg-number of garnets with a spinel core ranges between ~62 and 75 (Table 4). Compositionally, these garnets resemble the Cr-poor megacrystic garnets from Malaita (Delaney *et al.*, 1979) and Jagersfontein, South Africa (Hops *et al.*, 1989). Major-element variations in the large garnets are shown in Figs 6 and 13. The compositions of exsolved garnets in cpx are similar to those of large garnets with or without a spinel core (Table 4).

On the basis of the CaO–Cr_2O_3 empirical relation (Sobolev *et al.*, 1973), garnets in the SLC xenoliths form a relatively tight cluster in the websteritic field (Fig. 14a). In addition, in the pyrope–almandine–grossular (Py–Alm–Gr) ternary, the garnet compositions radiate from the Py corner toward the Alm apex (Fig. 14b).

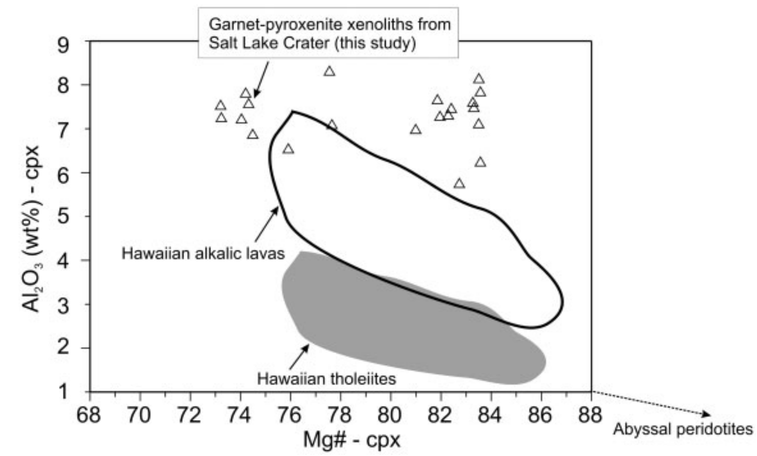

Fig. 7. Variation of Al_2O_3 vs Mg-number for garnet-pyroxenite cpx and comparison with phenocrysts in Hawaiian lavas and in abyssal peridotites (dotted line with an arrow; Johnson *et al.*, 1990; Johnson & Dick, 1992; data sources for Hawaiian lavas as in Fig. 6).

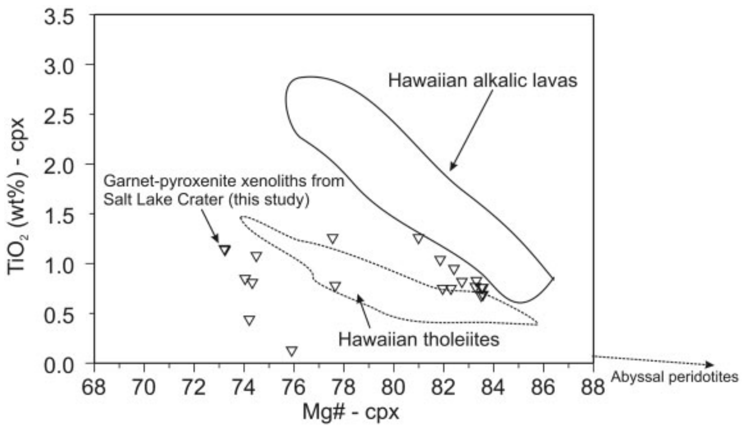

Fig. 8. Composition of cpx in the garnet-pyroxenite xenoliths in terms of their TiO_2 content and Mg-number. Also shown are compositions of the cpx phenocrysts in Hawaiian lavas (data sources as in Fig. 6) and the cpx compositional trend in abyssal peridotites (dotted line with an arrow; Johnson *et al.*, 1990; Johnson & Dick, 1992).

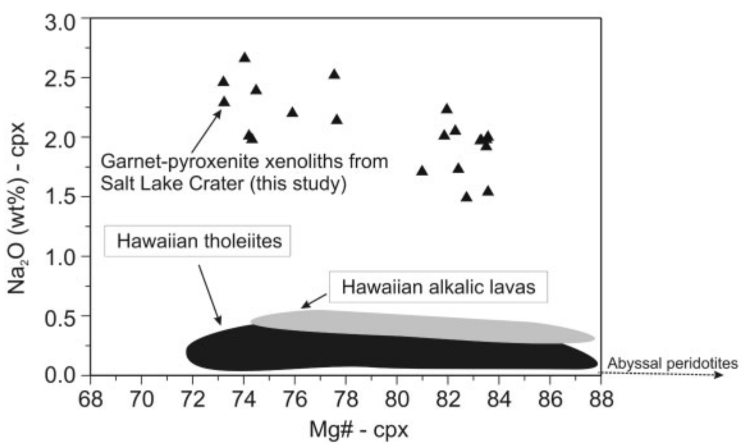

Fig. 9. Composition of cpx in the garnet-pyroxenite xenoliths in terms of their Na_2O content and Mg-number. Also shown are compositions of the cpx phenocrysts in Hawaiian lavas (data sources as in Fig. 6) and the cpx compositional trend in abyssal peridotites (dotted line with an arrow; Johnson *et al.*, 1990; Johnson & Dick, 1992).

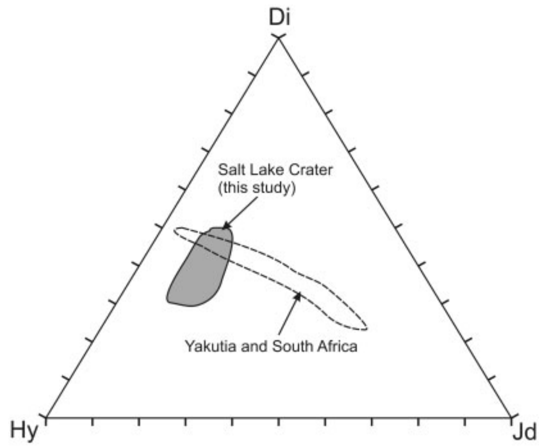

Fig. 10. Composition of cpx in the garnet-pyroxenite xenoliths in the hypersthene–diopside–jadeite (Hy–Di–Jd) ternary. Also shown are compositions of cpx in eclogites found as xenoliths in kimberlites from Yakutia, Russia, and South Africa (Snyder *et al.*, 1997, and references therein; S. E. Haggery, personal communication, 2003).

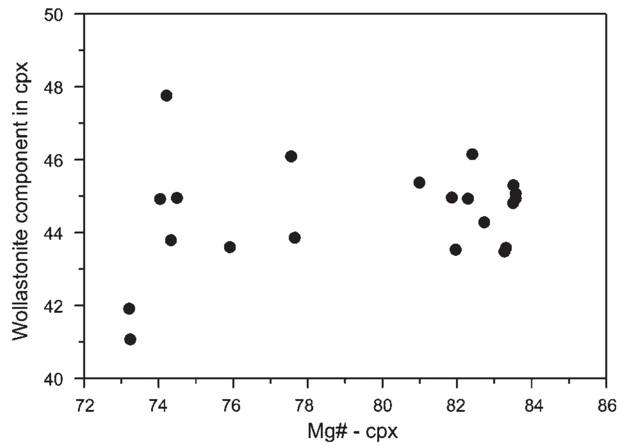

Fig. 11. Wollastonite component (mol %) vs Mg-number of cpx in the studied suite of xenoliths.

Table 3: Major element composition of orthopyroxenes

Sample no.:	1	1	1	1	2	2	2	3	3	3	6	6	8	9	9	9	10
Type:	P	H	R	E	P	E	Al	Al1	Al2	Al3	E	Al	P	P1	P2	Al	H
SiO_2	53·61	53·88	53·63	54·18	53·96	53·02	50·13	45·32	47·54	44·34	53·01	48·75	54·88	53·18	50·86	48·43	53·43
TiO_2	0·20	0·17	0·24	0·24	0·17	0·20	0·02	0·35	0·37	0·47	0·18	0·04	0·26	0·19	0·43	0·61	0·23
Al_2O_3	4·29	5·45	5·67	4·13	5·39	4·97	11·37	14·63	11·04	15·65	4·96	9·95	3·85	3·76	5·28	10·19	6·27
Cr_2O_3	0·19	0·22	0·24	0·10	0·19	0·03	0·09	0·03	0·03	0·04	0·02	0·06	0·06	0·03	0·00	0·17	0·10
FeO^*	9·01	9·28	8·83	10·61	9·31	14·69	10·52	15·88	15·56	15·87	14·71	15·51	11·61	13·54	17·78	11·28	10·21
MnO	0·00	0·16	0·15	0·14	0·16	0·16	0·35	0·31	0·46	0·31	0·17	0·25	0·12	0·17	0·37	0·44	0·19
MgO	30·42	29·25	27·66	29·35	29·37	26·58	26·13	20·73	19·84	20·78	26·30	22·95	28·75	26·44	23·39	20·76	28·09
CaO	0·73	0·69	2·46	0·79	0·74	0·71	1·50	2·15	4·04	1·72	0·72	1·94	0·71	0·77	1·71	1·74	0·83
Na_2O	0·13	0·16	0·32	0·12	0·09	0·13	0·00	0·00	0·04	0·00	0·16	0·06	0·07	0·12	0·04	0·01	0·14
K_2O	0·00	0·00	0·00	0·00	0·00	0·00	0·00	0·00	0·00	0·00	0·00	0·00	0·00	0·00	0·00	0·00	0·00
Sum	98·92	99·28	99·25	99·69	99·37	100·30	100·13	99·44	98·91	99·18	100·26	99·54	100·35	98·20	99·86	98·60	99·46
Si	1·901	1·883	1·856	1·889	1·885	1·838	1·709	1·529	1·606	1·500	1·834	1·667	1·907	1·869	1·758	1·646	1·854
Ti	0·005	0·004	0·006	0·005	0·006	0·005	0·000	0·009	0·009	0·011	0·004	0·001	0·006	0·005	0·011	0·015	0·006
Al(IV)	0·098	0·116	0·143	0·099	0·114	0·165	0·291	0·470	0·393	0·499	0·165	0·332	0·092	0·130	0·241	0·353	0·146
Al(VI)	0·081	0·108	0·087	0·071	0·109	0·036	0·166	0·112	0·044	0·124	0·036	0·068	0·064	0·025	0·024	0·054	0·108
Cr	0·005	0·006	0·006	0·002	0·004	0·000	0·002	0·000	0·000	0·001	0·001	0·001	0·001	0·001	—	0·004	0·002
Fe	0·277	0·271	0·243	0·310	0·276	0·354	0·239	0·263	0·266	0·265	0·362	0·304	0·337	0·353	0·364	0·335	0·233
Mn	—	0·003	0·002	0·004	0·002	0·003	0·003	0·005	0·006	0·004	—	0·003	0·002	0·004	0·002	0·003	0·003
Mg	1·598	1·575	1·559	1·580	1·573	1·543	1·536	1·521	1·522	1·525	1·559	1·541	1·565	1·584	1·558	1·531	1·568
Ca	0·027	0·026	0·091	0·029	0·027	0·026	0·054	0·078	0·146	0·062	0·026	0·071	0·026	0·125	0·063	0·063	0·030
Na	0·008	0·009	0·021	0·009	0·007	0·010	—	—	—	—	0·011	0·003	0·005	0·029	0·002	0·000	0·009
K	0·000	0·000	0·000	0·000	0·000	0·000	0·000	0·000	0·000	0·000	0·000	0·000	0·000	0·000	0·000	0·000	0·000
O	6	6	6	6	6	6	6	6	6	6	6	6	6	6	6	6	6
Sum	4·000	4·001	4·000	4·009	4·002	4·000	4·000	4·000	4·000	4·000	3·999	3·998	4·008	4·001	3·998	4·001	3·996
Mg-no.	85·89	85·48	86·49	83·54	85·48	81·59	86·49	85·22	85·12	85·15	81·46	83·85	82·26	82·06	81·46	85·18	86·79

(continued)

Table 3: Continued

Sample no.:	10	10	11	11	12	12	12	13	13	14	14	15	16	17	17	17
Type:	R	E	H	R	P	Al1	Al2	E1	E2	P	Al	Al	Al	H	R	E
SiO_2	54·29	54·17	54·23	53·82	53·80	49·86	47·69	53·85	54·70	54·78	46·27	49·80	49·93	52·35	51·50	53·26
TiO_2	0·29	0·19	0·16	0·24	0·22	0·17	0·17	0·20	0·17	0·14	0·13	0·11	0·48	0·17	0·24	0·25
Al_2O_3	5·16	4·49	5·10	5·45	3·76	11·34	14·81	5·33	3·82	3·73	14·41	8·90	9·43	6·41	7·21	3·64
Cr_2O_3	0·08	0·18	0·14	0·17	0·14	0·27	0·33	0·17	0·15	0·14	0·08	0·00	0·05	0·14	0·18	0·09
FeO^*	9·15	11·10	9·79	9·10	9·28	11·92	13·17	9·56	9·37	11·32	16·00	11·96	12·36	10·18	9·57	14·29
MnO	0·14	0·13	0·12	0·12	0·00	0·41	0·51	0·14	0·15	0·15	0·28	0·22	0·25	0·00	0·00	0·00
MgO	27·87	29·26	29·79	27·40	29·63	24·62	22·34	28·99	29·59	28·98	20·96	25·44	25·58	28·39	25·99	26·01
CaO	2·51	0·82	0·72	3·35	0·86	2·70	1·72	0·84	0·81	0·59	1·28	2·16	1·95	0·76	3·39	0·81
Na_2O	0·31	0·19	0·13	0·40	0·13	0·04	0·02	0·04	0·10	0·16	0·00	0·09	0·16	0·14	0·41	0·29
K_2O	0·00	0·00	0·00	0·00	0·00	0·00	0·01	0·00	0·00	0·00	0·00	0·00	0·00	0·00	0·00	0·00
Sum	99·84	100·01	100·22	100·08	99·70	101·3	100·77	99·21	98·89	100·01	99·68	98·70	100·19	98·52	98·53	99·01
Si	1·872	1·885	1·891	1·850	1·923	1·677	1·588	1·881	1·925	1·912	1·558	1·727	1·712	1·836	1·781	1·861
Ti	0·007	0·005	0·004	0·006	0·004	0·004	0·004	0·005	0·004	0·003	0·003	0·002	0·012	0·004	0·006	0·005
Al(IV)	0·127	0·112	0·108	0·149	0·076	0·322	0·411	0·118	0·074	0·087	0·441	0·272	0·287	0·163	0·218	0·139
Al(VI)	0·082	0·071	0·100	0·071	0·080	0·127	0·169	0·101	0·083	0·065	0·130	0·091	0·093	0·101	0·075	0·013
Cr	0·002	0·005	0·004	0·004	0·004	0·007	0·008	0·004	0·004	0·003	0·002	—	0·001	0·004	0·005	0·004
Fe	0·240	0·321	0·285	0·223	0·331	0·237	0·254	0·279	0·275	0·330	0·309	0·249	0·274	0·348	0·202	0·348
Mn	0·005	0·006	—	0·003	0·003	0·003	0·005	0·006	0·004	0·001	0·002	0·001	0·001	0·002	1·558	0·002
Mg	1·554	1·569	1·571	1·549	1·569	1·516	1·500	1·574	1·586	1·573	1·517	1·563	1·545	1·579	0·125	1·579
Ca	0·992	0·031	0·027	0·123	0·019	0·097	0·061	0·031	0·030	0·022	0·046	0·080	0·071	0·029	0·028	0·029
Na	0·021	0·010	0·009	0·027	0·012	0·002	0·001	0·006	0·007	0·011	0·003	0·006	0·010	0·013	0·000	0·013
K	0·000	0·000	0·000	0·000	0·000	0·000	0·000	0·000	0·000	0·000	0·000	0·000	0·000	0·000	0·000	0·000
O	6	6	6	6	6	6	6	6	6	6	6	6	6	6	6	6
Sum	4·000	4·004	4·002	3·998	3·993	3·997	4·001	4·004	3·995	4·006	3·999	3·998	4·002	4·001	3·999	4·001
Mg-no.	86·61	82·86	84·61	87·61	85·23	86·76	86·57	84·92	85·17	82·63	83·47	86·52	85·24	85·34	88·74	81·98

Sample no.:	19	19	19	19	19	19	20	20	20	21	21	22	22	22	23	24	24
Type:	P	Al	V	E	H	R	H	R	E	Al1	Al2	P	E	Inc	E3	H1	R1
SiO_2	54·29	50·04	53·63	53·99	52·89	52·62	53·42	54·78	53·99	50·86	50·11	53·43	54·09	54·15	53·26	54·68	54·25
TiO_2	0·22	0·18	0·20	0·27	0·3	0·30	0·20	0·15	0·27	0·03	0·03	0·20	0·19	0·18	0·26	0·17	0·27
Al_2O_3	5·56	9·94	4·33	4·50	5·98	6·19	6·29	4·40	4·51	9·66	11·13	6·24	4·49	4·43	3·64	4·66	4·97
Cr_2O_3	0·16	0·12	0·17	0·12	0·16	0·17	0·13	0·23	0·13	0·12	0·16	0·12	0·20	0·17	0·08	0·28	0·31
FeO^*	9·98	10·69	10·28	10·21	10·56	10·04	10·20	9·23	10·21	11·28	10·83	10·21	10·99	11·17	14·36	9·30	8·55
MnO	0·00	0·00	0·00	0·16	0·00	0·00	0·18	0·16	0·15	0·31	0·29	0·20	0·11	0·12	0·00	0·16	0·15
MgO	28·96	27·03	29·35	29·48	28·87	27·35	28·03	29·45	29·48	25·65	25·52	28·07	29·07	29·19	25·75	29·75	26·93
CaO	0·91	1·80	0·92	0·76	0·86	2·58	0·79	0·85	0·76	1·96	1·32	0·81	0·83	0·89	0·87	0·82	3·94
Na_2O	0·14	0·04	0·15	0·10	0·17	0·35	0·13	0·11	0·10	0·03	0·02	0·13	0·15	0·16	0·27	0·14	0·45
K_2O	0·00	0·00	0·00	0·00	0·00	0·00	0·01	0·00	0·00	0·00	0·00	0·00	0·00	0·00	0·00	0·00	0·00
Sum	99·69	99·96	99·05	99·59	99·73	99·62	99·46	99·40	99·59	99·96	99·41	99·42	99·89	100·47	98·50	99·98	99·86
Si	1·846	1·725	1·890	1·895	1·846	1·820	1·852	1·914	1·895	1·737	1·711	1·853	1·883	1·887	1·861	1·906	1·860
Ti	0·005	0·004	0·005	0·006	0·006	0·007	0·004	0·004	0·006	0·000	0·000	0·005	0·004	0·004	0·006	0·004	0·007
Al(IV)	0·151	0·274	0·109	0·105	0·153	0·179	0·146	0·085	0·105	0·262	0·288	0·146	0·115	0·112	0·138	0·093	0·139
Al(VI)	0·089	0·129	0·070	0·081	0·092	0·072	0·108	0·095	0·081	0·126	0·159	0·109	0·070	0·069	0·010	0·098	0·061
Cr	0·004	0·003	0·004	0·004	0·004	0·004	0·005	0·006	0·004	0·003	0·004	0·003	0·006	0·004	0·002	0·007	0·008
Fe	0·281	0·243	0·283	0·298	0·282	0·237	0·269	0·269	0·298	0·263	0·246	0·280	0·323	0·325	0·354	0·271	0·209
Mn	—	—	—	0·002	—	—	0·004	0·004	0·002	0·002	0·001	0·001	0·001	0·002	—	0·001	0·002
Mg	1·574	1·553	1·588	1·582	1·573	1·559	1·565	1·574	1·582	1·538	1·539	1·563	1·568	1·570	1·574	1·571	1·545
Ca	0·033	0·066	0·034	0·026	0·032	0·095	0·030	0·032	0·026	0·031	0·048	0·030	0·031	0·033	0·032	0·030	0·144
Na	0·009	0·002	0·010	0·008	0·011	0·023	0·007	0·007	0·008	0·002	0·001	0·009	0·010	0·010	0·018	0·009	0·030
K	0·000	0·000	0·000	0·000	0·000	0·000	0·000	0·000	0·000	0·000	0·000	0·000	0·000	0·000	0·000	0·000	0·000
O	6	6	6	6	6	6	6	6	6	6	6	6	6	6	6	6	6
Sum	4·002	3·999	4·002	4·001	3·996	3·999	4·002	3·994	4·001	4·001	3·999	4·003	4·008	4·005	4·001	3·996	4·001
Mg-no.	85·18	86·76	85·16	84·05	85·10	87·02	87·76	83·57	84·09	85·65	86·90	86·87	82·79	82·83	81·95	85·27	88·27

(continued)

Table 3: Continued

Sample no.:	24	24	25	25	25	28	28
Type:	H2	R2	P	Al1	Al2	H	E
SiO_2	53·63	53·26	52·38	47·07	48·20	54·18	54·43
TiO_2	0·19	0·28	0·24	0·18	0·05	0·24	0·24
Al_2O_3	6·28	6·58	4·80	12·27	9·85	4·13	3·71
Cr_2O_3	0·34	0·37	0·06	0·06	0·04	0·10	0·02
FeO*	9·59	8·91	14·23	17·16	18·20	10·61	10·24
MnO	0·14	0·13	0·14	0·38	0·37	0·13	0·16
MgO	29·06	26·74	26·05	21·03	20·78	29·35	29·36
CaO	0·81	3·41	1·11	1·41	2·20	0·77	0·54
Na_2O	0·15	0·42	0·16	0·02	0·01	0·11	0·08
K_2O	0·00	0·00	0·00	0·00	0·00	0·00	0·00
Sum	100·21	100·15	99·20	99·63	99·70	99·62	98·78
Si	1·858	1·819	1·827	1·594	1·637	1·900	1·920
Ti	0·004	0·007	0·006	0·004	0·001	0·006	0·006
Al(IV)	0·141	0·180	0·172	0·405	0·362	0·099	0·079
Al(VI)	0·114	0·084	0·024	0·084	0·032	0·071	0·074
Cr	0·009	0·010	0·001	0·001	0·001	0·002	—
Fe	0·277	0·209	0·346	0·333	0·353	0·311	0·302
Mn	0·001	0·001	0·001	0·002	0·002	0·004	0·001
Mg	1·561	1·539	1·571	1·526	1·531	1·581	1·589
Ca	0·030	0·125	0·041	0·051	0·080	0·028	0·020
Na	0·010	0·028	0·011	0·001	0·080	0·007	0·005
K	0·000	0·000	0·000	0·000	0·000	0·000	0·000
O	6	6	6	6	6	6	6
Sum	4·009	4·002	4·004	4·002	4·001	4·007	3·998
Mg-no.	84·89	88·27	82·26	82·48	83·50	83·54	84·03

P, no exsolution; H, host; R, reconstructed; E, exsolved in cpx; E1/E2, compositionally distinct opx exsolved in cpx; E3, exsolved in host garnet; V, vein; Al, highly aluminous; Inc, inclusion.
*Total Fe given as FeO.

In this respect the SLC garnets are considerably different from garnets in eclogite xenoliths from kimberlites (Fig. 14b; Snyder *et al.*, 1997, and references therein; S. E. Haggerty, personal communication, 2003). However, garnets in the SLC xenoliths appear to be similar to those in the garnet pyroxenites from the Lherz Massif (Bodinier *et al.*, 1987; not shown in Fig. 14b), in xenoliths and megacrysts from kimberlites in Canada (Kopylova *et al.*, 1999; Schmidberger & Francis, 1999), and the megacrystic suite from Malaita (Delaney *et al.*, 1979) and Jagersfontein, South Africa (Hops *et al.*, 1989). The trend from the Py corner to the Alm apex in Salt Lake Crater garnets is also seen in high-pressure (2·5–4·0 GPa) liquidus phase equilibrium experimental studies (Herzberg & Zhang, 1996; Walter, 1998; Keshav *et al.*, 2004), and at either a single pressure or range of pressures is consistent with progressive cooling (crystallization) of a partial melt.

Spinel

Spinels in the SLC xenoliths are variable in terms of their Cr-number and Mg-number (Table 5; Fig. 15a and b). When compared with the SLC spinel lherzolite xenoliths, spinels in these garnet-bearing xenoliths are dominantly Mg–Al pleonastes, compositionally similar to those documented in previous studies (Sen, 1983). These spinels are high in Fe/Mg, low in Cr-number, and high in TiO_2. Sen (1988) pointed out that in individual xenoliths, spinels surrounded by garnet are more Cr-rich than the spinels without a rim. However, in the present study garnet-rimmed spinels are not very different from those that are large and discrete. Spinels that occur near the grain boundaries of large garnets are always Mg–Al pleonaste and are lower in Cr than the other types. The spinels in SLC garnet pyroxenites are also distinct (Fig. 16) from those in abyssal peridotites (Dick & Bullen, 1984; Dick, 1989), dunite xenoliths from Koolau volcano, Hawaii (Sen & Presnall, 1986), and also those found as phenocrysts or microphenocrysts in Hawaiian lavas (Clague *et al.*, 1980; BVSP, 1981).

Phlogopite

Phlogopites are homogeneous and vary little in composition (Table 6). Compositional zoning was not detected. Compared with either the primary or secondary phlogopites in kimberlites (Carswell, 1975), the phlogopites in

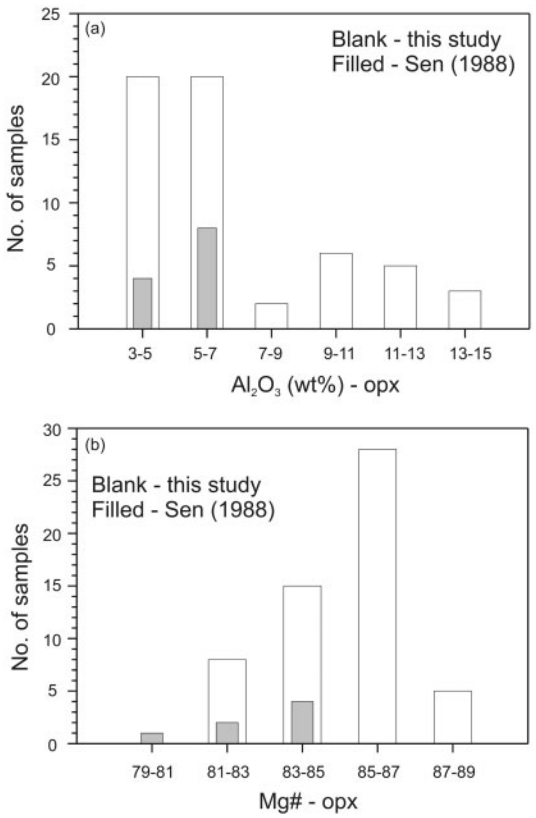

Fig. 12. Composition of opx in the garnet-pyroxenite xenoliths: (a) Al_2O_3 (wt %) and (b) molar Mg-number [Mg/(Mg + Fe)]. The alumina content of opx (with or without exsolution) clusters around 3–5 wt %, whereas the very high alumina contents represent samples where opx is of secondary origin (e.g. breakdown).

the SLC xenoliths are considerably higher in Fe/Mg and alumina. Phlogopites of different compositions are not seen in the same xenolith from Salt Lake Crater. Primarily on the basis of major-element chemistry and some textural arguments, Sen (1988) suggested a primary origin (that is, syngenetic with other silicates in the rock) for the phlogopites in some of the Salt Lake garnet pyroxenites. However, recent isotopic studies of these phlogopites indicate strong disequilibrium with the other anhydrous silicates in the same xenolith (Bizimis *et al.*, 2003*b*). Hence, it seems that formation of phlogopite in these xenoliths was a separate event.

Ilmenite

Ilmenites have variable TiO_2, FeO*, Al_2O_3, and MgO concentrations (Table 7). In the hematite–ilmenite–geikelite (Fe_2O_3–$FeTiO_3$–$MgTiO_3$) ternary, they are similar to those found as discrete xenoliths and macrocrysts in kimberlites (Haggerty, 1991). Although this similarity might imply some sort of relation between kimberlitic melts and the SLC xenoliths, the dataset on ilmenite compositions is not detailed enough to permit this evaluation.

PETROGENESIS OF THE GARNET-BEARING XENOLITHS

Equilibrium between minerals in the xenoliths and thermobarometry

In this section, we evaluate the major-element (Mg–Fe) chemical equilibrium between the major silicate minerals in the SLC xenoliths. We then place constraints on the thermal equilibration history of the xenoliths from chemical equilibrium (or lack thereof) between the coexisting phases. Thermal equilibration is discussed in the context of major element (Mg–Fe) chemical equilibrium between the major silicate minerals. Table 8 lists the Mg-number of olivine–cpx–opx–gt in the xenoliths.

A good positive correlation (almost 1:1; Fig. 17) exists between the Mg-number of coexisting cpx and olivine, suggesting chemical equilibrium between these two phases. This correlation is similar to that observed in high-pressure experiments (Brey & Kohler, 1990; Walter, 1998). In contrast, simple Mg–Fe exchange equilibrium is not readily evident for large olivine and opx crystals (Table 8). The chemical disequilibrium of opx with olivine is puzzling as the xenoliths lack supporting evidence (e.g. broken grain margins or resorbed rims). Some previous studies have also noted chemical disequilibrium between olivine and opx in SLC xenoliths (Sen, 1988; Sen & Jones, 1990). Varying alumina content is a good indication of disequilibrium between the large opx in individual xenoliths.

Good positive Mg-number correlations between large olivine and garnet suggest equilibrium (Fig. 18). These correlations are in accord with those observed in a high-pressure melting study of a fertile lherzolite (Walter, 1998). Significantly, demonstration of Mg–Fe equilibrium (or lack thereof) between opx and garnet is crucial, as both of these minerals are generally used to retrieve pressure(s) of final equilibration for garnet-bearing assemblages. Orthopyroxenes with variable alumina contents in individual xenoliths suggest disequilibrium (Table 3). The Mg-number values of various types of opx coexisting with garnet are given in Table 8. In contrast to this study, the opx–garnet pairs in SLC xenoliths described by Bizimis *et al.* (2005*c*) appear to be in broad Mg–Fe equilibrium. Similar garnet-pyroxenite lithologies from the Sierra Nevada (Mukhopadhyay & Manton, 1994), Lherz Massif (Bodinier *et al.*, 1987), and kimberlite-hosted xenoliths from Canada (Kopylova *et al.*, 1999; Schmidberger & Francis, 1999) have equilibrated opx–garnet pairs. In the SLC samples from this study, disequilibrium of opx with garnet persists whether or not olivine is present in the xenoliths (Table 8).

Correlations of Mg-number between large opx and cpx from individual SLC xenoliths are indicated in Table 8. The widely varying Mg-number of opx in individual xenoliths suggests disequilibrium. Good positive Mg-number

Table 4: Major element composition of garnets

Sample no.:	1	2	2	3	3	4	4	4	5	5	5	5	5	6	6	7
Type:	S	S	P	E1	P	P	E1	G	P	E1	S	H	R	P	S	P
SiO_2	41·05	40·88	42·02	41·67	41·75	40·92	41·48	41·29	41·53	40·57	40·63	40·69	39·88	40·45	41·52	41·08
TiO_2	0·19	0·19	0·21	0·46	0·45	0·39	0·25	0·26	0·29	0·46	0·30	0·35	1·21	0·00	0·18	0·00
Al_2O_3	22·71	23·31	23·61	22·71	22·7	22·72	22·70	22·76	22·77	22·86	22·73	22·71	22·28	22·95	22·77	23·26
Cr_2O_3	0·45	0·17	0·19	0·03	0·04	0·05	0·06	0·06	0·05	0·07	0·06	0·05	0·05	0·04	0·06	0·02
FeO*	10·94	11·32	11·42	15·65	15·55	15·31	15·96	16·10	14·70	14·49	14·77	16·04	16·65	15·86	15·97	13·97
MnO	0·00	0·45	0·44	0·32	0·31	0·39	0·41	0·22	0·00	0·39	0·00	0·41	0·40	0·42	0·43	0·35
MgO	17·96	17·83	17·73	15·55	15·56	15·13	14·75	14·87	15·70	15·66	15·81	15·50	15·32	14·84	14·64	16·38
CaO	4·82	4·97	5·09	4·72	4·76	5·14	5·14	5·19	5·03	5·09	4·99	5·05	4·95	5·05	5·11	5·95
Na_2O	0·04	0·01	0·03	0·04	0·04	0·03	0·03	0·01	0·03	0·04	0·03	0·04	0·03	0·02	0·03	0·03
K_2O	0·00	0·00	0·00	0·00	0·00	0·00	0·00	0·00	0·00	0·00	0·00	0·00	0·00	0·00	0·00	0·00
Sum	98·18	99·14	100·74	101·06	101·10	100·10	100·18	100·78	100·10	99·63	99·23	100·84	100·82	99·93	100·71	100·98
Si	2·999	2·969	2·990	3·014	3·018	2·995	3·020	3·000	3·021	2·975	3·007	2·969	2·926	2·987	3·025	2·978
Ti	0·010	0·010	0·011	0·025	0·024	0·021	0·014	0·014	0·015	0·025	0·016	0·019	0·067	—	0·009	—
Al(IV)	—	—	—	—	—	—	—	—	—	—	—	—	—	—	—	—
Al(VI)	1·960	1·999	1·980	1·936	1·935	1·961	1·948	1·955	1·953	1·976	1·983	1·953	1·928	1·998	1·956	1·988
Cr	0·025	0·009	0·010	0·002	0·002	0·003	0·003	0·003	0·002	0·004	0·003	0·003	0·002	0·002	0·003	0·001
Fe	0·668	0·667	0·712	0·947	0·940	0·937	0·971	0·981	0·894	0·878	0·914	0·924	0·981	0·953	0·973	0·778
Mn	0·000	0·027	0·026	0·019	0·018	0·024	0·025	0·013	0·000	0·024	0·000	0·025	0·025	0·026	0·026	0·021
Mg	1·956	1·929	1·880	1·676	1·676	1·650	1·600	1·615	1·702	1·711	1·668	1·685	1·676	1·633	1·589	1·770
Ca	0·377	0·386	0·388	0·366	0·368	0·403	0·401	0·405	0·392	0·399	0·386	0·394	0·389	0·400	0·398	0·462
Na	0·005	0·001	0·004	0·006	0·005	0·004	0·005	0·002	0·004	0·005	0·004	0·005	0·025	0·003	0·004	0·004
K	0·000	0·000	0·000	0·000	0·000	0·000	0·000	0·000	0·000	0·000	0·000	0·000	0·000	0·000	0·000	0·000
O	12	12	12	12	12	12	12	12	12	12	12	12	12	12	12	12
Sum	8·001	8·000	8·004	7·993	7·990	8·002	7·991	7·998	7·986	7·997	7·984	7·996	8·002	7·998	7·987	7·999
Py	65·15	64·67	64·56	56·07	56·15	55·18	53·82	53·80	56·95	57·38	56·87	56·09	55·15	53·86	53·67	59·39
Alm	22·27	22·36	22·41	31·67	31·49	31·33	32·67	32·69	29·92	29·21	29·99	30·76	32·02	32·70	32·85	27·29
Gr	12·56	12·96	13·02	12·24	12·35	13·47	13·49	13·49	13·11	13·40	13·28	13·14	12·81	13·43	13·46	14·78
Mg-no.	74·52	74·29	74·17	63·89	64·06	63·78	62·22	62·20	65·55	66·26	65·79	64·58	63·26	62·14	62·02	68·48

Sample no.:	7	7	8	8	9	9	10	11	12	13	13	13	14	15	16	17	17
Type:	S	E1	P	E1	P	S	S	S	P	P	S	E1	P	P	P	P	S
SiO_2	40·75	40·87	41·15	41·23	40·85	41·10	42·05	42·41	42·08	41·56	41·72	41·96	41·65	40·62	40·76	41·89	42·24
TiO_2	0·19	0·20	0·23	0·25	0·19	0·20	0·21	0·15	0·20	0·19	0·17	0·15	0·15	0·24	0·26	0·21	0·15
Al_2O_3	22·95	22·89	23·22	23·28	22·38	22·45	23·12	23·37	23·05	22·95	23·21	23·01	22·94	22·95	22·84	23·11	23·38
Cr_2O_3	0·04	0·02	0·19	0·14	0·03	0·07	0·18	0·35	0·35	0·39	0·33	0·32	0·03	0·05	0·09	0·29	0·13
FeO*	14·04	14·14	13·47	13·69	15·29	15·40	11·57	11·25	12·44	11·60	11·67	11·40	16·03	12·85	15·77	11·81	11·90
MnO	0·36	0·36	0·37	0·36	0·02	0·42	0·16	0·36	0·45	0·00	0·43	0·35	0·46	0·35	0·36	0·00	0·00
MgO	16·39	16·41	16·33	16·00	15·29	15·32	17·96	18·17	17·20	17·68	17·59	17·44	15·65	16·42	14·95	18·01	17·90
CaO	5·04	4·80	5·01	4·93	4·74	4·78	4·73	4·77	4·62	5·07	4·92	5·11	4·22	5·47	4·70	4·94	4·87
Na_2O	0·02	0·02	0·03	0·03	0·03	0·17	0·02	0·02	0·03	0·02	0·02	0·02	0·02	0·02	0·04	0·01	0·02
K_2O	0·00	0·00	0·00	0·00	0·00	0·00	0·00	0·00	0·00	0·00	0·00	0·00	0·00	0·00	0·00	0·00	0·00
Sum	99·78	99·71	100·03	99·94	100·25	100·08	100·04	100·77	100·46	99·47	99·94	99·80	101·10	99·02	98·80	100·31	100·59
Si	2·976	2·987	2·988	2·996	3·004	3·011	3·017	3·018	3·022	3·004	3·008	3·023	3·013	2·980	2·995	3·003	3·015
Ti	0·010	0·011	0·012	0·014	0·010	0·011	0·011	0·008	0·010	0·010	0·009	0·008	0·008	0·013	0·014	0·011	0·008
Al(IV)	—	—	—	—	—	—	—	—	—	—	—	—	—	—	—	—	—
Al(VI)	1·975	1·970	1·987	1·995	1·950	1·939	1·956	1·961	1·952	1·956	1·973	1·954	1·957	1·984	1·988	1·960	1·978
Cr	0·002	0·001	0·011	0·008	0·001	0·004	0·010	0·014	0·020	0·022	0·018	0·018	0·003	0·003	0·005	0·016	0·007
Fe	0·831	0·844	0·818	0·832	1·040	0·934	0·694	0·669	0·747	0·701	0·721	0·687	0·970	0·776	0·969	0·708	0·710
Mn	0·022	0·022	0·022	0·022	0·001	0·026	0·009	0·021	0·027	—	0·026	0·021	0·028	0·021	0·022	—	—
Mg	1·783	1·786	1·767	1·733	1·622	1·673	1·921	1·885	1·841	1·905	1·846	1·872	1·687	1·794	1·637	1·928	1·957
Ca	0·394	0·376	0·390	0·383	0·373	0·375	0·364	0·388	0·355	0·392	0·380	0·394	0·327	0·429	0·370	0·379	0·372
Na	0·002	0·003	0·004	0·004	0·004	0·024	0·002	0·003	0·005	0·003	0·002	0·003	0·003	0·003	0·006	0·001	0·002
K	0·000	0·000	0·000	0·000	0·000	0·000	0·000	0·000	0·000	0·000	0·000	0·000	0·000	0·000	0·000	0·000	0·000
O	12	12	12	12	12	12	12	12	12	12	12	12	12	12	12	12	12
Sum	7·986	7·989	8·002	7·990	7·997	7·998	7·989	7·987	7·985	7·997	7·987	7·984	7·999	8·002	7·997	8·001	7·998
Py	59·42	59·56	59·39	58·76	55·19	56·27	64·46	64·94	62·52	63·51	63·57	63·38	56·53	59·89	54·99	63·84	63·74
Alm	27·43	27·89	27·49	28·22	30·99	31·10	23·31	22·79	25·39	23·39	23·46	23·26	32·49	25·76	32·56	23·67	23·78
Gr	13·13	12·54	13·11	13·01	12·57	12·61	12·22	12·25	12·08	13·10	13·01	13·35	10·97	14·34	12·43	12·58	12·46
Mg-no.	68·40	68·10	68·35	67·55	64·27	64·39	73·44	74·20	71·11	73·08	72·98	73·15	63·50	69·92	62·80	73·07	72·82

(continued)

Table 4: Continued

Sample no.:	17	18	18	18	19	19	19	20	21	22	23	23	23	24	24	25	25
Type:	E1	P	E1	V	P	S	V	P	P	S	P	H	R	P	S	P1	P2
SiO_2	41·66	40·28	39·98	42·23	41·84	41·96	41·74	42·29	42·00	41·86	40·27	39·79	41·25	41·61	41·51	40·88	40·61
TiO_2	0·16	0·06	0·05	0·21	0·21	0·21	0·26	0·14	0·14	0·18	0·24	0·28	0·30	0·19	0·17	0·23	0·07
Al_2O_3	22·97	22·82	22·28	22·48	22·71	23·18	22·94	23·03	23·20	23·41	22·24	22·06	20·23	23·06	22·95	22·92	22·71
Cr_2O_3	0·33	0·03	0·02	0·03	0·45	0·42	0·39	0·49	0·38	0·30	0·19	0·32	0·37	0·71	0·87	0·11	0·10
FeO*	11·87	16·21	16·34	15·96	11·66	11·60	11·53	10·77	12·18	11·97	16·31	16·76	16·60	11·37	11·20	16·92	15·07
MnO	0·00	0·41	0·39	0·39	0·00	0·00	0·00	0·40	0·43	0·36	0·36	0·38	0·35	0·00	0·00	0·36	0·36
MgO	18·19	14·93	14·77	14·35	17·80	17·91	17·97	18·07	17·32	17·67	14·91	14·65	15·77	18·06	18·23	14·95	15·30
CaO	4·84	4·98	5·06	5·32	5·06	5·02	5·00	5·06	4·82	4·80	4·50	4·35	4·33	4·91	4·84	4·36	4·32
Na_2O	0·02	0·03	0·03	0·05	0·01	0·02	0·02	0·02	0·05	0·02	0·06	0·09	0·11	0·03	0·03	0·03	0·04
K_2O	0·00	0·00	0·00	0·00	0·00	0·00	0·00	0·00	0·00	0·00	0·00	0·00	0·00	0·00	0·00	0·00	0·00
Sum	100·04	99·75	99·63	99·02	100·07	100·32	99·85	100·31	100·52	100·61	99·08	98·07	99·34	99·94	99·80	100·79	98·61
Si	2·997	2·974	2·990	2·991	3·005	3·005	3·004	3·022	3·013	2·997	2·992	2·978	3·063	2·992	2·989	2·987	2·991
Ti	0·008	0·003	0·002	0·011	0·011	0·011	0·014	0·007	0·007	0·009	0·017	0·015	0·016	0·010	0·009	0·012	0·014
Al(IV)	—	—	—	—	—	—	—	—	—	—	—	—	—	—	—	—	—
Al(VI)	1·950	1·989	1·964	1·970	1·956	1·957	1·946	1·941	1·962	1·976	1·948	1·946	1·771	1·955	1·948	1·974	1·967
Cr	0·018	0·001	0·001	0·001	0·021	0·023	0·022	0·028	0·021	0·017	0·011	0·018	0·021	0·040	0·049	0·006	0·004
Fe	0·705	0·972	1·018	0·987	0·700	0·695	0·694	0·644	0·730	0·717	0·995	1·020	1·002	0·684	0·674	1·022	0·933
Mn	—	0·025	0·024	0·024	—	—	—	0·024	0·026	0·021	0·022	0·024	0·022	—	—	0·022	0·017
Mg	1·950	1·642	1·543	1·590	1·906	1·912	1·927	1·925	1·851	1·885	1·651	1·634	1·745	1·936	1·956	1·628	1·668
Ca	0·373	0·393	0·450	0·423	0·389	0·385	0·385	0·388	0·370	0·368	0·358	0·348	0·344	0·378	0·373	0·341	0·405
Na	0·003	0·004	0·004	0·007	0·001	0·002	0·002	0·003	0·006	0·003	0·008	0·013	0·015	0·004	0·004	0·005	0·003
K	0·000	0·000	0·000	0·000	0·000	0·000	0·000	0·000	0·000	0·000	0·000	0·000	0·000	0·000	0·000	0·000	0·000
O	12	12	12	12	12	12	12	12	12	12	12	12	12	12	12	12	12
Sum	7·996	7·999	8·001	7·999	7·994	7·993	7·998	7·986	7·992	7·997	7·999	8·002	7·999	7·995	8·001	7·997	7·999
Py	64·51	54·73	54·69	53·09	63·60	64·04	64·09	65·09	62·70	63·46	55·05	54·50	56·52	64·55	65·40	54·55	56·94
Alm	23·13	32·14	31·99	32·74	23·37	23·04	23·08	21·78	24·74	23·13	33·00	33·86	32·31	22·81	22·10	34·00	31·47
Gr	12·34	13·12	13·19	14·15	13·02	12·90	12·82	13·12	12·54	12·39	11·95	11·63	11·15	12·63	12·48	11·45	11·57
Mg-no.	73·60	63·00	63·11	61·86	73·12	73·34	73·51	74·92	71·70	72·44	62·52	61·67	63·62	73·89	74·36	61·60	64·33

(continued)

correlations between large cpx and garnet suggest equilibrium (Fig. 19).

The presence of exsolution textures in pyroxenes (mainly cpx) suggests that these xenoliths have had at least a two-stage thermal history: the pre-exsolution stage is probably a melt-equilibrated stage, whereas the exsolution occurred when the xenoliths cooled to subsolidus temperatures. On the basis of Mg–Fe exchange between coexisting clinopyroxene and garnet, we assess the state of thermal equilibrium of the SLC xenoliths. Where possible, we also employ two-pyroxene thermometry to retrieve information on the thermal equilibration of these xenoliths. First, two gt–cpx thermometers, developed by Ellis & Green (1979; hereafter called EG79) and Krogh (1988; hereafter called K88) are used. The exchange reaction governing this equilibrium can be written as

$$Mg^{2+}(cpx) + Fe^{2+}(gt) = Mg^{2+}(gt) + Fe^{2+}(cpx).$$

As the Fe^{3+} and Fe^{2+} contents of cpx and garnet are unknown, we first calculate temperatures at which subsolidus cooling might have occurred; because the experimental and model calibrations for the gt–cpx thermometers are most extensive at 2·5–3 GPa, the temperatures retrieved here are calculated assuming a pressure of 3 GPa. Some garnet-bearing pyroxenite xenoliths from SLC, however, contain majoritic garnets (Keshav & Sen, 2001) and microdiamonds (Wirth & Rocholl, 2003; Frezzotti and Peccerillo, 2005), suggesting that these have originated at pressures of at least 5–6 GPa. Hence, the

Table 4: Continued

Sample no.:	26	27	28	28
Type:	P	P	P/G	E1
SiO_2	40·98	40·32	41·66	41·94
TiO_2	0·25	0·21	0·22	0·22
Al_2O_3	22·86	22·64	22·89	22·97
Cr_2O_3	0·07	0·03	0·25	0·18
FeO*	15·38	16·63	11·60	11·81
MnO	0·27	0·36	0·39	0·37
MgO	15·34	14·33	17·32	17·38
CaO	5·19	4·17	5·03	5·12
Na_2O	0·02	0·03	0·01	0·02
K_2O	0·00	0·00	0·00	0·00
Sum	100·40	98·73	99·37	100·05
Si	2·991	3·003	3·017	3·019
Ti	0·014	0·009	0·011	0·012
Al(IV)	—	—	—	—
Al(VI)	1·967	1·988	1·954	1·949
Cr	0·004	0·001	0·014	0·010
Fe	0·933	1·036	0·702	0·711
Mn	0·017	0·023	0·023	0·022
Mg	1·668	1·600	1·869	1·864
Ca	0·405	0·332	0·390	0·395
Na	0·003	0·004	0·001	0·003
K	0·000	0·000	0·000	0·000
O	12	12	12	12
Sum	7·998	7·992	7·998	7·989
Py	55·63	53·75	63·10	62·75
Alm	30·83	35·00	23·71	23·93
Gr	13·53	11·25	13·18	13·31
Mg-no.	64·33	60·56	72·68	72·38

S, sp-cored; E1, exsolved in cpx; G, grain boundary; P, primary; V, vein; R, reconstructed; H, host; P/G, primary/grain boundary?
*Total Fe given as FeO.

3 GPa pressure input value in the temperature calculations should be regarded as a minimum. To estimate subsolidus thermal state (where exsolution might have occurred), in the temperature calculations, we have used, for the most part, host cpx and garnet (with or without spinel core). We have also used the P-type of cpx (the type of cpx that lacks exsolution; Table 2) to retrieve temperature information. Additionally, in samples with two or more compositionally distinct types of cpx and garnet, we also calculate temperatures for these compositions using both the thermometric formulations (i.e. EG79 and K88). The results of the thermometric calculations are presented in Table 9 and Fig. 20. With a few exceptions, temperatures (of last equilibration) calculated by both the thermometers yield

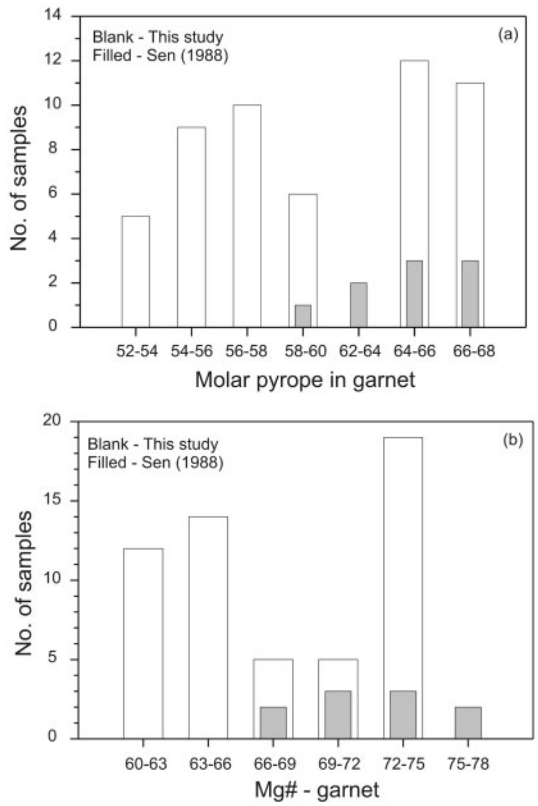

Fig. 13. Composition of garnet in the Salt Lake Crater garnet-pyroxenite xenoliths: (a) molar% pyrope [Mg/(Mg + Fe + Ca)]; (b) molar% Mg-number [Mg/[Mg + Fe)]. Garnets with or without spinel core are compositionally very similar to each other.

similar results, with most of the temperatures clustering around 1200–1320°C. When the pressure input value is lowered to 2·5 GPa, the retrieved temperature estimates are lower by 30–60°C. The temperatures calculated using the K88 thermometer range from ~1150°C to ~1320°C (Fig. 20), and are to a large degree in the temperature range given by the EG79 thermometer. An exception to this generalization is sample SL-7 (b), for which the temperature estimate with EG79 is actually lower by almost 150°C than that calculated with K88. With two exceptions (>1400°C), the temperature estimates reported here are similar to those of Bizimis *et al.* (2005*c*). Additionally, on the basis of new experimental data on the solid solution properties of Ca–Mg–Fe garnets, Ganguly *et al.* (1996) presented an optimized thermodynamic model, and concluded that the K88 thermometer consistently provided temperature estimates that were lower by at least 75°C, and also that at higher temperatures the relative difference increases. Ganguly *et al.* (1996) also concluded that the agreement between EG79 and their own formulation was better. The conclusion drawn above has been confirmed in two recent studies (Bizimis *et al.*, 2005*c*; Sen *et al.*, 2005). Hence, for the rest of the paper we use the EG79 results. As an aside, Sen *et al.* (2005), on the basis of the

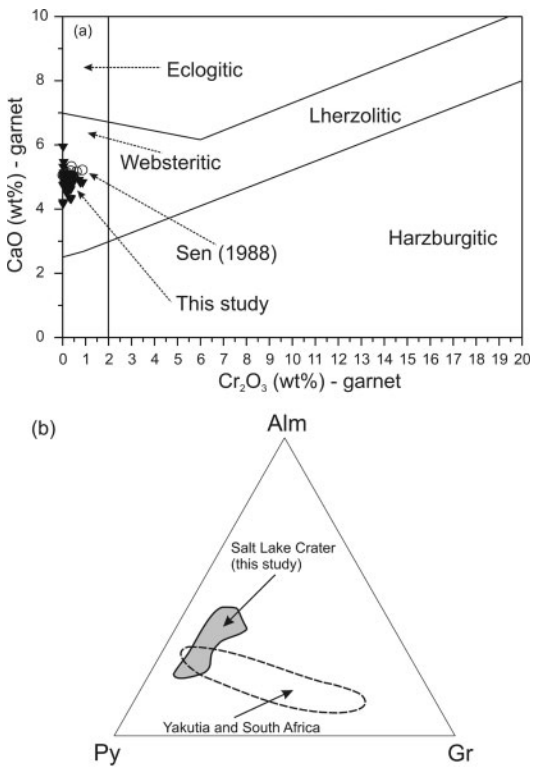

Fig. 14. Garnet compositions in Salt Lake Crater garnet-pyroxenite xenoliths in terms of (a) CaO (wt %) vs Cr_2O_3 (wt %), modified after Sobolev *et al.* (1973); (b) pyrope–almandine–grossular (Py–Alm–Gr) ternary. Also shown are compositions of garnets in eclogite found as xenoliths in kimberlites from Yakutia, Russia, and South Africa (data sources as in Fig. 10).

composition of Hawaiian lavas, a variety of mantle xenoliths dominantly from Salt Lake Crater, the trace element systematics of these xenoliths and the presence of amphibole, phlogopite, and exotic glass pockets in some of the pyroxenites-suite xenoliths, concluded that the ambient temperature in the Salt Lake Crater lithosphere is perhaps no more than 1150°C. As mentioned above, recent work has shown that phlogopite in some of these xenoliths is in isotopic disequilibrium with cpx and garnet (Bizimis *et al.*, 2003*b*), and hence, on this basis, we conclude that the subsolidus temperature estimates provided here are only for the anhydrous silicate mineralogy, and may have nothing to do the subsequent phlogopite formation event.

For samples where the composition of the exsolved phase in the host cpx could be determined, reconstructed cpx compositions were used along with coexisting garnet in the same xenolith to estimate pre-exsolution temperatures (Table 10). In these calculations, with the pressure input of 3 GPa, only the thermometric formulation of Ellis & Green (1979; EG79) was used. We note, however, that these calculations critically hinge upon the estimated volume of the exsolved phase dissolved back into the host cpx, which, in the absence of multiple sections of the same rock, can have a fairly large uncertainty. Hence, besides the inherent uncertainty in the retrieval of temperature from the thermometric formulation itself, there is this added unknown regarding the precision with which the original composition of the cpx can be reconstructed. Notwithstanding these issues, the pre-exsolution temperatures, using the EG79 thermometer, range from as low as 1216°C to as high as 1608°C, and hence, are moderately to significantly higher than the post-exsolution temperatures. However, out of 20 samples for which pre-exsolution temperatures could be calculated, 18 fall in the range ~1250–1420°C. This difference in the temperature estimates [i.e. between post- and pre-exsolution stage(s)], suggests that the xenoliths must have resided and cooled below the solidus of the mantle from which they were derived.

Both pre- and post-exsolution temperatures, although generally higher (by ~200–400°C) than the geotherm (~1100°C at 3·0 GPa) expected for a ~90 Ma oceanic lithosphere, are also lower by ~100–200°C than the anhydrous solidus of mantle peridotite in the 3–4 GPa pressure range (Walter, 1998). Sen *et al.* (2005) suggested, on the basis of similar observations (post-exsolution temperatures and the presence of phlogopite in some of these xenoliths), that the higher temperatures recorded for the garnet pyroxenites were a result of heating of the wall-rock by the ascending magmas that perhaps erupted as Honolulu Volcanics. However, the model of Sen *et al.* (2005) supposes that the garnet-pyroxenite xenoliths were already in place during the passage of these magmas, a suggestion seemingly in contradiction to the results of Bizimis *et al.* (2005*c*), who on the basis of isotope and trace-element work, interpreted these garnet-pyroxenite xenoliths as cumulates genetically related to 'HV-type' melts. Additionally, the difference in post- and pre-exsolution temperatures suggests that for phlogopite to be present as a stable phase in at least some of these xenoliths, this cooling must have occurred. Furthermore, the pre-exsolution temperatures of these xenoliths are also lower than the recently determined liquidus temperatures (1455–1485°C at 2–2·5 GPa) of one of the garnet-pyroxenite xenoliths (Keshav *et al.*, 2004), which suggests that the garnet pyroxenites are not frozen melts. Temperature estimates obtained using the two-pyroxene thermometers (Brey & Koehler, 1990) are also very similar to those obtained using the garnet–cpx thermometers. For example, the presence of opx exsolution in the host cpx allows the use of two-pyroxene thermometry to retrieve thermal re-equilibration temperatures. The results are in the range 1170–1290°C, which overlaps the estimates obtained from the garnet–cpx thermometers. Hence, on the basis of the temperature estimates presented here, if the previous suggestions that the higher temperatures recorded for garnet-pyroxenite xenoliths are a reflection of their interaction with passing

Table 5: Major element composition of spinels

Sample no.:	1	1	1	1	2	2	2	3	3	3	4	6
Type:	E2	I	In	G	I	E1	G	I	R1	R2	R	E1
SiO_2	0·21	0·14	0·17	0·18	0·27	0·06	0·04	0·12	0·16	0·09	0·24	0·06
TiO_2	0·34	0·27	0·21	0·38	11·98	0·37	0·36	16·88	0·57	0·78	0·50	1·19
Al_2O_3	55·9	57·72	59·38	55·38	11·16	61·39	60·52	9·61	59·75	57·78	56·64	49·84
Cr_2O_3	7·35	6·4	4·39	7·55	0·85	1·99	2·21	0·03	0·16	0·14	0·13	0·63
FeO^*	16·62	17·10	17·31	18·27	69·79	18·96	17·82	64·87	23·12	28·15	25·96	35·76
MnO	0·13	0·11	0·21	0·00	0·12	0·10	0·09	0·23	0·12	0·23	0·19	0·08
MgO	17·80	18·28	18·43	17·76	5·82	18·16	17·99	8·21	15·91	13·31	15·25	13·01
CaO	0·10	0·01	0·00	0·00	0·18	0·07	0·00	0·09	0·08	0·08	0·02	0·07
Na_2O	0·02	0·02	0·01	0·01	0·03	0·00	0·01	0·02	0·00	0·00	0·05	0·03
K_2O	0·00	0·00	0·00	0·00	0·00	0·00	0·00	0·00	0·00	0·00	0·00	0·00
Sum	98·49	100·07	100·02	99·54	100·22	101·10	99·05	100·07	99·87	100·60	98·98	100·69
Si	0·005	0·003	0·004	0·004	0·010	0·001	0·001	0·004	0·004	0·002	0·006	0·001
Ti	0·006	0·005	0·004	0·007	0·338	0·001	0·007	0·464	0·011	0·015	0·010	0·025
Al(IV)	—	—	—	—	—	—	—	—	—	—	—	—
Al(VI)	1·768	1·790	1·831	1·745	0·494	1·871	1·876	0·414	1·876	1·850	1·826	1·676
Cr	0·155	0·133	0·090	0·159	0·025	0·040	0·046	0·001	0·003	0·003	0·002	0·014
Fe^{3+}	0·074	0·094	0·075	0·081	0·548	0·077	0·056	0·555	0·118	0·140	0·157	0·281
Fe^{2+}	0·276	0·248	0·281	0·297	1·245	0·299	0·302	1·113	0·353	0·446	0·375	0·446
Mn	0·002	0·002	0·002	—	0·003	0·002	0·000	0·007	0·002	0·005	0·004	0·002
Mg	0·711	0·717	0·718	0·707	0·326	0·700	0·705	0·447	0·631	0·538	0·621	0·553
Ca	0·001	0·001	0·003	0·002	0·001	0·001	0·001	0·002	0·001	0·002	0·000	0·000
Na	0·001	0·001	0·001	0·001	0·002	0·001	0·000	0·001	0·000	0·000	0·002	0·002
K	0·000	0·000	0·000	0·000	0·000	0·000	0·000	0·000	0·000	0·000	0·000	0·000
O	4	4	4	4	4	4	4	4	4	4	4	4
Sum	3·000	3·000	3·000	3·000	3·000	3·000	3·000	3·000	3·000	3·000	3·000	3·000
Sp	72·03	74·23	71·84	70·43	20·74	70·02	69·99	28·66	64·10	54·67	62·33	55·32
Chr	7·77	6·58	4·53	8·00	1·79	2·04	2·31	0·07	0·17	0·14	0·14	0·71
Usp	2·42	2·10	1·44	2·50	21·37	2·37	2·30	29·43	3·12	3·44	2·66	5·40
Mt	3·71	4·65	3·78	4·09	38·98	3·90	2·86	38·70	5·89	6·99	7·88	14·09
Her	14·04	12·43	18·38	14·96	17·10	21·65	22·52	3·11	26·69	34·72	26·97	24·46
Mg-no.	72·03	74·23	71·84	70·43	20·74	70·02	69·99	28·66	64·10	54·67	62·33	55·32
Cr-no.	8·09	6·92	4·72	8·37	4·85	2·13	2·39	0·66	0·18	0·16	0·15	0·84

Sample no.:	6	6	7	8	10	10	11	11	11	12	12
Type:	E1	G	G	G	G1	G2	G1	G2	E1	I1	I2
SiO_2	0·18	0·06	0·08	0·06	0·06	0·07	0·07	0·10	0·06	0·11	0·06
TiO_2	11·30	0·85	0·00	1·00	0·34	0·35	0·25	0·42	0·49	0·20	0·94
Al_2O_3	15·83	59·84	61·14	56·73	61·35	59·29	61·66	53·41	51·52	61·89	45·84
Cr_2O_3	0·61	0·15	0·06	2·67	1·38	3·21	0·84	7·03	8·40	1·44	12·80
FeO^*	62·06	23·78	22·05	22·76	17·22	18·80	20·00	22·75	23·85	18·20	25·83
MnO	0·19	0·22	0·22	0·08	0·02	0·00	0·07	0·10	0·09	0·20	0·15
MgO	9·66	15·25	15·68	16·27	18·56	18·25	18·97	16·87	16·94	17·81	14·59
CaO	0·09	0·05	0·04	0·02	0·01	0·00	0·01	0·01	0·17	0·01	0·01
Na_2O	0·00	0·00	0·023	0·03	0·05	0·00	0·01	0·00	0·01	0·00	0·00
Sum	99·94	100·20	99·32	99·62	99·37	100·01	101·80	100·69	101·20	99·96	100·22
Si	0·003	0·001	0·002	0·001	0·001	0·001	0·001	0·002	0·001	0·003	0·001
Ti	0·302	0·017	—	0·020	0·006	0·009	0·004	0·008	0·010	0·004	0·020
Al(IV)	—	—	—	—	—	—	—	—	—	—	—
Al(VI)	0·663	1·878	1·917	1·801	1·886	1·836	1·868	1·703	1·650	1·898	1·530
Cr	0·017	0·003	0·001	0·056	0·034	0·066	0·017	0·150	0·180	0·029	0·286
Fe^{3+}	0·498	0·172	0·073	0·128	0·082	0·090	0·116	0·146	0·154	0·069	0·152
Fe^{2+}	0·996	0·317	0·387	0·337	0·258	0·284	0·269	0·312	0·321	0·288	0·382
Mn	0·005	0·004	0·005	0·001	0·001	0·000	0·001	0·002	0·002	0·005	0·003
Mg	0·511	0·605	0·621	0·653	0·721	0·714	0·726	0·680	0·686	0·690	0·615
Ca	0·000	0·000	0·000	0·000	0·000	0·000	0·000	0·000	0·000	0·000	0·000
Na	0000	0·000	0·000	0·000	0·002	0·000	0·000	0·000	0·000	0·000	0·000
K	0·000	0·000	0·000	0·000	0·000	0·000	0·000	0·000	0·000	0·000	0·000
O	4	4	4	4	4	4	4	4	4	4	4
Sum	3·000	3·000	3·000	3·000	3·000	3·000	3·000	3·000	3·000	3·000	3·000
Sp	33·94	65·58	61·61	65·94	73·64	71·55	72·91	68·54	68·06	70·51	61·69
Chr	1·15	0·15	0·06	2·83	1·72	3·33	0·85	7·48	9·04	1·48	14·40
Usp	23·27	5·08	0·00	5·66	2·55	2·42	1·72	2·66	6·08	1·38	4·73
Mt	33·63	8·31	3·69	6·38	4·11	4·54	5·78	7·30	7·74	3·46	7·68
Her	7·98	20·86	34·62	19·17	17·96	18·14	18·72	14·00	9·05	23·15	11·48
Mg-no.	33·94	65·58	61·61	65·94	73·64	71·55	72·91	68·54	68·06	70·51	61·69
Cr-no.	2·51	0·16	0·07	3·05	1·80	3·50	0·90	8·11	9·85	1·54	15·77

(continued)

Table 5: Continued

Sample no.:	13	13	15	15	16	17	17	18	18	19	19	21
Type:	E1	G	G	E1	I	E2	G	V	V	G	E2	I
SiO_2	0·15	0·12	0·06	0·09	0·27	0·10	0·07	0·12	0·06	0·12	0·11	0·07
TiO_2	0·33	0·33	0·55	0·45	11·98	0·33	0·27	9·53	0·99	0·25	0·40	0·26
Al_2O_3	58·45	58·55	58·55	59·06	11·16	59·05	61·42	11·71	51·10	59·65	56·92	57·83
Cr_2O_3	3·82	3·35	0·85	0·43	0·85	2·67	1·48	0·72	0·64	0·58	4·15	3·72
FeO*	17·89	18·11	22·22	21·10	69·79	18·18	17·13	71·34	33·69	21·56	18·85	20·36
MnO	0·12	0·17	0·07	0·03	0·12	0·00	0·00	0·15	0·05	0·00	0·00	0·09
MgO	17·91	18·00	17·02	17·08	5·82	18·18	18·49	5·18	12·63	18·75	17·91	17·59
CaO	0·13	0·14	0·02	0·08	0·12	0·00	0·00	0·01	0·00	0·02	0·02	0·02
Na_2O	0·01	0·02	0·01	0·00	0·03	0·00	0·00	0·01	0·02	0·00	0·01	0·02
K_2O	0·00	0·00	0·00	0·00	0·00	0·00	0·00	0·00	0·00	0·00	0·00	0·00
Sum	98·83	98·78	99·37	98·32	100·22	98·51	98·87	98·77	99·18	100·94	98·37	99·99
Si	0·003	0·003	0·001	0·002	0·010	0·002	0·001	0·004	0·001	0·003	0·002	0·001
Ti	0·006	0·006	0·011	0·009	0·338	0·006	0·005	0·276	0·021	0·004	0·008	0·005
Al(IV)	—	—	—	—	—	—	—	—	—	—	—	—
Al(VI)	1·831	1·836	1·846	1·870	0·494	1·849	1·895	0·532	1·723	1·841	1·803	1·811
Cr	0·080	0·070	0·018	0·009	0·025	0·056	0·030	0·022	0·014	0·012	0·088	0·078
Fe^{3+}	0·079	0·080	0·136	0·132	0·559	0·080	0·075	0·805	0·231	0·091	0·084	0·099
Fe^{2+}	0·274	0·285	0·310	0·301	1·247	0·278	0·263	1·060	0·472	0·315	0·292	0·311
Mn	0·002	0·003	0·001	—	0·003	—	—	0·004	0·001	—	—	0·002
Mg	0·709	0·713	0·678	0·683	0·326	0·719	0·721	0·297	0·538	0·731	0·717	0·696
Ca	0·000	0·000	0·000	0·002	0·003	0·000	0·000	0·000	0·000	0·000	0·000	0·000
Na	0·000	0·000	0·000	0·000	0·000	0·000	0·000	0·000	0·000	0·000	0·000	0·000
K	0·000	0·000	0·000	0·000	0·000	0·000	0·000	0·000	0·000	0·000	0·000	0·000
O	4	4	4	4	4	4	4	4	4	4	4	4
Sum	3·000	3·000	3·000	3·000	3·000	3·000	3·000	3·000	3·000	3·000	3·000	3·000
Sp	72·11	71·39	68·59	69·38	20·73	72·09	73·26	21·93	53·28	69·85	71·05	69·13
Chr	4·02	3·53	0·89	0·41	1·78	2·81	1·52	1·34	0·72	0·61	4·43	3·91
Usp	2·34	2·25	3·45	2·92	21·34	2·31	1·97	20·68	4·31	1·53	2·69	1·64
Mt	3·98	4·05	6·79	6·56	39·45	4·05	3·73	49·22	11·62	4·69	4·27	4·99
Her	17·53	18·75	20·25	20·70	16·70	18·72	19·48	6·81	30·05	23·29	17·53	20·31
Mg-no.	72·11	71·39	68·59	69·38	20·73	72·09	73·26	21·93	53·28	69·85	71·05	69·13
Cr-no.	4·20	3·69	0·97	0·48	4·81	2·94	1·59	3·97	0·80	0·64	4·66	4·13

Sample no.:	22	22	24	24	25	26	27	27
Type:	G	E1	I	G	R	G	E1	I
SiO_2	0·07	0·10	0·09	0·08	0·15	0·12	0·15	0·11
TiO_2	0·34	0·45	0·40	0·54	0·05	1·79	9·70	9·63
Al_2O_3	59·30	54·29	53·61	54·25	62·01	46·13	11·00	11·02
Cr_2O_3	2·66	6·97	7·53	7·09	0·19	1·16	0·15	0·40
FeO*	19·02	21·83	21·50	21·89	21·32	37·81	73·12	74·92
MnO	0·09	0·09	0·09	0·02	0·19	0·09	0·11	0·10
MgO	17·85	17·24	17·66	16·99	16·71	12·86	5·10	5·14
CaO	0·01	0·08	0·00	0·00	0·00	0·01	0·00	0·00
Na_2O	0·01	0·00	0·00	0·00	0·00	0·00	0·00	0·00
K_2O	0·00	0·00	0·00	0·00	0·00	0·00	0·00	0·00
Sum	99·37	101·05	100·89	100·86	100·63	100·00	99·33	101·30
Si	0·002	0·002	0·002	0·002	0·003	0·003	0·005	0·004
Ti	0·006	0·009	0·008	0·010	—	0·039	0·282	0·275
Al(IV)	—	—	—	—	—	—	—	—
Al(VI)	1·848	1·715	1·697	1·717	1·909	1·590	0·501	0·494
Cr	0·055	0·147	0·159	0·150	0·003	0·026	0·004	0·012
Fe^{3+}	0·276	0·132	0·130	0·132	0·093	0·360	0·556	0·560
Fe^{2+}	0·002	0·300	0·296	0·301	0·338	0·414	1·356	1·366
Mn	—	0·002	0·002	—	0·004	0·002	0·003	0·003
Mg	0·703	0·688	0·707	0·679	0·650	0·560	0·294	0·291
Ca	0·000	0·000	0·001	0·000	0·000	0·000	0·000	0·000
Na	0·000	0·000	0·000	0·000	0·000	0·000	0·000	0·000
K	0·000	0·000	0·000	0·000	0·000	0·000	0·000	0·000
O	4	4	4	4	4	4	4	4
Sum	3·000	3·000	3·000	3·000	3·000	3·000	3·000	3·000
Sp	71·77	69·63	70·46	69·26	69·85	57·49	17·82	17·60
Chr	2·76	7·36	8·01	7·48	0·61	1·33	0·34	0·90
Usp	2·43	2·93	2·65	3·48	1·53	8·69	17·22	16·78
Mt	5·21	6·59	6·53	6·59	4·69	17·87	41·35	41·72
Her	17·81	13·47	12·34	13·16	23·29	14·60	23·25	22·97
Mg-no.	71·77	69·63	69·26	20·73	69·85	57·49	17·82	17·60
Cr-no.	2·92	7·92	8·05	4·81	0·647	1·66	0·91	2·38

E1, exsolved in cpx; E2, exsolved in opx; I, interstitial; G, garnet-rimmed; In, inclusion; R, reaction product. Two E1s, different kinds of spinel in the same pyx; G1 and G2, spinels of different compositions rimmed by different garnet grains in the same xenolith; R1 and R2, reaction products.

*Total Fe given as FeO.

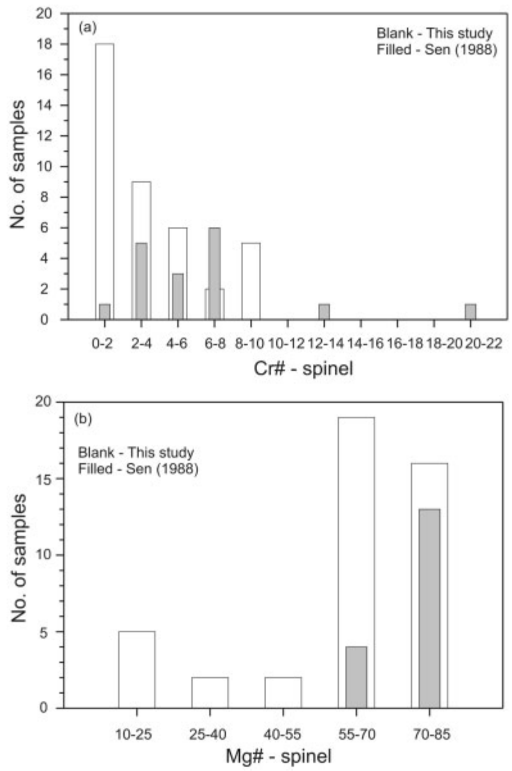

Fig. 15. Composition of spinel in the garnet-pyroxenite xenoliths in terms of (a) Cr-number [Cr/(Cr + Al)]; (b) molar Mg-number [Mg/(Mg + Fe)]. Data shown are dominantly for spinels occurring as cores in large garnets. (See text for further explanation.)

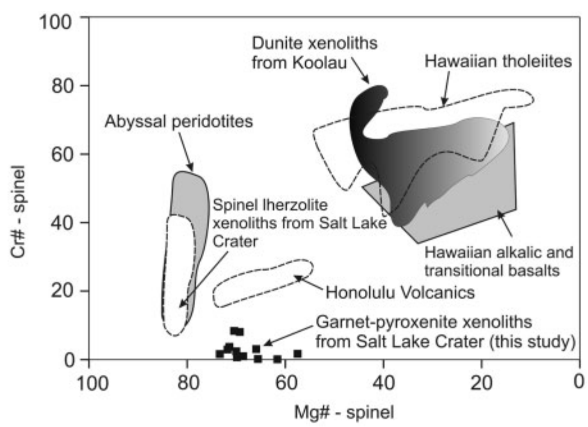

Fig. 16. Compositions (Cr-number vs Mg-number) of spinels in the garnet-pyroxenite xenoliths. Also shown are spinel compositions in abyssal peridotites (Dick & Bullen, 1984; Dick, 1989), Hawaiian lavas (Clague *et al.*, 1980; BVSP, 1981), Hawaiian (Koolau) dunites (Sen & Presnall, 1986), and spinel lherzolite xenoliths from Salt Lake Crater (Sen, 1988).

magmas (Sen, 1988; Sen *et al.*, 2005), then an unsettling question is, why do the spinel lherzolite xenoliths (also brought to the surface by HV lavas at Salt Lake Crater) not record temperatures [most are in the range 900–1100°C; Sen (1988)] as high as those calculated for

Table 6: Major element composition of phlogopites

Sample no.:	5	19	19	22	24
Type:	P	P	V	P	P
SiO_2	37·35	37·67	37·18	37·91	37·59
TiO_2	4·75	4·80	4·64	4·32	4·26
Al_2O_3	17·26	16·08	16·09	16·63	16·35
Cr_2O_3	0·37	0·41	0·35	0·25	0·45
FeO*	6·86	7·02	6·95	7·03	6·54
MnO	0·12	0·00	0·00	0·03	0·00
MgO	18·66	18·22	18·36	18·27	18·72
CaO	0·08	0·04	0·04	0·02	0·18
Na_2O	0·75	0·56	0·56	0·71	0·62
K_2O	9·10	9·24	9·14	9·00	8·72
Sum	94·60	94·04	93·13	94·19	93·43
Si	5·368	5·488	5·460	5·500	5·485
Ti	0·513	0·525	0·512	0·471	0·467
Al(IV)	—	—	—	—	—
Al(VI)	2·924	2·762	2·785	2·845	2·812
Cr	0·042	0·047	0·040	0·028	0·051
Fe	0·824	0·855	0·853	0·853	0·798
Mn	0·014	—	—	0·004	—
Mg	3·998	3·956	4·018	3·951	4·071
Ca	0·012	0·006	0·006	0·003	0·028
Na	0·209	0·158	0·159	0·199	0·175
K	1·338	1·717	1·712	1·667	1·623
O	22	22	22	22	22
Sum	15·461	15·518	15·548	15·524	15·514
Mg-no.	82·91	82·22	83·46	82·24	83·61

P, primary?; V, vein.
*Total Fe given as FeO.

garnet pyroxenite xenoliths? That is, why are spinel lherzolites apparently colder than the garnet-bearing pyroxenites? In other words, it is possible that the temperature estimates for the garnet pyroxenites reported here might represent a thermal 'kink' similar to that observed in continental mantle xenoliths (Boyd & Gurney, 1986). As noted above, some of these xenoliths contain majoritic garnets and diamonds, and are definitely sampling different mantle depths (and temperatures) than inferred previously (Sen, 1983, 1988). In contrast to temperatures, obtaining estimates on the final equilibration depth(s) of these xenoliths is considerably more difficult simply because there are compositionally multiple generations of discrete, large opx crystals in individual xenoliths. Not only do these opx crystals have distinct alumina concentrations, they also have variable Mg/Fe in individual xenoliths; these factors render unusable the pressure dependence of $(opx)^{Al_2O_3}$ isopleths in the garnet lherzolite stability field

Table 7: Major element composition of ilmenites

Sample no.:	4	5	9	9	16	26	27
Type:	E1/I1	E2/I2	E1	E2/I2	P	P	P
SiO_2	0·01	0·07	0·01	0·00	0·02	0·02	0·00
TiO_2	47·45	46·63	44·94	41·27	50·98	45·40	41·27
Al_2O_3	1·94	1·01	0·93	1·21	0·52	1·84	1·21
Cr_2O_3	0·15	0·10	0·48	0·02	0·07	0·34	0·02
FeO^*	45·51	45·19	45·82	50·61	39·56	46·51	50·61
MnO	0·23	0·16	0·18	0·11	0·44	0·08	0·11
MgO	4·67	7·05	6·10	5·14	6·19	6·81	5·14
CaO	0·00	0·13	0·02	0·01	0·26	0·03	0·01
Na_2O	0·00	0·00	0·00	0·00	0·00	0·00	0·00
K_2O	0·00	0·00	0·00	0·00	0·00	0·00	0·00
Sum	99·94	100·31	98·52	98·45	98·04	101·08	98·45
Si	—	0·001	—	—	—	—	—
Ti	0·89	0·871	0·863	0·813	0·953	0·844	0·813
Al(IV)	—	—	—	—	—	—	—
Al(VI)	0·057	0·029	0·028	0·037	0·015	0·053	0·037
Cr	0·002	0·001	0·009	—	0·001	0·007	—
Fe^{3+}	0·056	0·103	0·096	0·144	0·034	0·086	0·144
Fe^{2+}	0·818	0·727	0·772	0·801	0·757	0·753	0·801
Mn	0·004	0·003	0·004	0·002	0·009	0·001	0·002
Mg	0·173	0·261	0·232	0·200	0·229	0·251	0·200
Ca	—	0·003	—	—	0·003	—	—
Na	0·000	0·000	0·000	0·000	0·000	0·000	0·000
K	0·000	0·000	0·000	0·000	0·000	0·000	0·000
O	3	3	3	3	3	3	3
Sum	2·000	2·000	2·000	2·000	2·000	2·000	2·000
Ilm	78·04	66·62	70·11	69·90	72·91	69·03	69·90
Geik	16·53	23·91	21·09	17·51	22·62	23·02	17·51
Hem	5·42	9·46	8·79	12·58	4·46	7·93	12·58

E1/I1, exsolution or inclusion in cpx (exsolution?); E2/I2, exsolution or an inclusion in garnet; E1, exsolution in cpx; P, discrete.
*Total Fe given as FeO.

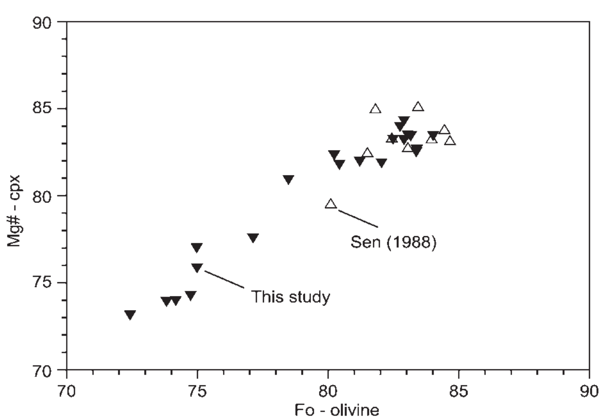

Fig. 17. Mg-number of cpx vs forsterite content of olivine in the garnet-pyroxenite xenoliths (modified after Keshav & Sen, 2004).

Table 8: Mg-number of minerals in samples with large olivine, opx, cpx, and garnet

Sample	Mg-number			
Number	Opx	Cpx	Gt	Ol
1	85·89(P)	83·51	74·52	84·13
1	85·48(H)			
1	83·54(E)			
2	85·48(P)	82·41	74·17	82·75
2	81·59(E)			
9	82·06(P1)	74·04	64·27	74·17
9	81·46(P2)			
10	86·79(H)	83·27	73·44	82·90
10	82·86(E)			
11	84·61(H)	82·58	74·20	82·52
12	85·23(P)	82·40	71·11	82·19
14	82·63(P)	75·56	63·50	75·97
17	85·34(H)	82·47	73·07	82·90
17	81·98(E)			
19	85·18(P)	83·31	73·12	82·96
19	85·10(H)			
19	84·04(E)			
20	86·76(H)	83·50	74·92	83·16
20	84·09(E)			
22	86·87(P)	81·96	72·44	82·04
22	82·79(E)			

The type of opx (P, without exsolution; H, with exsolution; E, exsolved in cpx) is indicated in parentheses.

(Macgregor, 1970, 1973; Wood & Banno, 1973; Nickel & Green, 1985) and its application as a suitable barometer. Hence, on this basis, we are not in a position to obtain estimates of the depth(s) of last equilibration for the suite of xenoliths described here. Instead, we focus on estimating the depth(s) of origin of these xenoliths by an alternative method described below.

Salt Lake Crater xenoliths as high-pressure crystals from magmas

Several lines of evidence indicate an igneous (cumulate) origin for the garnet-pyroxenite xenoliths. We arrive at this conclusion on the basis of the following observations and inferences.

(1) Although the minerals in these xenoliths have undergone some subsolidus deformation and recrystallization, distinct cumulate textures are still preserved in some xenoliths (e.g. Kuno, 1969; Frey, 1980; Sen, 1988; Sen & Jones, 1990). For example, in a few xenoliths discontinuous layers of garnet and spinel

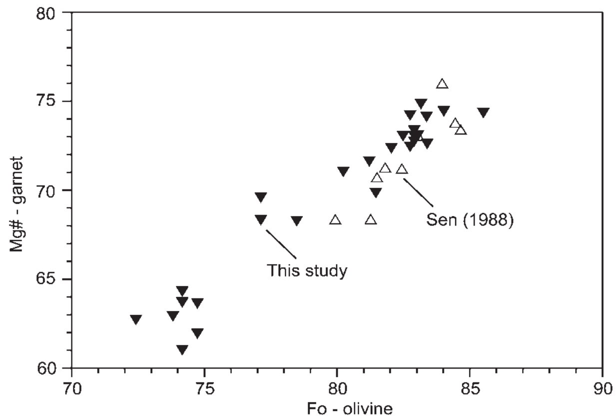

Fig. 18. Correlation of Mg-number in garnet and forsterite content in olivine in the garnet-pyroxenite xenoliths (modified after Keshav & Sen, 2004).

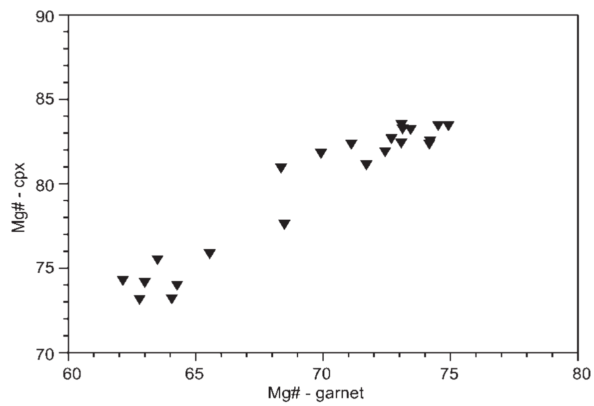

Fig. 19. Correlation of Mg-number in cpx vs Mg-number in garnet in the garnet-pyroxenite xenoliths (modified after Keshav & Sen, 2004). Data from this study.

are interlayered with grains of olivine. Garnet is found dispersed not only in the spinel–garnet zones, but also in the so-called 'transition zone'. In other xenoliths, either the entire rock is composed solely of garnet or it has a much smaller proportion of cpx and olivine grains that in turn are sometimes layered with subhedral garnet. Similar 'layered' textures have been observed in mantle xenoliths from the Delegate Pipe in Australia (Irving, 1974). It is possible that the layering may have developed in response to *in situ* oscillatory crystallization processes of the type proposed for giant mafic–ultramafic layered intrusions (McBirney, 1984). In some other xenoliths, there are two generations of spinel and garnet grains that occur with one generation of olivine crystals. The first generation of these spinel and garnet crystals exhibits intercumulus textures interspersed with euhedral olivine and subhedral cpx. The second generation of spinel and garnet crystals occurs as 'intrusive veins' in the host-rock, composed of spinel, garnet, olivine, and cpx. This second generation

Table 9: Temperature (T) estimates (post-exsolution) for the garnet-pyroxenite xenoliths

Sample no.	Kind of grains	T (K88,°C)	T (EG79,°C)
1	P-cpx/S-gt	1218	1232
1	H-cpx/S-gt	1229	1248
2	H-cpx/P-gt	1208	1283
2	H-cpx/S-gt	1223	1288
3	H-cpx/P-gt	1291	1330
6	H-cpx/P-gt	1294	1256
7	H-cpx/P-gt	1272	1311
7	H-cpx/S-gt	1249	1282
8	H-cpx/P-gt	1125	1183
9	H-cpx/P-gt	1253	1353
10	H-cpx/S-gt	1194	1225
11	P-cpx/S-gt	1263	1281
12	P-cpx/P-gt	1239	1263
13	H-cpx/P-gt	1187	1212
14	P1-cpx/P-gt	1176	1218
14	P2-cpx/P-gt	1142	987
15	H-cpx/P-gt	1244	1250
16	H-cpx/P-gt	1285	1295
17	H-cpx/P-gt	1235	1326
18	H-cpx/P-gt	1189	1244
19	H-cpx/P-gt	1273	1283
20	H-cpx/P-gt	1266	1274
21	P-cpx/P-gt	1201	1260
22	H-cpx/S-gt	1260	1254
24	H-cpx/P-gt	1223	1268
24	H-cpx/S-gt	1229	1281
25	H-cpx/P1-gt	1213	1247
25	H-cpx/P2-gt	1334	1342
27	H-cpx/P-gt	1139	1161
28	H-cpx/P/G-gt	1211	1237

H, host cpx; P, large cpx without exsolution; S, large garnet with spinel core; P/G (?), primary/grain boundary garnet; P1/P2, two or more compositionally distinct cpx.

of spinel and garnet crystals also exhibits cumulus textures, and, near the contact, reaction textures are seen between the intrusive vein and the pre-existing wall-rock. These intrusive events provide fairly robust textural evidence for an igneous origin of these xenoliths. Sen (1988), Sen & Jones (1990), and Keshav & Sen (2003) also described such cumulate textures. In general, subsolidus recrystallization appears to have occurred at temperatures of 1200–1300°C.

(2) Coexisting silicate minerals in chemical equilibrium with each other have high Fe/Mg [low molar Mg-number, Mg/(Mg + Fe)], and if the constituent

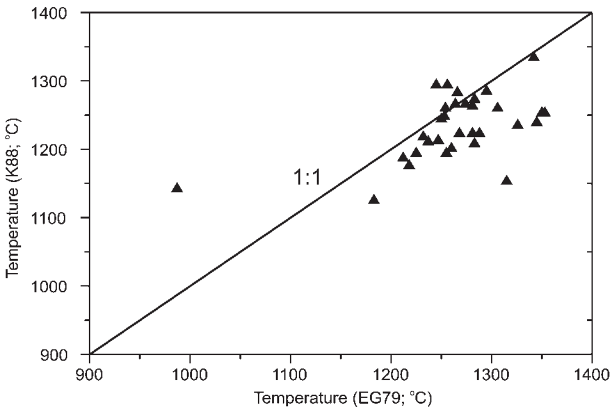

Fig. 20. Comparison of temperatures (post-exsolution) calculated using Ellis & Green (1979; EG79) and Krogh (1988; K88). With a few exceptions, there appears to be a reasonably good agreement between temperatures retrieved using these two routines. (See text for further details.)

Table 10: Temperature (T) estimates (pre-exsolution) for the garnet-pyroxenite xenoliths

Sample no.	Kind of grains	*T* (EG79, °C)
1	R-cpx/S-gt	1249
2	R-cpx/P-gt	1414
2	R-cpx/S-gt	1421
3	R-cpx/P-gt	1366
6	R-cpx/P-gt	1269
6	R-cpx/S-gt	1258
7	R-cpx/P-gt	1392
7	R-cpx/S-gt	1362
8	R-cpx/P-gt	1218
10	R-cpx/S-gt	1216
13	R-cpx/P-gt	1219
15	R-cpx/P-gt	1306
16	R-cpx/P-gt	1536
17	R-cpx/P-gt	1253
18	R-cpx/P-gt	1296
19	R-cpx/P-gt	1266
20	R-cpx/P-gt	1264
22	R-cpx/S-gt	1304
27	R-cpx/P-gt	1608
28	R-cpx/P/G-gt	1290

R, reconstructed cpx; P, large garnet without spinel core; S, large garnet with spinel core; P/G (?), primary/grain boundary garnet.

minerals in these xenoliths were residues of partial melting as observed for abyssal peridotites (Dick & Bullen, 1984; Johnson & Dick, 1992; Johnson *et al.*, 1990), they would have had lower Fe/Mg ratios, higher Cr_2O_3, and lower Al_2O_3, Na_2O, and TiO_2 concentrations. On the basis of the compositional similarity of the constituent minerals in these xenoliths to the phenocrysts in the Hawaiian lavas (Fodor *et al.*, 1975; Clague *et al.*, 1980; BVSP, 1981; Baker *et al.*, 1996; Garcia, 1996; Frey *et al.*, 2000), a magmatic origin for these xenoliths is implied. Additionally, the cpx crystals in these xenoliths are substantially richer in Al_2O_3 (Fig. 7), TiO_2 (Fig. 8), and Na_2O (Fig. 9) than those found in residual abyssal peridotites and harzburgites (lower-pressure residues of melting that have not been affected by subsequent melt impregnation events; Dick & Bullen, 1984; Dick, 1989). On the basis of this comparison, cpx in these xenoliths must have a cumulate (or broadly igneous) rather than a residual origin. In addition, garnets in the Salt Lake Crater xenoliths are low in Cr_2O_3 and high in Fe/Mg, two chemical traits that rule out a residual origin.

(3) Trace element studies have demonstrated that garnet-bearing xenoliths at Salt Lake Crater cannot be either restites or crystallized melts. This conclusion has been reached on the basis of the low abundance of incompatible elements (Frey, 1980; Bizimis *et al.*, 2005*c*), and the chondrite-normalized rare earth element (REE) patterns of the constituent minerals of these xenoliths, which are consistent with a cumulate origin (Frey, 1980; Sen *et al.*, 1993; Bizimis *et al.*, 2005*c*).

(4) High supersolidus temperatures that are estimated from the reconstituted cpx and garnet compositions also support an igneous origin. These temperatures correspond to solidus to supersolidus temperatures for anhydrous mantle lherzolite over a plausible pressure range of 2·5–5·0 GPa (Walter, 1998; Herzberg *et al.*, 2000; Hirschmann, 2000) and garnet clinopyroxenites (Ito & Kennedy, 1968; Hirschmann *et al.*, 2003; Keshav *et al.*, 2004).

On the basis of the arguments presented above, olivine, cpx, and garnet are considered to be cumulus phases that coexisted with magma at high pressure. In an effort to determine the pressure (depth) of origin where such cumulus phases could have crystallized from magmas, we use high-pressure liquidus experimental studies in the $CaO–MgO–Al_2O_3–SiO_2$ (CMAS) system. The CMAS system is chosen for the following reasons: (1) it can be used to represent 85–90% of the Earth's mantle (Presnall, 1999); (2) phase relations are relatively well constrained; (3) phase relations in CMAS are similar to those in $CMAS–Na_2O$ (CMASN; Walter & Presnall, 1994) and CMAS–FeO (CMASF; Gudfinnsson & Presnall, 2000); (4) most importantly, this system is the best-studied analog system for mafic magmas. In discussing the petrogenesis of the SLC garnet-pyroxenite xenoliths, additional

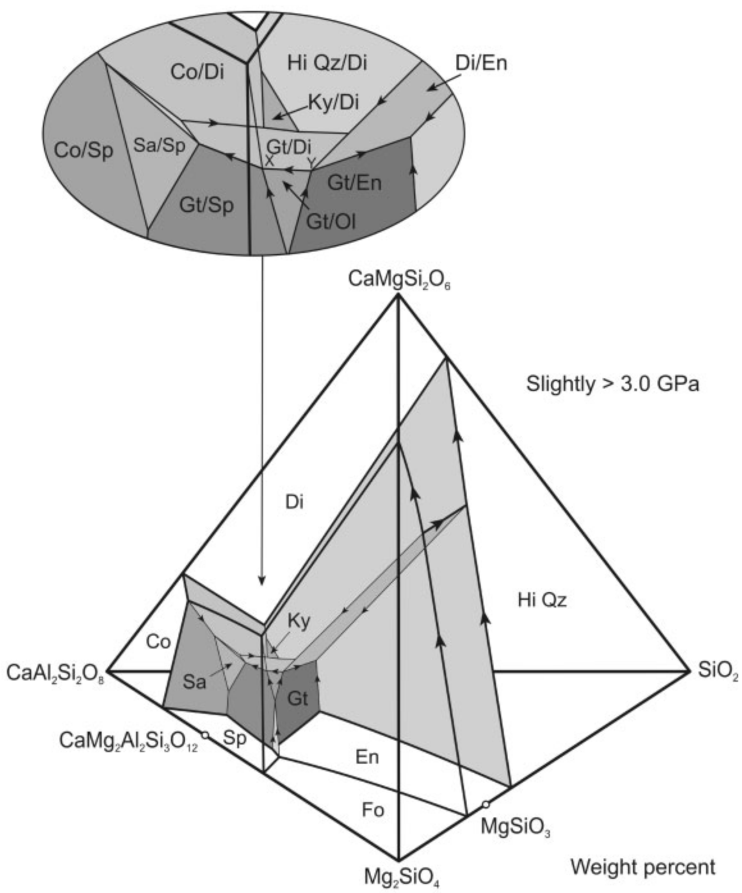

Fig. 21. $CaO–MgO–Al_2O_3–SiO_2$ (CMAS) liquidus phase relations in the tholeiitic portion of the basalt tetrahedron at a pressure slightly greater than 3 GPa (modified after Milholland & Presnall, 1998). Arrows show direction of decreasing temperature. Sp, spinel ($MgAl_2O_4$); Fo, forsterite (Mg_2SiO_4); En, enstatite ($MgSiO_3$); Wo, wollastonite ($CaSiO_3$); Di, diopside ($CaMgSi_2O_6$); Gr, grossular ($Ca_3Al_2Si_3O_{12}$); An, anorthite ($CaAl_2Si_2O_8$); Gt, garnet ($CaMg_2Al_2Si_3O_{12}$); Sa, sapphirine; Qz, quartz (SiO_2); Co, corundum (Al_2O_3); Ky, kyanite. Isobarically divariant liquidus surfaces in the inset are labeled according to the coexisting crystalline phases. The boundary line X–Y (in the inset) and other relevant features of this quaternary are discussed in the text.

textural constraint of garnet rims around spinel grains is also considered. Majoritic garnets and microdiamonds (not in the suite described here) in similar xenoliths from Salt Lake Crater also provide additional constraints on the depth of formation of these rocks (Keshav & Sen, 2001; Wirth & Rocholl, 2003; Frezzotti and Peccerillo, 2005).

Olivine–clinopyroxene–garnet in Salt Lake Crater xenoliths: insights from CMAS at high pressures

To model the petrogenesis of the xenoliths, we focus on the Si-poor portion of the tholeiitic part of the basalt tetrahedron in the CMAS system. Although model system liquidus data as a function of pressure are not available for the alkalic parts of the CMAS, CMASN, and CMASF systems, phase relations in the adjacent tholeiitic regions of these systems have been extensively studied (Kushiro, 1968; Presnall *et al.*, 1979; Walter & Presnall, 1994; Milholland & Presnall, 1998; Presnall, 1999; Liu & Presnall, 2000; Gudfinnsson & Presnall, 2000). In comparison with the tholeiitic portion of CMAS, liquid compositions in CMASN are shifted toward and into the alkalic portion of the basalt tetrahedron, while maintaining many of the topological features of the tholeiitic part of the CMAS basalt tetrahedron.

For pressures <3 GPa, the characteristic xenolith assemblage, olivine + clinopyroxene + garnet, does not exist in equilibrium with liquid (Milholland & Presnall, 1998). As pressure increases from 3 GPa, the liquidus boundary line for this assemblage becomes increasingly prominent and is shown in Fig. 21 as the short line, X–Y (in the inset), at a pressure slightly above 3 GPa. It is likely that at pressures >3 GPa, and at least up to 5 GPa (Weng, 1997), the fate of basaltic liquids is controlled by crystallization of olivine, clinopyroxene, and garnet. These phase relations indicate that the olivine + cpx + garnet assemblage could have crystallized from a liquid only at pressures above 3 GPa. With increasing pressure and addition of Na_2O to the system, this assemblage would shift out of the tetrahedron to the alkalic side of the forsterite–diopside–anorthite plane.

Spinel-cored garnets: precipitation from a liquid? Indications from CMAS

It was noted above that the spinel occurring as cores in garnets is of two types: (1) generally round and fairly uniform in size; (2) more irregular and amoeboidal types with embayed grain boundaries. Also, other phases (cpx, opx, or olivine) are not intergrown with the spinel–garnet assemblage. In addition, in almost all the xenoliths described here, two types of garnets are present, one that has a spinel core, and one that does not. It is possible that garnets lacking a spinel core are merely artifacts of the thin-sectioning process. However, it is also possible that these two different forms of garnets are real. For the rest of the discussion we assume the latter. Previous studies on similar xenoliths have hypothesized that spinel-cored garnets developed exclusively during subsolidus, near-isobaric cooling of a spinel-bearing assemblage through the spinel- to garnet-lherzolite boundary, by either of the two reactions sp + opx = gt + ol or sp + cpx + opx = gt + ol (Sen, 1988; Sen & Leeman, 1991; Sen *et al.*, 1993). However, if pyroxenes are reacting with spinel in the subsolidus regime, then this hypothesis is unlikely to be correct, as it would beg the question of why neither opx nor olivine is present in the spinel–garnet zones.

Interestingly, garnet-clinopyroxenite xenoliths from Dish Hill, California, and the Dominican Republic also have similar spinel-cored garnets, as noted by Shervais *et al.* (1973) and Abbott *et al.* (2004), respectively. It was concluded by those researchers, both on the basis of petrography and arguments from phase equilibrium studies, that there is no simple way, in the absence of either opx or olivine in the spinel–garnet zones, to generate spinel-cored garnets by a subsolidus reaction. However, the genesis of spinel-cored garnets could be explained if they formed in an 'open system' (Shervais *et al.*, 1973; via a melt-present reaction). Thus, an alternative explanation must also be found to model the generation of spinel-cored garnets in the Salt Lake Crater xenoliths. In so doing, it should be noted that such a model must also take into account the assemblage olivine, cpx, and garnet, that occurs at a minimum pressure of >3 GPa.

In Fig. 21, the univariant line fo–di–gt–liq (X–Y, the inset) meets the sp–gt–liq divariant surface at X. This surface is a reaction surface, where spinel reacts with the liquid to produce garnet. The coefficient for spinel in reaction with the liquid will be small, as the spinel composition plots far to the left on the $MgO–Al_2O_3$ join, whereas the garnet and liquid compositions are close together. On the assumption that the garnet–spinel surface is planar, the coefficients for this reaction at 3 GPa are approximately 97 liq + 3 sp = 100 gt. With increasing pressure, the garnet–spinel surface will move away from the SiO_2 apex, and at some higher pressure (perhaps ~5–6 GPa), spinel will change sides in the equation to produce the reaction liq = gt + sp. That is, the spinel–garnet divariant surface would no longer be a reaction surface.

We suggest the following explanation for the spinel-cored garnets. We assume the existence of a deep and large magma chamber that crystallizes garnet, clinopyroxene, and olivine along the univariant line, X–Y (Fig. 21; inset). We assume further that at the top cooling surface of this magma chamber, olivine, clinopyroxene, and garnet are crystallizing from a liquid on the line X–Y and close to X. The high density of spinel would cause it to sink to greater depths in the magma chamber, where the pressure would be slightly higher. At this pressure, the garnet–spinel surface would be slightly shifted toward the anorthite–forsterite–diopside face and the spinel would lie in a magma that would crystallize garnet alone, not garnet + spinel + olivine. The spinel would be out of equilibrium with this melt and would start to dissolve. However, it would also serve as a nucleation surface for garnet. This would explain both the corroded appearance of some of the spinel cores (Fig. 3c) and the garnet rims. Because garnet would be the phase crystallizing from this part of the magma chamber, some of the garnets would initiate their crystallization directly from the melt and would contain no spinel cores.

In the model presented above, the important thing to note is that the entire crystallization must occur at these high pressures (>3·0 GPa), as the fo + di + gt + liq univariant line disappears below 3 GPa. In addition, phase relations also indicate that the liquid precipitating olivine, cpx, garnet, and spinel-cored garnet could have been slightly alkalic.

The estimated pressure of crystallization of the Salt Lake Crater xenoliths is higher than that in all but two of the previous studies (Sen & Jones, 1990; Keshav & Sen, 2003). However, this minimum pressure of 3·0 GPa also raises a few concerns. For example, as mentioned above, majoritic garnets and diamonds occur in some of these garnet-pyroxenite xenoliths from Salt Lake Crater. As the formation of majoritic garnets and diamonds requires pressures of at least 5–6 GPa, one way to reconcile this discrepancy between the two pressure estimates is if the entire crystallization process (formation of ol + cpx + gt, spinel-cored garnets, majoritic garnets, and diamonds in the xenoliths) occurs at a pressure of at least 5 GPa. This pressure is also in excellent agreement with phase relations determined in the tholeiitic portion of the CMAS system at 5 GPa (Weng, 1997), which show that with increasing pressure the boundary line fo–di–gt–liq becomes increasingly prominent in dictating the crystallization path of mafic magmas. The estimated pressure of 5 GPa is also in seemingly reasonable agreement with the suggested depth of generation estimates (equivalent to ~5 GPa) of the primary tholeiitic magmas at Hawaii (Gudfinnsson & Presnall, 2004). Hence, taken together, it seems that the primary crystallization pressure for the xenoliths described in this study could be about 5 GPa, corresponding to a depth of ~150–160 km. This depth estimate also requires that the Honolulu Volcanics that brought the xenoliths to the surface must originate at similar or greater depths; this is greater than that based on some earlier geochemical studies of these lavas (Clague & Frey, 1982; Class & Goldstein, 1997; Yang *et al.*, 2003), which postulated that they originated in the lithosphere (Clague & Frey, 1982; Yang *et al.*, 2003).

Possible melts in equilibrium with the xenoliths

In this section we use major-element partition coefficients from the high-pressure peridotite melting experimental data of Walter (1998) to calculate the putative melt composition in equilibrium with the individual minerals in the xenoliths. We also use the parameterization provided by Walter (1998, 1999) to calculate near-solidus melt compositions at 3 and 5 GPa. It is assumed that melting, melt segregation, and fractional crystallization occur exclusively in the garnet lherzolite stability field (also as required by the phase equilibria discussed above). The source is also assumed to be homogeneous. These calculated melt compositions are then compared with late-stage, strongly alkalic lavas belonging to the Honolulu Volcanic Series on Oahu (Clague & Frey, 1982). The following parameters have been used in these numerical experiments: $K_D{}^{ol/melt}$ and $K_D{}^{cpx/melt}$ of 0·3 and 0·35, respectively. K_D is the Fe–Mg exchange coefficient between crystalline phase and melt. We also use D_{Na} and D_{Al} of 0·39 and 0·64, respectively, where D is the partition coefficient (by weight) of Na and Al between cpx and melt. Some experimental studies suggest that $K_D{}^{ol/melt}$ and $K_D{}^{cpx/melt}$ increase with pressure (Takahashi & Kushiro, 1983; Ulmer, 1989; Gudfinnsson & Presnall, 2000), whereas Kushiro & Walter (1998) proposed that melt composition has more effect than pressure or temperature. However, for our purpose, we use the values mentioned above. Other parameterizations (Longhi, 2002) are not likely to significantly affect the calculations presented here.

The calculated Mg-number, Na_2O, and Al_2O_3 of the melts in equilibrium with olivine and cpx in the xenoliths vary in the range of ~48–62, 3·8–7·8 wt %, and ~9·1–12·6 wt %, respectively. Honolulu Volcanics with Mg-number, Na_2O, and Al_2O_3 of ~62–69, ~2·5–5·5 wt %, and ~10–12 wt %, respectively, have been proposed to be the parental magmas for the pyroxenite xenoliths from Salt Lake Crater (Frey, 1980; Sen, 1988). The calculated melts in equilibrium with the compositions of olivine and cpx in the SLC xenoliths are similar to the HV in terms of their Na_2O and Al_2O_3 contents. However, compared with the published data on the HV, the calculated melts extend to much lower Mg-number (48–62), and thus appear to be significantly more fractionated. Although the calculated melt compositions, in terms of their Mg-number, resemble some of the Hawaiian tholeiites (Baker *et al.*, 1996; Garcia, 1996; Yang *et al.*, 1996), they differ in being too alkalic, and poorer in Al_2O_3. Thus, on the basis of major elements (this study), it appears that there may not be a genetic link between the HV and the garnet-pyroxenite xenoliths. Comparison of the calculated melts with the experimental data of Walter (1998) at pressures of 3–5 GPa indicates that even the most primitive calculated melt with ~4 wt % Na_2O, ~9 wt % Al_2O_3, and Mg-number of ~62 is far removed from the reported moderate-degree partial melts (F ~13%), which have ~1–1·5 wt % Na_2O and Mg-number of ~75–77 (Walter, 1998). When the parameterizations provided by Walter (1999) are used to retrieve the compositions of the near-solidus melts of a fertile, garnet lherzolite, the following results are obtained: ~1·8 wt % Na_2O, 14 wt % Al_2O_3, and ~13·8 wt % MgO at 3 GPa, and ~1·6 wt % Na_2O, ~7·8 wt % Al_2O_3, and ~20 wt % MgO at 5 GPa. More recently, Clague *et al.* (2006) reported major and trace element data for alkalic (nephelinites and alkalic basalts) lavas from the submarine stage of the HV activity. Clague *et al.* (2006) reported glass as well as bulk-rock analyses for these samples. The glass compositions are particularly significant as these represent liquid compositions. Whereas the submarine glasses have fairly evolved compositions with low MgO contents (4·5–7·8 wt %), the offshore HV bulk-rocks have high MgO (11·2–12·9 wt %), Ni (254–307 ppm), Cr (414–539 ppm), and Sc (22–27), reflecting their primitive magmatic nature. In this respect, the submarine lavas (bulk) are chemically similar to the HV onshore. The Na_2O and Al_2O_3 concentrations in the submarine HV glasses are ~4·5–8·4 wt % and ~13·5–15·5 wt %, respectively. Concentrations of Na_2O and Al_2O_3 in the bulk-rock lavas are in the range ~2·5–4·2 wt % and 10·8–13·9 wt %, respectively, and the submarine lavas appear to have lower Na_2O than the onshore HV. Additionally, the offshore lavas extend to slightly higher Al_2O_3 concentrations than the onshore HV lavas. In spite of these differences, the submarine lavas, in general, have compositional trends similar to those of the rejuvenated stage lavas (HV) on land. On the basis of the MgO contents of the glasses and petrography of the submarine samples recovered, Clague *et al.* (2006) suggested that the submarine HV lavas had cooled considerably during their passage through the lithospheric mantle and crust, and also that the crystals and melt did not efficiently separate. From the above, although it is clear that the melts hypothesized to be in equilibrium with the SLC garnet pyroxenites are also similar, in terms of their Na_2O and MgO contents, to the submarine HV glasses, the calculated melts are too poor in Al_2O_3. Hence, there is no clear relationship between alkalic lavas (either glasses or bulk-rock) belonging to the HV stage and the xenoliths described here.

To make a more convincing case regarding the above conclusions, it is tempting to compare the lava compositions with the near-solidus partial melt compositions of fertile garnet lherzolite. For this task, we use the parameterizations of Walter (1999) at 3–5 GPa. It is possible that in detail these parameterizations do not provide a rigorous insight into the actual process of melting, melt segregation, and fractional crystallization. In these calculations, a homogeneous garnet lherzolite source is assumed. The 3 GPa near-solidus (F ~0·5–2 wt %) compositions (by weight) obtained using the parameterizations (for equilibrium melting) are as follows: SiO_2 45·21%; Al_2O_3 14·26%; FeO^* 9·97%; MgO 14·52%; CaO 10·13%; Na_2O 1·48%. At 5 GPa, the near-solidus melt compositions are: SiO_2 ~44·9%; Al_2O_3 7·8%; FeO^* 12·8%; MgO 20·2%; CaO 9·7%; Na_2O 1·62%. These melt compositions are significantly different from the melts calculated to be in equilibrium with the mineral assemblage in the SLC garnet-pyroxenite xenoliths. More significantly, none of the melt compositions calculated to be in equilibrium with the xenoliths can, in normal mantle melting circumstances, represent primary or near-primary magma compositions.

On the basis of the arguments presented above, the suite of garnet-pyroxenite xenoliths described here cannot be treated as crystal cumulates that grew from the Honolulu Volcanics during their passage through the overlying mantle. The melt compositions calculated to be in equilibrium with the xenolith minerals could only be achieved after a significant degree of fractional crystallization of the parental magmas. At this stage, it is difficult to conclude if the parental magmas of the melts inferred to be in equilibrium with the xenolith minerals were tholeiitic or alkalic in nature. However, judging from the position of the boundary line fo–di–gt–liq at a pressure slightly greater than 3 GPa (Fig. 21), and also at 5 GPa (Weng, 1997), it appears that the parental melts could range from being tholeiitic to transitional. Whatever the case might be, it is fairly certain that melts similar to those inferred to be in equilibrium with the garnet-pyroxenite xenoliths never erupted on the island of Oahu.

The origin(s) of orthopyroxene

Chemical disequilibrium between opx and other major silicate minerals in the garnet-pyroxenite xenoliths is an issue that remains unresolved. Obvious chemical or textural evidence suggesting chemical disequilibrium (e.g. broken grain margins, chemical zoning, or resorbed rims) is lacking. In addition, opx, unlike large olivine, cpx, and garnet, has a restricted range of Mg-number (83–86). It could be argued that this opx comes from the lithosphere beneath Oahu. In this case, the opx initially formed part of spinel lherzolite wall-rocks, and thus had a higher Mg-number; however, as the rising magma(s) ponded, some of the opx became entrained in the magmas that ultimately precipitated olivine–cpx–gt–spinel-cored garnet assemblages. One argument against this model is that the opx lacks textural evidence (e.g. resorbed margins) for such melt–mantle interaction(s). Of course, it is possible that melt–mantle interaction did indeed occur but that its effects were very efficiently erased. However, even if such interaction did occur, it would beg the question of why this opx has a restricted Mg-number. Unlike previous studies where textural evidence, for example, the presence of composite xenoliths, could be cited as suggesting disequilibrium of opx (Sen, 1988; Sen & Leeman, 1991), the studied suite of xenoliths does not offer any such clues.

Some large opx have exsolved cpx and spinel, indicating that some cooling did occur, implying residence of opx at some level(s) in the mantle. However, compared with the thick blebs of opx, spinel, and garnet in the host cpx, the exsolved phases in host opx form rather thin exsolution lamellae, which are locally very closely spaced. These two features imply rather rapid cooling, indicating that exsolution may have occurred close to the solidus. Owing to the disequilibrium of opx with cpx and garnet, thermometric calculations cannot be used to address the origin(s) of the opx.

Two possibilities that lack arguments to either prove or disprove the origin of opx are: (1) if opx is a result of melt–mantle interaction, then obvious evidence for this interaction is lacking; (2) opx could be a cumulus mineral from some previous episode of melt crystallization.

Where does phlogopite fit in?

A puzzling observation is the virtual absence of phlogopite from the hundreds of spinel lherzolite xenoliths examined so far from Salt Lake Crater. In other words, why is phlogopite present only in garnet-bearing pyroxenites, even though the spinel lherzolites seem to be recording re-equilibration temperatures (900–1100°C) that are lower than those of the garnet pyroxenites? In this respect, the following observations or inferences may be significant.

(1) Texturally, phlogopites in the garnet-pyroxenite xenoliths are of two kinds. One has corroded margins and is in physical contact with large, discrete cpx and garnet. The second kind lacks imperfections (i.e. it is subhedral to euhedral), and is also in physical with contact large, discrete cpx or garnet. Although interstitial, both kinds of phlogopite appear to be in textural equilibrium with the rest of the xenolith. Similar, interstitially occurring phlogopite has been described in kimberlite-hosted continental mantle xenoliths

(Francis, 1976; Girod *et al.*, 1981; Canil & Scarfe, 1989). However, unlike in the Salt Lake Crater xenoliths, the phlogopite in continental mantle xenoliths is dominantly found in lherzolite xenoliths.

(2) The remarkably similar Fe/Mg of these SLC phlogopites with each other also suggests that these grains have attained major-element equilibrium. The distribution coefficients of Fe and Mg between phlogopite and coexisting olivine and cpx ($K_D = [Fe/Mg]_{phlogopite}/[Fe/Mg]_{olivine,\ cpx}$) are close to unity and similar to those observed in continental mantle xenoliths. Unfortunately, the influence of pressure, temperature, oxygen fugacity, and bulk composition on the mineral chemistry and phase relations of Ti-bearing phlogopites has not been systematically evaluated, and this prevents us from performing a rigorous comparison of the Salt Lake K_D values with those derived from experimental data (Esperanca & Holloway, 1986, 1987).

Experimental studies in which phlogopite has been equilibrated with olivine, cpx, or garnet show a wide range of K_D values (0·65–3·00). Further, these values seem to be uncorrelated with temperature, oxygen fugacity, water pressure, total pressure, or bulk composition (Esperanca & Holloway, 1986, 1987). Thus, in addition to the reasons cited above, the presence of interstitial phlogopite in the Salt Lake xenoliths provides few clues to its secondary or primary nature.

Possible clues to the origin of the phlogopite might come from isotopic data. For example, preliminary studies (Bizimis *et al.*, 2003*b*; M. Bizimis, unpublished data) indicate that some of the phlogopites in the garnet pyroxenites from Salt Lake Crater have identical $^{143}Nd/^{144}Nd$ ratios to the coexisting cpx. However, these phlogopites also have considerably more radiogenic $^{87}Sr/^{86}Sr$ than the coexisting cpx. The Sr isotope compositions of these phlogopites are even more radiogenic than the recently described offshore alkalic lavas that appear to be contemporaneous with the onshore HV lavas (Clague *et al.*, 2006). All these observations suggest that there is a more radiogenic Sr isotope component that is not recorded in the erupted lavas, but is 'seen' only in these phlogopites, indicating that the phlogopite in the Salt Lake Crater garnet pyroxenites is a phase introduced after the crystallization of the anhydrous silicate minerals. This discussion still does not offer any resolution to the question we asked at the beginning of this section; that is, why, in hundreds of spinel lherzolite xenoliths (also from Salt Lake Crater; brought up by HV lavas) examined so far, is phlogopite completely absent? What we can infer is that the association of phlogopite only with garnet-bearing xenoliths suggests that the processes responsible for its crystallization in the mantle beneath Oahu are restricted to greater depths. This observation also indicates that, even though phlogopite appears to be in major-element and sometimes textural equilibrium with the other crystalline phases in the garnet pyroxenites, its formation in the garnet pyroxenites and the formation of the parental HV magmas and HV lavas (the carriers) are perhaps not coeval events. The melt(s) responsible for the precipitation of phlogopite in the garnet pyroxenites do not infiltrate the shallower, more depleted spinel lherzolite 'stratum' in the lithospheric mantle section of Oahu, pointing to a deeper origin for these melts.

Magma chambers and deep magma ponding beneath Oahu: a unified model?

The two interfaces in the upper mantle where rising magmas might stall and fractionally crystallize are the Moho and the deeper lithosphere–asthenosphere boundary. In reality, these two interfaces are more likely to be diffuse zones. On the basis of the suite of xenoliths from Salt Lake Crater, we evaluate the minimum depth of magma generation and subsequent ponding beneath Oahu. Identification of magma storage zones at depth has implications for understanding sub-volcanic plumbing systems, and in this respect, the xenoliths described in this study offer valuable insights.

Hawaiian volcanism commences with rather small-volume, small-degree alkalic lavas (pre-shield) that erupt infrequently, ultimately giving way to large-volume, relatively large-degree melts (tholeiitic lavas; shield stage) that erupt more frequently. A reasonably good connection can be made between the nature of the magma storage system at a certain depth and the eruption rate (Clague, 1987). From dunite and lherzolite xenoliths entrained in the pre-shield alkalic stage lavas, the depth of such storage systems has been estimated at 20–25 km (Clague, 1988). This contrasts with the shield lavas, which are associated mostly with dunite cumulates, reflecting the presence of shallower (crust–mantle boundary; ~10 km depth) magma storage systems (Sen & Presnall, 1986). In contrast to the shield lavas, the garnet-bearing xenoliths in the post-erosional lavas (late-stage lavas) indicate a lack of shallow magma storage reservoirs during this period of rejuvenation and low eruption rates. This inference is also supported by the primitive geochemical characteristics of the late-stage lavas (Clague & Frey, 1982).

The Salt Lake Crater garnet-pyroxenite xenoliths described here are not simply cumulates related to the Honolulu Volcanics that bring them up to the surface. The magmas from which the protoliths to the xenoliths crystallized probably never erupted. Such magma compositions could exist at depth, solidified in conduits or small magma chambers within the mantle. On the basis of these arguments, a schematic model is proposed in Fig. 22. In this model the mantle lithosphere beneath Oahu is depicted as riddled with the solidified products of previous magmatic episodes that built the island. Ponding of shield-tholeiites happens mostly at the crust–mantle boundary

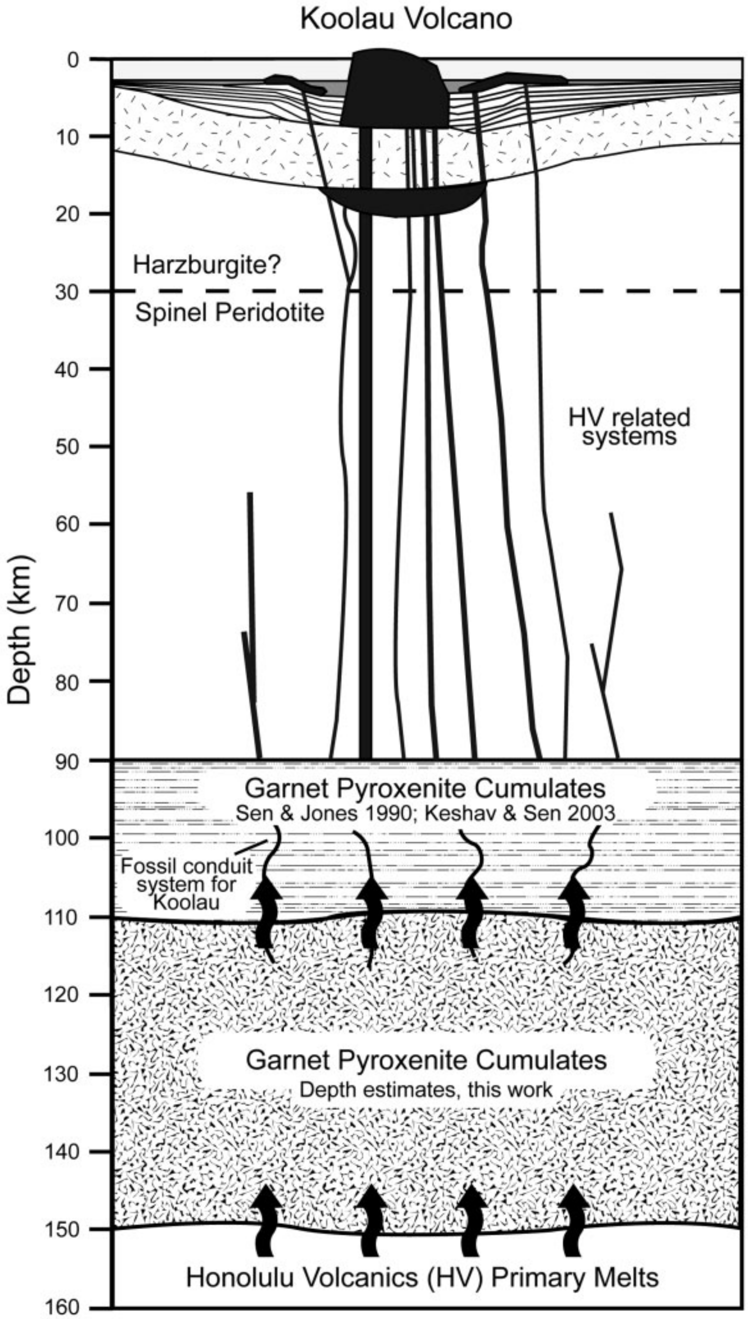

Fig. 22. A schematic model developed on the basis of petrography, mineralogy, mineral chemistry, and phase equilibria, for the petrogenesis of the Salt Lake Crater garnet-pyroxenite xenoliths. In this model, the mantle portion of the Oahu lithosphere is made up almost entirely of depleted spinel lherzolite and minor harzburgite (Sen, 1988). The thickness of the mantle lithosphere is ~65–70 km. The crust is about 11–15 km thick. The total thickness of the lithosphere beneath Oahu is ~90 km. This thickness is consistent with seismic studies (Bock, 1991). Tholeiitic basalts originating at a depth of ~80–90 km pond at the crust–mantle interface (~11–15 km) and undergo differentiation before erupting. The lower part (~60–90 km) of the Oahu lithosphere is extensively veined with fractional crystallization products resembling the garnet-clinopyroxenite xenoliths (shown as branching veins) that are intermixed with the more depleted spinel lherzolite residuum (Sen, 1988; Sen et al., 1993). Some fossil tholeiitic conduits are also shown to exist at these depths (~90–100 km). The garnet-pyroxenite suite of xenoliths is inferred to have originated at depths of ~150 km (corresponding to ~5 GPa) beneath Oahu. This depth estimate is ~60–70 km deeper than the top of the seismically detected lithosphere–asthenosphere transition. It is envisioned that at this depth 'blind' conduits exist where magmas (that never erupt) pond and 'plate' their fractional crystallization products in the form of the Salt Lake Crater garnet-pyroxenite xenoliths. A later magmatic event (the generation of Honolulu Volcanics) brings these cumulate-type xenoliths to the surface.

(Moho; ~10 km depth; Sen & Presnall, 1986; Clague, 1987). The lithospheric mantle is composed mostly of depleted peridotite; some highly depleted harzburgite may also be present. In contrast to the tholeiites, the parental magmas to the Honolulu Volcanics ascend directly from the deep mantle and exhume cumulate material (in form of garnet-bearing xenoliths) from great depths (>140 km; ~5 GPa). An attractive aspect of the model presented here is that it is also consistent with the presence of majoritic garnets (Keshav & Sen, 2001) and microdiamonds (Wirth & Rocholl, 2003; Frezzotti and Peccerillo, 2005) in some garnet-pyroxenite xenoliths, two additional features that bear testimony to the deep magmatic crystallization processes envisioned here. It is possible that the ponded material corresponds to a network of 'magma chambers'. The model developed here argues for the existence of magma chambers deep in the mantle beneath Oahu, and provides evidence that tholeiitic liquids undergo fractional crystallization deep in the mantle. In a later episode, low-degree, strongly alkalic magmas bring these cumulates (of broadly tholeiitic parentage) with them up to the surface. Salt Lake Crater is the only locality, to the best of our knowledge, in the oceanic regions where processes related to deep magma storage have been recognized; this has wide-ranging implications for furthering our understanding of magmatic processes at depth in the Earth and of the inner workings of volcanic systems.

CONCLUSIONS

Salt Lake Crater, Oahu is one of the very few locations in the ocean basins where abundant garnet-bearing xenoliths are found. Even though there is considerable heterogeneity in the xenoliths, some fairly robust conclusions, on the basis of petrography, major-element mineral chemistry, thermobarometry, high-pressure liquidus phase relations in the CMAS system and some simple calculations, can be reached, as follows.

(1) Subhedral clinopyroxene is the dominant mineral in all the xenoliths studied. Extensive exsolution textures are seen in the cpx. The common exsolved phases are opx and garnet, and to a lesser extent also spinel. Large, discrete olivine and garnet are the two other phases next in abundance to the cpx. Olivine is mostly euhedral to subhedral, whereas garnet is mostly subhedral and is also kelyphitized. Orthopyroxene occurs mostly in clusters, and in most xenoliths is present only in small amounts. Opx has exsolved cpx (and sometimes spinel) but lacks garnet exsolution. Many xenoliths do not have large, discrete opx. Spinel occurs as garnet-rimmed grains, as an exsolved phase in cpx or opx, and rarely also as interstitial grains.

(2) Although there is a wide range in the composition of the olivine, cpx and garnet, the major-element compositions are homogeneous on the scale of a single xenolith. Good Mg-number correlations exist between olivine, cpx, and garnet, suggesting that they represent an equilibrium assemblage. On the other hand, opx consistently appears to be out of major-element equilibrium with these three phases. Cpx-garnet and, in some instances, two-pyroxene thermometry indicates temperatures of subsolidus equilibration that are higher than equilibration temperatures in spinel lherzolites. On the basis of recalculated cpx compositions, temperatures that are moderately to considerably higher than subsolidus temperatures are retrieved, suggesting crystallization of the minerals in these garent-pyroxenite xenoliths from a magma.

(3) On the basis of major-element systematics and the presence of cumulate-type textures in some of the xenoliths, their comparison with other types of xenoliths from Salt Lake Crater, and phenocrysts in Hawaiian lavas, the garnet-pyroxenite xenoliths described in this study cannot be of residual origin. Instead, they are interpreted as cumulates from high-pressure melts.

(4) The mineral association olivine–cpx–garnet [the olivine eclogites of Kuno (1969)] in the studied xenoliths is unusual and in oceanic regimes, to the best of our knowledge, has so far been described only from Salt Lake Crater.

(5) Liquidus phase equilibrium experiments in the CMAS system at 3 GPa, slightly higher than 3 GPa, and also at 5·0 GPa can be used to model the petrogenesis of the Salt Lake Crater garnet pyroxenites. In the proposed model, spinel-cored garnets are the earliest cumulus minerals to crystallize from a slightly Si-poor melt (that is, still within the tholeiitic volume of the basalt tetrahedron). In this respect, the proposed model differs from the earlier models that seek to explain the spinel-cored garnets as products of near-isobaric subsolidus cooling. The assemblage olivine, cpx, and garnet in these xenoliths is stable only at a pressure >3·0 GPa. This pressure is critical, as below this pressure the univariant line fo–di–gt–liq disappears. The melts calculated to be in equilibrium with the dominant minerals in the xenoliths are similar, in terms of their Na_2O and Al_2O_3 contents, to the Honolulu Volcanics, but are significantly more fractionated. On this basis, previous models suggesting that the Honolulu Volcanics were the parental melts of these xenoliths would need to be reconsidered. However, it appears, on the basis of phase equilibria arguments presented here and the composition of the melts

inferred to be in equilibrium with the xenolith mineral assemblage, that the parental melts could have been transitional in composition. Additionally, even though the compositions of cpx in the xenoliths overlap the compositions of cpx found as phenocrysts in the erupted Hawaiian alkalic and tholeiitic lavas, it is fairly difficult to make a strict genetic connection between the lava-types and cpx compositions in the xenoliths.

(6) The origin of opx in the xenoliths remains unresolved; it could be a product of melt–mantle interaction or an earlier cumulate phase. Similar arguments can also be extended to the nature and origin of phlogopite that has been found so far only in the garnet pyroxenites. Phlogopite locally appears to be in textural and major-element chemical equilibrium with the other crystalline phases in the xenoliths. Preliminary Sr–Nd isotope data on phlogopites from a different batch of garnet-pyroxenite xenoliths to those studied here, however, indicates that formation of phlogopite was an event unrelated to the formation of the host xenoliths.

(7) It is suggested here that the minimum depth of crystallization of these xenoliths was ~5 GPa, which corresponds to a depth of ~150 km. This depth estimate is around 60–70 km deeper than the top of the seismically modeled asthenosphere beneath Oahu. Thus, it is argued that, contrary to popular belief, significant magma ponding and subsequent magmatic differentiation can indeed occur in the asthenosphere. Salt Lake Crater appears to be the only locality among the oceanic islands where deep magmatic fractional crystallization processes have been recognized.

ACKNOWLEDGEMENTS

S.K. thanks Tom Beasley at FCAEM, FIU for his help in acquisition of probe data on the described suite of mantle xenoliths. Barbara Maloney, also in the probe lab (FIU), makes the trains run on time and enforces good discipline in the lab through various draconian edicts. The University Graduate School, FIU, is acknowledged for the Dissertation Year Fellowship award to the first author. S.K. thanks Andrew Macfarlane and Grenville Draper for their critiques of several versions of this manuscript. Their comments led to a better and more focused presentation and are much appreciated. Michael Bizimis, Grenville Draper, Gummi Gudfinnsson, Claude Herzberg, Andrew Macfarlane, and Mike Walter are acknowledged for discussions on various aspects of the petrogenesis of these xenoliths and mantle petrology. The authors thank Fred Frey, Tom Sisson, and an anonymous referee for their sharp reviews on the original version of the manuscript, and Marjorie Wilson for a critique of a version of the revised manuscript. All the referees made important criticisms, while allowing us our point of view, even where they may not have completely agreed with the way we weighted the evidence. The result is a much-improved manuscript. The authors acknowledge Dennis Geist (editor) for his handling of the original version of the manuscript and for his amazing patience. The authors also warmly thank Marjorie Wilson for her editorial efforts and for challenging us to beat the manuscript into shape. This research was supported by US National Science Foundation grants OCE-9810961, OIA-9977642, and OCE-0241681 to GS and EAR-0106645 to D.C.P.

REFERENCES

Abbott, R. N., Jr, Draper, G. & Keshav, S. (2004). UHP magma paragenesis, garnet peridotite, and garnet clinopyroxenite: an example from Dominican Republic. *International Geology Review* **47**, 233–247.

Baker, M., Alves, S. & Stolper, E. M. (1996). Petrography and petrology of the Hawaii Scientific Drilling Project lavas: inferences from olivine phenocrysts abundances and compositions. *Journal of Geophysical Research* **101**, 11715–11728.

Basaltic Volcanism Study Project (1981). Oceanic intraplate volcanism. In: *Basaltic Volcanism on Terrestrial Planets*. New York: Pergamon Press, pp. 161–192.

Beeson, M. & Jackson, E. D. (1970). Origin of garnet pyroxenite xenoliths at Salt Lake Crater, Oahu. In: Morgan, B.A. (ed.) *Fiftieth Anniversary Symposia – Mineralogy and Petrology of the Upper Mantle; Sulfides; Mineralogy and Geochemistry of Non-marine Evaporites. Mineralogical Society of America, Special Papers* **3**, 95–112.

Bizimis, M., Sen, G. & Salters, V. J. M. (2003*a*). Hf–Nd isotope decoupling in the oceanic lithosphere: constraints from spinel peridotites from Oahu, Hawaii. *Earth and Planetary Science Letters* **217**, 43–58.

Bizimis, M., Sen, G. & Salters, V. J. M. (2003*b*). Volatile-rich mineral phases in the Hawaiian lithosphere: phlogopites and carbonates from 0-age garnet pyroxenite xenoliths from Salt Lake Crater (Oahu, Hawaii). *Transactions of the American Geophysical Union, Fall Meeting Supplement* **84**(46), V42H–05.

Bizimis, M., Sen, G., Salters, V. J. M., Lassiter, J. C. & Keshav, S. (2005*a*). Recycled oceanic mantle lithosphere in Hawaii: the samples and the models. *Transactions of the American Geophysical Union, Spring Meeting Supplement* **86**(18), V42A–04.

Bizimis, M., Sen, G., Salters, V. J. M., Lassiter, J. C. & Keshav, S. (2005*b*). The heterogeneous Hawaiian lithosphere: new isotope data from Kauai and Oahu peridotites. *Transactions of the American Geophysical Union, Fall Meeting Supplement* **86**(52), V51A–1467.

Bizimis, M., Sen, G., Salters, V. J. M. & Keshav, S. (2005*c*). Hf–Nd–Sr isotope systematics of garnet pyroxenites from Salt Lake Crater, Oahu, Hawaii: evidence for a depleted component in Hawaiian volcanism. *Geochimica et Cosmochimica Acta* **69**, 2629–2646.

Bock, G. (1991). Long-period S to P converted waves and the onset of partial melting beneath Oahu, Hawaii. *Geophysical Research Letters* **18**, 869–872.

Bodinier, J., Guiraud, M., Fabriès, J., Dostal, J. & Dupuy, C. (1987). Petrogenesis of layered pyroxenites from the Lherz, Freychinede and Prades ultramafic bodies, Ariege, French Pyrenees. *Geochimica et Cosmochimica Acta* **51**, 279–290.

Boyd, F. R. (1971). Enstatite–ilmenite and diopside–ilmenite intergrowths from the Monastery Mine. *Carnegie Institution of Washington Yearbook* **70**, 134–138.

Boyd, F. R. & Gurney, J. J. (1986). Diamonds and the African lithosphere. *Science* **232**, 472–477.

Boyd, F. R. & Nixon, P. H. (1973). Origin of the ilmenite–silicate nodules in kimberlites from Lesotho and South

Africa. In: Nixon, P. H. (ed.) *Lesotho Kimberlites*. Maseru: Lesotho National Development Corporation, pp. 254–268.

Brey, G. P. & Koehler, T. (1990). Geothermobarometry in four-phase lherzolites: II. New thermobarometers, and practical assessment of existing thermobarometers. *Journal of Petrology* **31**, 1353–1378.

Canil, D. & Scarfe, C. M. (1989). Origin of phlogopite in mantle xenoliths from Kostal Lake, Wells Gray Park, British Columbia. *Journal of Petrology* **30**, 1159–1179.

Carswell, D. (1975). Primary and secondary phlogopite and clinopyroxenes. *Physics and Chemistry of the Earth* **9**, 417–429.

Clague, D. A. (1987). Hawaiian xenolith populations, magma supply rates, and development of magma chambers. *Bulletin of Volcanology* **49**, 577–587.

Clague, D. A. (1988). Petrology of ultramafic xenoliths from Loihi Seamount, Hawaii. *Journal of Petrology* **29**, 1161–1186.

Clague, D. A. & Frey, F. A. (1982). Petrology and trace element geochemistry of the Honolulu Volcanics, Oahu: implications for the oceanic mantle below Hawaii. *Journal of Petrology* **23**, 447–504.

Clague, D. A., Fisk, M. R. & Bence, A. E. (1980). Mineral chemistry of basalts from Ojin, Nintoku, and Suiko seamounts, leg 55, DSDP. In: Jackson, E.D., Koisumi, I. *et al* (eds). *Initial Reports of the Deep Sea Drilling Project, 55.* Washington, DC: US Government Printing Office, pp. 607–637.

Clague, D. A., Paduan, J. B., McIntosh, W. C., Cousens, B. L., Davis, A. S., & Reynolds, J. R. (2006). A submarine perspective of the Honolulu Volcanics, Oahu. *Journal of Volcanology and Geothermal Research* **151**, 279–307.

Class, C. & Goldstein, S. L. (1997). Plume–lithosphere interactions in the ocean basins: constraints from the source mineralogy. *Earth and Planetary Science Letters* **150**, 245–260.

Dawson, J. B. & Reid, A. (1970). A pyroxene–ilmenite intergrowth from the Monastery Mine, South Africa. *Contributions to Mineralogy and Petrology* **26**, 296–301.

Delaney, J., Smith, J. V. & Nixon, P. H. (1979). Model for upper mantle below Malaita, Solomon Islands, deduced from chemistry of lherzolite and megacryst minerals. *Contributions to Mineralogy and Petrology* **70**, 209–218.

Dick, H. J. B. (1989). Abyssal peridotites, very slow spreading ridges and ocean ridge magmatism. In: Saunders, A. D. & Norry, M. J. (eds) *Magmatism in the Ocean Basinsı. Geological Society, London, Special Publications* **42**, 71–105.

Dick, H. J. B. & Bullen, T. (1984). Chromium spinel as a petrogenetic indicator in oceanic environments. *Contributions to Mineralogy and Petrology* **86**, 54–76.

Ducea, M., Sen, G., Eiler, J. M. & Fimbres, J. (2002). Melt depletion and subsequent metasomatism in the shallow mantle beneath Koolau volcano, Oahu (Hawaii). *Geochemistry, Geophysics, Geosystems* **3**, paper number 2001GC000184.

Ellis, D. J. & Green, D. H. (1979). An experimental study of the effect of Ca upon garnet–clinopyroxene Fe–Mg exchange equilibria. *Contributions to Mineralogy and Petrology* **71**, 13–22.

Esperanca, S. & Holloway, J. R. (1986). The origin of the high-K latites from Camp Creek, Arizona: constraints from experiments with variable f_{O_2} and a_{H_2O}. *Contributions to Mineralogy and Petrology* **93**, 504–512.

Esperanca, S. & Holloway, J. R. (1987). On the origin of mica-lamprophyres: experimental evidence from a mafic minette. *Contributions to Mineralogy and Petrology* **95**, 207–216.

Fodor, R. V., Keil, K. & Bunch, T. E. (1975). Contributions to the mineral chemistry of Hawaiian rocks. IV. Pyroxenes in rocks from Haleakala and West Maui volcanoes, Maui, Hawaii. *Contributions to Mineralogy and Petrology* **50**, 173–195.

Fodor, R. V., Keil, K. & Bunch, T. E. (1977). Contributions to the mineral chemistry of Hawaiian rocks. VI. Olivines in rocks from Haleakala and West Maui volcanoes, Maui, Hawaii. *Pacific Science* **31**, 299–308.

Francis, D. (1976). The origin of amphibole in lherzolite xenoliths from Nunivak Islands, Alaska. *Journal of Petrology* **17**, 357–378.

Frezzotti, M. & Peccerillo, A. (2005). High flux of (diamond CO_2–H_2O–H_2S) fluids in the mantle beneath Hawaii: evidence from fluid inclusions in garnet pyroxenites from Salt Lake Crater (Oahu, Hawaii). *Transactions of the American Geophysical Union, Fall Meeting Supplement* **86**(52), V33D–08.

Frey, F. A. (1980). The origin of pyroxenites and garnet pyroxenites from Salt Lake Crater, Oahu, Hawaii. *American Journal of Science* **280-A**, 427–449.

Frey, F. A., Clague, D. A., Mahoney, J. & Sinton, J. (2000). Volcanism at the edge of the Hawaiian plume: petrogenesis of submarine alkalic lavas from the North Arch volcanic field. *Journal of Petrology* **41**, 667–691.

Ganguly, J., Cheng, W. & Tirone, M. (1996). Thermodynamics of aluminosilicate garnet solid solution: new experimental data, an optimized data, and thermometric applications. *Contributions to Mineralogy and Petrology* **126**, 137–151.

Garcia, M. O. (1996). Petrography and olivine and glass chemistry of lavas from the Hawaii Scientific Drilling Project. *Journal of Geophysical Research* **101**, 11701–11714.

Garcia, M. O. & Presti, A. A. (1987). Glass in garnet pyroxenite xenoliths from Kaula Island, Hawaii: product of infiltration of host nephelinites. *Geology* **15**, 904–906.

Girod, M., Dautria, J. M. & deGiovanni, R. (1981). A first insight into the constitution of the upper mantle under the Hoggar area (southern Algeria): the lherzolite xenoliths in the alkali basalts. *Contributions to Mineralogy and Petrology* **77**, 66–73.

Green, D. H. (1966). The origin of 'eclogites' from Salt Lake Crater, Hawaii. *Earth and Planetary Science Letters* **1**, 414–420.

Gudfinnsson, G. H. & Presnall, D. C. (2000). Melting relations of model lherzolite in the system CaO–MgO–Al_2O_3–SiO_2–FeO at 0·7–2·8 GPa. *Journal of Petrology* **41**, 1241–1269.

Gudfinnsson, G. H. & Presnall, D. C. (2004). Generation of primary Kilauea magmas: constraints on pressure, temperature, and composition of melts. Transactions of the American Geophysical Union, Fall Meeting Supplement **85**(47), V51B–0552.

Gurney, J., Hesq, H. & Kable, E. (1973). Clinopyroxene–ilmenite intergrowths from kimberlite: a re-appraisal. In: Nixon, P. H. (ed.) *Lesotho Kimberlites*. Maseru: Lesotho National Development Corporation, pp. 238–253.

Haggerty, S. E. (1991). Oxide mineralogy of the upper mantle. In: Lindsley, D. H. (ed.) *Oxide Minerals: Petrologic and Magnetic Significance. Mineralogical Society of America, Reviews in Mineralogy* **25**, 355–407.

Herzberg, C. (1978). The bearing of phase equilibria in simple and complex systems on the origin and evolution of some well-documented garnet-websterites. *Contributions to Mineralogy and Petrology* **66**, 375–382.

Herzberg, C. & Zhang, J. (1996). Melting experiments on anhydrous peridotite KLB-1; composition of magmas in the upper mantle and transition zone. *Journal of Geophysical Research* **101**, 8271–8295.

Herzberg, C., Raterron, P. & Zhang, J. (2000). New experimental observations on the anhydrous solidus for peridotite KLB-1. *Geochemistry, Geophysics, Geosystems* **1**, paper number 2000GC000089.

Hirschmann, M. M. (2000). Mantle solidus: experimental constraints and the effects of peridotite composition. *Geochemistry, Geophysics, Geosystems* **1**, paper number 2000GC000070.

Hirschmann, M. M., Kogiso, T., Baker, M. & Stolper, E. M. (2003). Alkalic magmas generated by partial melting of garnet pyroxenite. *Geology* **31**, 481–484.

Hops, J., Gurney, J., Harte, B. & Winterburn, P. (1989). Megacrysts and high temperature nodules from the Jagersfontein kimberlite pipe. In: O'Reilly, S. Y. (ed.) *The Upper Mantle and Lower Crust in Continental Regions. Proceedings of the Fourth International Kimberlite Conference, Perth, 1986, Volume 2. Geological Society of Australia Special Publication* **14**, 759–770.

Irving, A. J. (1974). Geochemical and high pressure experimental studies of garnet pyroxenite and pyroxene granulite xenoliths from the Delegate basaltic pipes, Australia. *Journal of Petrology* **15**, 1–40.

Ito, K. & Kennedy, G. C. (1968). Melting and phase relations in the plane tholeiite–lherzolite–nepheline basanite to 40 kilobars with geological implications. *Contributions to Mineralogy and Petrology* **19**, 177–211.

Jackson, E. D. (1968). The character of the lower crust and upper mantle beneath the Hawaiian Islands. In: *XXIII International Geological Congress, Prague, Proceedings, Volume 1*, pp. 135–150.

Jackson, E. D. & Wright, T. L. (1970). Xenoliths in the Honolulu volcanic series, Hawaii. *Journal of Petrology* **11**, 405–430.

Johnson, K. T. M. & Dick, H. J. B. (1992). Open system melting and temporal and spatial variation of peridotite and basalt at the Atlantis II fracture zone. *Journal of Geophysical Research* **97**, 9219–9241.

Johnson, K. T. M., Dick, H. J. B. & Shimizu, N. (1990). Melting in the oceanic upper mantle: an ion microprobe study of diopsides in the abyssal peridotites. *Journal of Geophysical Research* **95**, 2661–2678.

Keshav, S. & Sen, G. (2001). Majoritic garnets in Hawaiian xenoliths: preliminary results. *Geophysical Research Letters* **28**, 3509–3512.

Keshav, S. & Sen, G. (2002). Exsolution times of Hawaiian garnet-pyroxenites. Transactions of the American Geophysical Union, Fall Meeting Supplement **83**(47), V62B–1409.

Keshav, S. & Sen, G. (2003). A rare composite xenolith from Salt Lake Crater, Oahu: high-pressure fractionation and implications for kimberlitic melts in the Hawaiian mantle. *Contributions to Mineralogy and Petrology* **144**, 548–558.

Keshav, S. & Sen, G. (2004). The depth of magma fractionation in the oceanic mantle: insights from garnet-bearing xenoliths from Oahu, Hawaii. *Geophysical Research Letters* **31**, doi:10.1029/2003GL018990.

Keshav, S., Sowerby, J. & Sen, G. (2001). Ilmenite exsolution in xenolithic garnets from the Hawaiian hot spot: evidence for the existence of high-titanium garnets in the Earth's mantle. *Transactions of the American Geophysical Union, Fall Meeting Supplement* **82**(17), V12B–0975.

Keshav, S., Gudfinnsson, G. H., Sen, G. & Fei, Y. (2004). High-pressure melting experiments on garnet clinopyroxenite and the alkalic to tholeiitic transition in ocean island basalts. *Earth and Planetary Science Letters* **223**, 365–379.

Kopylova, M., Russell, J. & Cookenboo, H. (1999). Petrology of peridotite and pyroxenite xenoliths from Jericho Kimberlite; implications for the thermal state of the mantle beneath the Slave Craton, northern Canada. *Journal of Petrology* **40**, 79–104.

Krogh, E. J. (1988). The garnet–clinopyroxene Fe–Mg thermometer—a reinterpretation of existing experimental data. *Contributions to Mineralogy and Petrology* **99**, 44–48.

Kuno, H. (1969). Mafic and ultramafic nodules in basaltic rocks of Hawaii. *Geological Society of America, Memoirs* **115**, 189–234.

Kushiro, I. (1968). Compositions of magmas formed by partial zone melting in the Earth's upper mantle. *Journal of Geophysical Research* **7**, 337–362.

Kushiro, I. & Walter, M. J. (1998). Mg–Fe partitioning between olivine and mafic–ultramafic melts. *Geophysical Research Letters* **25**, 2337–2340.

Lanphere, M. & Dalrymple, G. B. (1980). Age and strontium isotopic composition of the Honolulu Volcanic Series, Oahu, Hawaii. *American Journal of Science* **280-A**, 794–819.

Lassiter, J. C., Hauri, E. H., Reiners, P. & Garcia, M. O. (2000). Generation of Hawaiian post-erosional lavas by melting of a mixed lherzolite/pyroxenite source. *Earth and Planetary Science Letters* **178**, 269–284.

Li, X., Kind, R., Priestley, K., Sobolev, S. V., Tilmann, F., Yuan, X. & Weber, M. (2000). Mapping the Hawaiian plume conduit with converted seismic waves. *Nature* **405**, 938–941.

Liu, T.-C. & Presnall, D. C. (2000). Liquidus phase relations in the system $CaO–MgO–Al_2O_3–SiO_2$ at 2·0 GPa: applications to basalt fractionation, eclogites, and igneous sapphirine. *Journal of Petrology* **41**, 3–20.

Longhi, J. (2002). Some phase equilibrium systematics of lherzolite melting: 1. *Geochemistry, Geophysics, Geosystems* **3**, doi:10.1029/2001GC000204.

Macgregor, I. D. (1970). The effect of CaO, Cr_2O_3, Fe_2O_3, and Al_2O_3 on the stability of spinel and garnet peridotites. *Physics of the Earth and Planetary Interiors* **3**, 372–377.

Macgregor, I. D. (1973). The system $MgO–Al_2O_3–SiO_2$: solubility of Al_2O_3 in enstatite for spinel and garnet peridotite. *American Mineralogist* **59**, 110–119.

McBirney, A. R. (1984). *Igneous Petrology.* San Francisco, CA: Freeman and Cooper.

Milholland, C. S. & Presnall, D. C. (1998). Liquidus phase relations in the $CaO–MgO–Al_2O_3–SiO_2$ system at 3·0 GPa: the aluminous pyroxene thermal divide and high-pressure fractionation of picritic and komatiitic magmas. *Journal of Petrology* **38**, 3–27.

Morgan, W. J. (1971). Convection plumes in the lower mantle. *Nature* **230**, 42–43.

Mukhopadhyay, B. & Manton, W. I. (1994). Upper-mantle fragments from beneath the Sierra Nevada Batholith; partial fusion, fractional crystallization, and metasomatism in a subduction-related ancient lithosphere. *Journal of Petrology* **35**, 1417–1450.

Mysen, B. O. & Kushiro, I. (1977). Compositional variations of coexisting phases with degree of melting of peridotite in the upper mantle. *American Mineralogist* **62**, 843–865.

Nickel, K. G. & Green, D. H. (1985). Empirical geothermobarometry for garnet peridotites and implications for the nature of the lithosphere, kimberlites, and diamonds. *Earth and Planetary Science Letters* **73**, 158–170.

Presnall, D. C. (1999). Effect of pressure on fractional crystallization of basaltic magma. In: Fei, Y., Bertka, C. & Mysen, B. (eds) *Mantle Petrology: Field Observations and High Pressure Experimentation: a Tribute to Francis R. Boyd. Geochemical Society, Special Publications* **6**, 209–224.

Presnall, D. C., Dixon, J. R., O'Donnell, T. H. & Dixon, S. A. (1979). Generation of mid-ocean ridge tholeiites. *Journal of Petrology* **20**, 3–35.

Ringwood, A. E. & Lovering, J. F. (1970). Significance of pyroxene–ilmenite intergrowths among xenoliths in kimberlites. *Earth and Planetary Science Letters* **7**, 371–375.

Sautter, V. & Fabriès, J. (1990). Cooling kinetics of garnet websterites from the Freychinede orogenic lherzolite massif, French Pyrenees. *Contributions to Mineralogy and Petrology* **105**, 533–549.

Schmidberger, S. & Francis, D. (1999). Nature of the mantle roots beneath the North American Craton; mantle xenolith evidence from Somerset Island kimberlites. *Lithos* **48**, 195–216.

Sen, G. (1983). A petrologic model for the constitution of the upper mantle and crust of the Koolau shield, Oahu, Hawaii, and Hawaiian magmatism. *Earth and Planetary Science Letters* **62**, 215–228.

Sen, G. (1987). Xenoliths associated with the Hawaiian hot spot. In: Nixon, P. H. (ed.) *Mantle Xenoliths*. New York: John Wiley, pp. 359–375.

Sen, G. (1988). Petrogenesis of spinel lherzolite and pyroxenite-suite xenoliths from the Koolau shield, Oahu, Hawaii: implications for the petrology of the post eruptive lithosphere beneath Oahu. *Contributions to Mineralogy and Petrology* **100**, 61–91.

Sen, G. & Jones, R. (1988). Exsolved silicates and oxide phases from clinopyroxenes in a single Hawaiian xenolith: implications for oxidation state of the Hawaiian upper mantle. *Geology* **16**, 69–72.

Sen, G. & Jones, R. (1990). Cumulate xenolith in Oahu, Hawaii: implications for deep magma chambers and Hawaiian volcanism. *Science* **249**, 1154–1157.

Sen, G. & Leeman, W. (1991). Iron-rich lherzolite xenoliths from Oahu: origin and implications for Hawaiian magma sources. *Earth and Planetary Science Letters* **102**, 45–57.

Sen, G. & Presnall, D. C. (1986). Petrogenesis of dunite xenoliths from Koolau volcano, Oahu, Hawaii: implications for Hawaiian volcanism. *Journal of Petrology* **27**, 197–217.

Sen, G., Frey, F., Shimizu, N. & Leeman, W. (1993). Evolution of the lithosphere beneath Oahu, Hawaii: trace element abundances in mantle xenoliths. *Earth and Planetary Science Letters* **119**, 53–69.

Sen, G., Keshav, S., Presnall, D. C. & Weng, Y.-H. (2002). High-pressure polybaric fractionation and spinel–garnet–liquid reactions in garnet-bearing xenoliths from Oahu: evidence from CMAS. Transactions of the American Geophysical Union, Fall Meeting Supplement **83**(47), V62B–1410.

Sen, G., Keshav, S. & Bizimis, M. (2005). Hawaiian mantle xenoliths and magmas I. Composition and thermal structure of the lithosphere. *American Mineralogist* **90**, 871–887.

Shervais, J., Pike, J. E. N. & Schwarzmann, E. (1973). Garnet clinopyroxenite xenolith from Dish Hill, California. *Earth and Planetary Science Letters* **19**, 120–130.

Snyder, G., Taylor, L., Crozaz, G., Halliday, A., Beard, B., Sobolev, V. & Sobolev, N. (1997). The origin of Yakutian eclogite xenoliths. *Journal of Petrology* **38**, 85–113.

Sobolev, N., Lavrent'ev, Yu. G., Pokhilenko, N. & Usova, L. (1973). Chrome-rich garnets from the kimberlites of Yakutia and their parageneses. *Contributions to Mineralogy and Petrology* **40**, 39–52.

Takahashi, E. & Kushiro, I. (1983). Melting of dry peridotite at high pressures and magma genesis. *American Mineralogist* **68**, 129–145.

Ulmer, P. (1989). The dependence of Fe^{2+}–Mg cation partitioning between olivine and basaltic liquid on pressure, temperature, and composition. *Contributions to Mineralogy and Petrology* **101**, 261–273.

Vance, D., Stone, O. & O'Nions, R. K. (1989). He, Sr, and Nd isotopes in xenoliths from Hawaii and other oceanic islands. *Earth and Planetary Science Letters* **96**, 147–160.

Walter, M. J. (1998). Melting of garnet peridotite and the origin of komatiite and depleted lithosphere. *Journal of Petrology* **39**, 29–60.

Walter, M. J. (1999). Melting residues of fertile peridotite. In: Fei, Y., Bertka, C. & Mysen, B. (eds) *Mantle Petrology: Field Observations and High Pressure Experimentation: a Tribute to Francis R. Boyd. Geochemical Society, Special Publications* **6**, 225–240.

Walter, M. J. & Presnall, D. C. (1994). Melting behavior of simplified lherzolite in the system CaO–MgO–Al_2O_3–SiO_2–Na_2O from 7 to 35 kbar. *Journal of Petrology* **35**, 329–359.

Weng, Y.-H. (1997). Liquidus phase relations for the model basaltic tetrahedron diopside–anorthite–forsterite–quartz in the system CaO–MgO–Al_2O_3–SiO_2 at 5 GPa. PhD dissertation, University of Texas at Dallas.

White, R. W. (1966). Ultramafic inclusions in basaltic rocks from Hawaii. *Contributions to Mineralogy and Petrology* **12**, 245–314.

Wilkinson, J. F. G. (1976). Some sub-calcic clinopyroxenites from Salt Lake Crater, Oahu, and their petrogenetic significance. *Contributions to Mineralogy and Petrology* **58**, 181–201.

Wilson, J. T. (1963). A possible origin of the Hawaiian Islands. *Canadian Journal of Physics* **41**, 863–870.

Wirth, R. & Rocholl, A. (2003). Nanocrystalline diamond from the Earth's mantle underneath Hawaii. *Earth and Planetary Science Letters* **211**, 357–369.

Wood, B. J. & Banno, S. (1973). Garnet–orthopyroxene and orthopyroxene–clinopyroxene relationships in simple and complex systems. *Contributions to Mineralogy and Petrology* **42**, 109–124.

Woods, M. T. & Okal, E. (1996). Rayleigh-wave dispersion along the Hawaiian Swell; a test of lithospheric thinning by thermal rejuvenation at a hotspot. *Geophysical Journal International* **125**, 325–339.

Wyatt, B. (1977). The melting and crystallization behavior of a natural clinopyroxene–ilmenite intergrowth. *Contributions to Mineralogy and Petrology* **61**, 1–9.

Yang, H.-J., Frey, F. A., Rhodes, J. M., & Garcia, M. O. (1996). Evolution of Mauna Kea volcano: Inferences from lava compositions recovered in the Hawaii Scientific Drilling Project. *Journal of Geophysical Research* **101**, 11747–11767.

Yang, H.-J., Sen, G. & Shimizu, N. (1998). Mid-ocean ridge melting: constraints from lithospheric xenoliths at Oahu, Hawaii. *Journal of Petrology* **39**, 277–295.

Yang, H.-J., Frey, F. A. & Clague, D. (2003). Constraints on the source components of lavas forming the Hawaiian North Arch and Honolulu Volcanics. *Journal of Petrology* **44**, 403–427.

Yoder, H. S. & Tilley, C. E. (1962). Origin of basalt magma: an experimental study of natural and synthetic systems. *Journal of Petrology* **3**, 342–532.

APPENDIX A

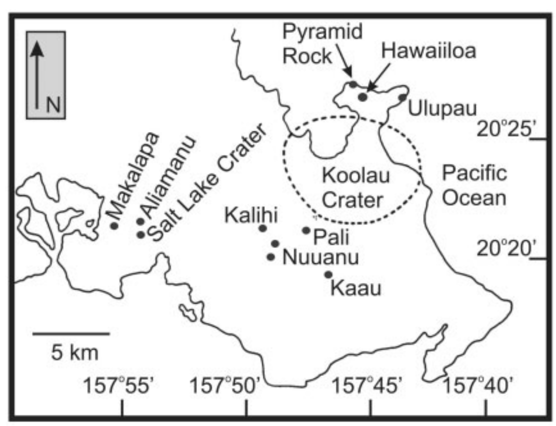

Fig. A1. A map of the Koolau volcanic area on the island of Oahu (eastern part), showing post-erosional (related to HV) vent locations. Vents proximal to the Koolau crater are characterized largely by the presence of spinel lherzolite and shallow cumulates (crust–mantle depth). All the garnet-bearing xenoliths described in the present study come from Salt Lake Crater, a vent on the apron of the Koolau shield. Garnet-bearing xenoliths are also found at Aliamanu. Modified after Sen & Presnall (1986) and Sen (1988).

APPENDIX B

Table B1: Sample numbers

Sample number in tables	True sample number
1	114697-42
2	114923-167
3	114923-172
4	114954-20A
5	115954-20B
6	115954-20C
7	69SAL-204
8	69SAL-214
9	77SL-10
10	77SL-35
11	77SL-7
12	77SL-8
13	77SL-9
14	SL-7
15	SLC-20-175
16	SLC-20-185
17	114923-55
18	69SAL-28
19	114923-158
20	77SL-77
21	77SL-54
22	77SL-62
23	114954-28A
24	114923-95
25	114954-28B
26	69SAL-80
27	SLC-20-180
28	77SL-48

APPENDIX C

Brief petrography of the studied suite of xenoliths

Samples are listed by their short code number as in Appendix B. Modal proportions are in volume per cent.

(1) $Ol_8Cpx_{85}Gt_7$: fairly coarse-grained olivine-bearing garnet clinopyroxenite. Olivine has minor deformation lamellae, with triple junctions, and besides being a discrete phase, also occurs as an inclusion in large cpx. Trace of large, discrete opx. Spinel occurs as an exsolved phase in large opx. Spinel dominantly found as blobs in large garnet. Cpx lacks garnet exsolution, but has opx as an exsolved phase.

(2) $Ol_5Cpx_{89}Gt_6$: medium-grained xenolith. Garnets with and without spinel cores. Cpx occurs with exsolution of opx. Opx lacks exsolution, and primarily occurs on the edges of the specimen. Blades of spinel exsolved in large cpx.

(3) $Ol_3Cpx_{91}Gt_6$: dominantly a garnet-bearing clinopyroxenite with minor olivine; lacks large opx. A fair amount of garnet occurs as an exsolved phase in large cpx. Spinel occurs interstitially, as well as near grain margins of large garnet. Large garnets do not have spinel cores.

(4) $Ol_{10}Cpx_{82}Gt_8$: coarse-grained olivine-bearing garnet clinopyroxenite. Olivine occurs as a large, discrete phase randomly distributed throughout the thin section; it also occurs as an inclusion in large, primary cpx. Cpx has a fair amount of garnet exsolved in it, with garnet achieving a maximum thickness of ~300–400 μm. Garnet also occurs as grains with or without spinel cores. In some places it is not entirely clear if garnet is a primary, discrete phase or occurs as a grain boundary phase garlanding primary cpx. Spinel cores are fairly thick (~200–300 μm). Ilmenite also occurs either as an exsolved phase or as an inclusion in large cpx. This xenolith lacks opx in any form.

(5) $Ol_7Cpx_{83}Gt_{10}$: medium- to coarse-grained olivine-bearing garnet clinopyroxenite. Olivine is stubby and appears to be uniformly distributed in the thin section. Cpx is subhedral and has a fair amount of garnet exsolution. Exsolved garnet is amoeboid in shape. Garnet also occurs as a phase with or without spinel cores; when with a spinel core, it appears to be more round than the garnet that lacks a spinel core. A few garnet grains lacking spinel cores also have radially oriented ilmenite needles. Phlogopite occurs as a trace phase and is almost euhedral.

(6) $Ol_{10}Cpx_{80}Gt_{10}$: fairly coarse-grained xenolith with plenty of spinel cores in large garnet grains. There are also garnet grains without spinel cores. In places primary olivine has deformation lamellae. Olivine is largely euhedral, although in places it appears to be of a slightly fractured nature. Large, primary cpx has marked exsolution of opx. In some cpx grains, exsolved opx is thinly spaced. Opx is absent as a large, discrete phase. Spinel also occurs as an exsolved phase in cpx and is of two forms: greenish, blade-like grains and brown–black needles.

(7) $Ol_2Cpx_{15}Gt_{83}$: almost a pure garnetite, and hence, a very interesting xenolith. Olivine is slightly broken and has a few deformation lamellae. Thick, blebby exsolution of garnet in large, primary cpx. Garnet is granular in appearance, and in some grains has a spinel core. Spinel in the core is generally irregular in shape. This xenolith lacks large, discrete opx.

(8) $Ol_4Cpx_{91}Gt_5$: a fairly granular and coarse-grained xenolith, with plenty of stubby garnet exsolution in large cpx. In places, exsolved garnet forms garlands around cpx, and can be physically traced back to garnet exsolved in the core of cpx. Garnet also occurs in two other forms, with and without a spinel core. Spinel grains in the core are almost as big as their host garnet.

(9) $Ol_6Cpx_{86}Gt_8$: coarse-grained xenolith with all the primary phases uniformly distributed. Cpx has abundant, very closely spaced exsolution lamellae of opx. Olivine grains are euhedral, and appear to lack either deformation lamellae or fractures. Opx tends to occur in clusters largely at the edges of the xenolith. Garnet grains without a spinel core appear to be slightly altered at their grain margins. Spinel cores are very small in their garnet host. Ilmenite occurs as needles in the host cpx, and it is not certain if it is an inclusion or an exsolved phase.

(10) $Ol_6Cpx_{87}Gt_7$: medium- to coarse-grained xenolith. Both cpx and opx have fairly abundant exsolution. Exsolved opx in host cpx is coarse-grained and occurs in lamellae that are evenly spaced; exsolved cpx lamellae in host opx are thin and closely spaced, and are also restricted to the center of the opx. Spinel cores in large, primary garnets appear to be of two textural kinds, one that is fairly round in form and the other that has an amoeboid outline; both types are almost black in their appearance.

(11) $Ol_{10}Cpx_{80}Gt_{10}$: a coarse-grained xenolith with abundant large, discrete garnet and olivine grains. A few olivine grains have deformation lamellae, and in places also exhibit triple-junction like features. A few of the olivine grains also have melt/fluid inclusion trails. Discrete cpx has greenish brown blade-like spinel as an exsolved phase, and large opx has a moderate amount of thin, exsolved cpx lamellae largely in the center. Large, primary garnets appear to have two textural types of spinels in their cores: one that is fairly round in its form and the other that has embayed grain margins.

(12) $Ol_{11}Cpx_{81}Gt_8$: a medium- to coarse-grained xenolith with cpx that has abundant spinel exsolution. Spinel exsolved in cpx is light green in color, and is largely of tabular nature, although in places it also has a needle-like form. Spinel exsolved in opx is brownish in color and is more needle-like than that in cpx. There are also cpx grains that are free of exsolution. Olivine is euhedral in form, and in places has a trail of melt/fluid inclusions in the core of the grains. Opx with spinel exsolution is stubby and is of well-developed prismatic nature.

(13) $Ol_9Cpx_{81}Gt_{10}$: a fine- to medium-grained xenolith with well-developed olivine grains that appear to be free of either deformation features or melt/fluid inclusions. Cpx is well developed and is blue–green in color, with some coarse opx exsolution; opx lamellae seem to be regularly spaced and are also uniformly distributed in the host cpx. It also has spinel in blade-like form as an exsolved phase. Some cpx grains have both spinel and opx as exsolved phases, whereas the neighboring cpx grains have only vermicular garnet as an exsolved phase. Primary garnet is large and has both round and irregular spinel in its core. Spinel in garnet cores is very dark in color. There are garnet grains that lack spinel cores; the margins of these garnets are brownish in color.

(14) $Ol_3Cpx_{91}Gt_6$: a very altered xenolith with significant deformation lamellae in large olivine. Olivine grains appear to be fractured locally and altered grain margins are common. Cpx is free of exsolution and in places appears to be highly altered at the grain margins. Garnet is free of spinel cores, and is round in form. Opx is largely restricted to the edges of the xenolith. This rock is also free of spinel in any form.

(15) $Ol_{10}Cpx_{80}Gt_{10}$: a medium- to coarse-grained xenolith with fresh-looking olivine grains that are euhedral in outline. Olivine grain size appears to be uniform in the xenolith. Cpx is subhedral in outline and is full of greenish, tabular spinel grains as an exsolved phase. Garnet is large and has spinel cores that are almost as large as the host garnet. Spinel in the garnet cores is very dark in color and attains round as well as highly irregular forms. This xenolith is free of large opx.

(16) $Ol_{12}Cpx_{79}Gt_9$: a medium- to coarse-grained xenolith with many well-developed primary olivine, cpx, and garnet grains. Large olivine is stubby, of uniform grain size and shape throughout the xenolith, and in places exhibits deformation features. Cpx is subhedral in outline and has abundant very thin lamellae of opx as an exsolved phase. Large garnet grains are free of spinel cores; although there are traces of spinel as an interstitial phase. Needle-like ilmenite also occurs as an interstitial, discrete phase in the xenolith.

(17) $Ol_{10}Cpx_{82}Gt_8$: a coarse-grained xenolith with abundant exsolution features in both types of pyroxene. Olivine is euhedral, stubby, and in places has deformation lamellae. Large subhedral cpx has abundant, coarse opx exsolution. Cpx exsolved in large opx (traces) is thin, and is also closely spaced. Large opx also has blades of greenish brown spinel as an exsolved phase. Spinel in the cores of large garnet grains is black in color and has fairly strongly embayed margins. Garnet exsolved in large

cpx is vermicular in outline, and in places is fairly coarse.

(18) $Ol_{11}Cpx_{80}Gt_9$: a medium- to coarse-grained xenolith with large euhedral olivine grains that exhibit minor variations in grain size. There is a vein of spinel and garnet in this xenolith that cuts the heart of the xenolith, which is made up of primary olivine, cpx, and garnet. The primary olivine, cpx, and garnet grains near the vein have a 'burnt' appearance. Spinel in the veins is of two types: one that is very reflective and the other that is not. 'Burnt' olivines near the veins have embayed margins, whereas similarly 'burnt' garnet has a more round appearance. Garnet exsolved in host cpx is thick and assumes an vermicular form. Sometimes, it also garlands the host cpx. The modal abundance of phases provided is for the main body of the xenolith.

(19) $Ol_{12}Cpx_{78}Gt_{10}$: a very coarse-grained xenolith cut by a vein composed of opx, garnet, phlogopite, and olivine. Olivine in the vein is not texturally very different from that found in the main body of the xenolith. In the main xenolith, olivine is stubby and euhedral, and occurs as large, discrete grains as well as an inclusions in large, discrete cpx. All the three types of olivine seem to have similar grain size. The margins of large olivines near the vein have an embayed appearance. Cpx in the xenolith is well developed and has plenty of opx exsolution. Opx in the vein is more round than that in the main body of the xenolith, which is prismatic and has exsolution of cpx and blade-like spinel. There is also opx in the main body of the xenolith that is free of exsolution. Garnet in the main body of the xenolith has a spinel core, whereas that in the vein is free of spinel. Phlogopite appears to occur dominantly in the vein part of the xenolith. Texturally, it is euhedral, does not seem to have irregular grain margins, and is well cleaved. There are also some grains of phlogopite in the main body of the xenolith but it is not clear if this phlogopite is part of that seen in the vein.

(20) $Ol_6Cpx_{85}Gt_9$: a medium- to coarse-grained xenolith with large olivine and garnet grains. Olivine is fresh and only slightly altered in places. It is euhedral in form and seems to have deformation features in a few grains. Garnet is large and lacks a spinel core. Large cpx has fairly coarse and uniformly spaced opx lamellae as exsolution features. Large opx has cpx exsolution. Cpx lamellae in host opx are thin and are very closely spaced, and in places they are present only in the center of the host opx.

(21) $Ol_{11}Cpx_{82}Gt_7$: a medium- to coarse-grained xenolith with a few deformation features in olivine grains. Olivine grains do not vary in size across the xenolith, and are fractured in a few places. Cpx is stubby and lacks exsolution of any kind. Large, discrete opx is absent in this xenolith, as is garnet with a spinel core. Large garnet is uniformly distributed in the xenolith. Although cpx and garnet are devoid of spinel, there are traces of interstitial spinel in the xenolith.

(22) $Ol_8Cpx_{81}Gt_{11}$: a medium-grained xenolith with two texturally distinct kinds of cpx. One type of cpx has exsolution of opx and spinel and the other type is free of exsolution features. Exsolved opx in cpx is lamellar and spinel in cpx ranges from being almost colorless to mild green and blade-like in form. There is also a large cpx grain without exsolution that has an inclusion of opx that is also free of exsolution. The opx inclusion is stubby and prismatic in form. Large olivine in the xenolith is euhedral and, although unstrained, is fractured in a few places. Large garnet in the xenolith has a spinel core, and spinel is amoeboid in form with slightly embayed margins. There are traces of phlogopite. Whereas a few of these grains have perfect outlines, others appear to have embayed grain margins. The textural relationship between phlogopite and rest of the phases in the xenolith is not entirely clear.

(23) $Cpx_{90}Gt_{10}$: a pure garnet clinopyroxenite with large cpx and garnet grains. Large cpx and garnet grains apparently form layers in the rock and alternate with each other. Cpx is free of inclusions or exsolution features. Most of the large garnet grains are elongated in outline and are free of spinel cores. A few garnet grains that are round in outline have exsolved opx. This feature makes this xenolith especially significant, as it demonstrates that at some point all the opx might have been fully dissolved in the host garnet, giving garnet a majoritic composition.

(24) $Cpx_{91}Gt_9$: a coarse-grained garnet clinopyroxenite with well-developed large cpx that has unaltered grain margins. Cpx has very fine lamellae of exsolved opx. Large garnet is both with and without spinel in the core; that with a spinel core is more round than that without spinel in the core. Spinel core in garnet is very dark in color and has an irregular outline. There is also interstitial subhedral spinel. Large opx occurs at the margins of the xenolith and contains two texturally distinct kinds of exsolved cpx: one that is present dominantly in the center of host opx, is tightly spaced, and is relatively thin; the other kind of exsolved cpx is thicker and appears to be more uniformly distributed. The host opx in each case seems to be of normal prismatic kind.

(25) $Cpx_{93}Gt_7$: a coarse-grained garnet clinopyroxenite with subhedral cpx that is devoid of exsolution features. Garnet is round and lacks a spinel core.

In places, a few garnet grains have altered margins. Prismatic opx is a trace phase, is present only at the edges of the xenolith, and lacks exsolution.

(26) $Cpx_{89}Gt_{11}$: a medium- to coarse-grained xenolith that has large, discrete cpx without exsolution structures of any kind. Cpx is uniformly distributed in the xenolith. A few of the large garnets grains have spinel in their core, with spinel being almost as large as the host garnet. Spinel in the core is greenish black in color and appears to have uniformly round margins. This xenolith has traces of needle-like, very dark ilmenite.

(27) $Cpx_{91}Gt_{9}$: a medium-grained garnet clinopyroxenite with significant spinel exsolution in large, discrete cpx. Large cpx is subhedral in outline and is uniformly distributed in the xenolith. Spinel in cpx occurs as flat, rhomb-like features that are light green in color. Very dark, subhedral–euhedral spinel also occurs as an interstitial phase in the xenolith, largely between primary cpx and garnet grains. Large garnet occurs uniformly in the xenolith and is free of spinel cores. Fine, needle-like grains of ilmenite also occur interstitially in parts of this xenolith.

(28) $Cpx_{90}Gt_{10}$: a very coarse-grained garnet clinopyroxenite with abundant coarse-grained garnet exsolution in large, discrete cpx grains. Large cpx is generally in subhedral form and is uniformly distributed throughout the xenolith. Garnet exsolved in large cpx is thick and amoeboid in form, and frequently garlands its host cpx. It is not certain in places if the garnet outside the large cpx was once a part of that exsolved in cpx and simply migrated out of the cpx host during subsolidus cooling. There are other large cpx grains with moderately thick exsolved opx lamellae. Cpx does not have both garnet and opx exsolution in the same grain. There are traces of large opx grains around the edges of the xenolith. These opx grains have fine-grained exsolved cpx lamellae.